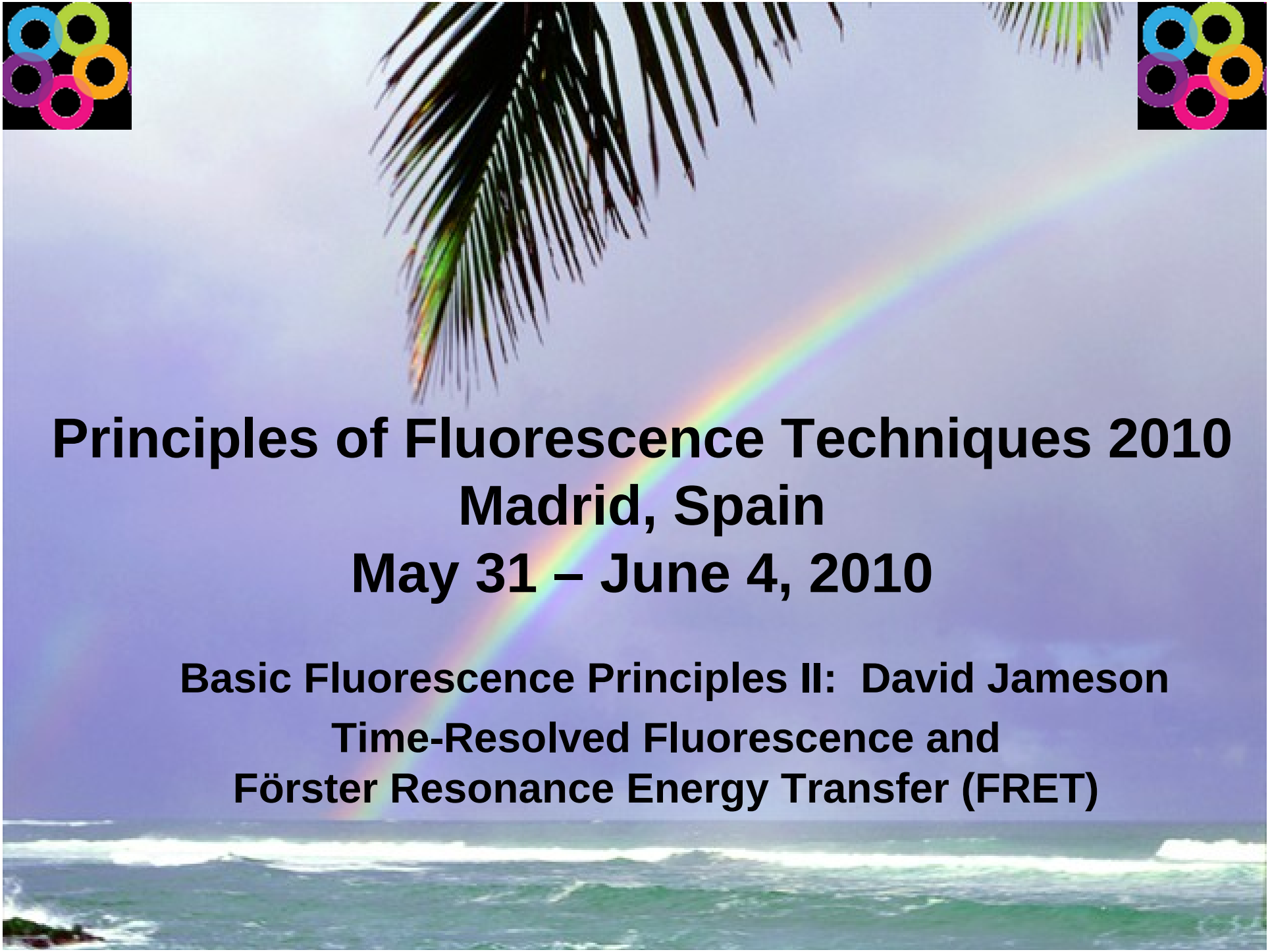

Principles of Fluorescence Techniques 2010
Madrid, Spain
May 31 – June 4, 2010

Basic Fluorescence Principles II: David Jameson

Time-Resolved Fluorescence and
Förster Resonance Energy Transfer (FRET)

The Time Interval between Absorption and Emission of Light in Fluorescence.

By R. W. Wood, For. Mem. R.S., Johns Hopkins University, Baltimore.

(Received June 12, 1921.)

Some experiments were then made at the University of Wisconsin, in collaboration with Prof. C. E. Mendenhall, during my visit to Madison in December. We used a high pressure, six-cylinder pump, and obtained a jet velocity of about 200 metres per second, with a fine glass nozzle about 0·2 mm. in diameter. More recently, Prof. Mendenhall has increased the velocity to 230 metres per second, and, by blackening one side of the jet tube, leaving a small clear space for the entrance of the sunlight, has assured himself that there is no displacement as great as 0·1 mm. (observing the fluorescent patch with a short-focus lens). This means that the duration of the fluorescence is less than 1/2,300,000 second.

The Time Interval between Absorption and Emission of Light in Fluorescence.

lem. R.S., Johns Hopkins University, Baltimore.

(Received June 12, 1921.)

Some experiments were niversity of Wisconsin, in collaboration with Prof. C. ng my visit to Madison in December. We used a high der pump, and obtained a jet velocity of about 200 metres th a fine glass nozzle about 0·2 mm. in diameter. More re lendenhall has increased the velocity to 230 metres per secc blackening one side of the jet tube, leaving a small clear spa entrance of the sunlight, has assured himself that there is no di as great as 0·1 mm. (observing the fluorescent patch with a short-f). This means that the duration of the fluorescence is less than 1/2,3 second.

The Time Interval between Absorption and Emission of Light in Fluorescence.

By R. W. Wood, For. Mem. R.S., Johns Hopkins University, Baltimore.

(Received June 12, 1921.)

Some experiments were then made at the University of Wisconsin, in collaboration with Prof. C. E. Mendenhall, during my visit to Madison in December. We used a high pressure, six-cylinder pump, and obtained a jet velocity of about 200 metres per second, with a fine glass nozzle about 0·2 mm. in diameter. More recently, Prof. Mendenhall has increased the velocity to 230 metres per second, and, by blackening one side of the jet tube, leaving a small clear space for the entrance of the sunlight, has assured himself that there is no displacement as great as 0·1 mm. (observing the fluorescent patch with a short-focus lens). This means that the duration of the fluorescence is less than 1/2,300,000 second.

i.e. < 435ns

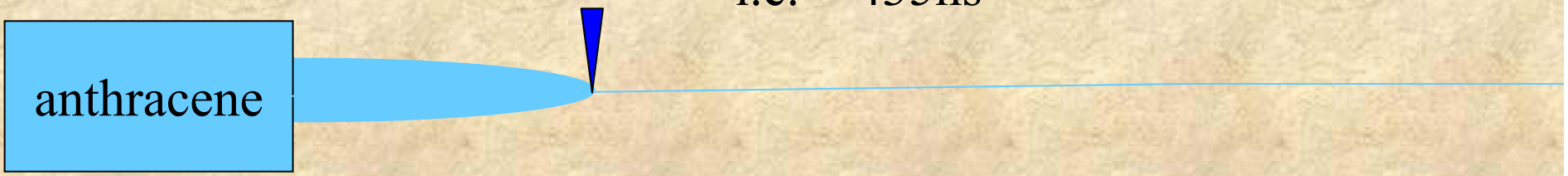

This work was followed by a report by Philip Gottling in 1923 who used a Kerr Cell – as originally suggested by Lord Rayleigh in 1905.

THE DETERMINATION OF THE TIME BETWEEN EXCITATION AND EMISSION FOR CERTAIN FLUORESCENT SOLIDS

By Philip F. Gottling

Abstract

Time lag between excitation and emission of fluorescence by barium platino-cyanide and rhodamine.—The work begun in 1921 by R. W. Wood on the measurement of fluorescent intervals and phosphorescent times has been continued. The method of Abraham and Lemoine, somewhat modified, was used for determining the very short periods of time involved. The fluorescent light is polarized and then passed through a condenser, containing nitrobenzene as dielectric, which had begun to be discharged when the illuminating spark started. The later the light arrives the lower the average field of the condenser and the smaller the angular setting of the analyzing nicol to match the two images produced by a double image prism. The apparatus was calibrated by means of light reflected from a mirror at different distances from the spark. The interval of time between the occurrence of a spark and the emission of the fluorescent light excited by that spark, was found to be $(2.12 \pm .01) \times 10^{-7}$ sec. for barium platino-cyanide and $(2.11 \pm .14) \times 10^{-8}$ sec. for rhodamine.

He found 21.1 ns for a solution of rhodamine in acetone, acetic acid and glycerol. Possibly he was observing a combination of fluorescence and phosphorescence

Enrique Gaviola

Ein Fluorometer.
Apparat zur Messung von Fluoreszenzabklingungszeiten.

Von **E. Gaviola** in Berlin.

Mit 9 Abbildungen. (Eingegangen am 24. März 1927.)

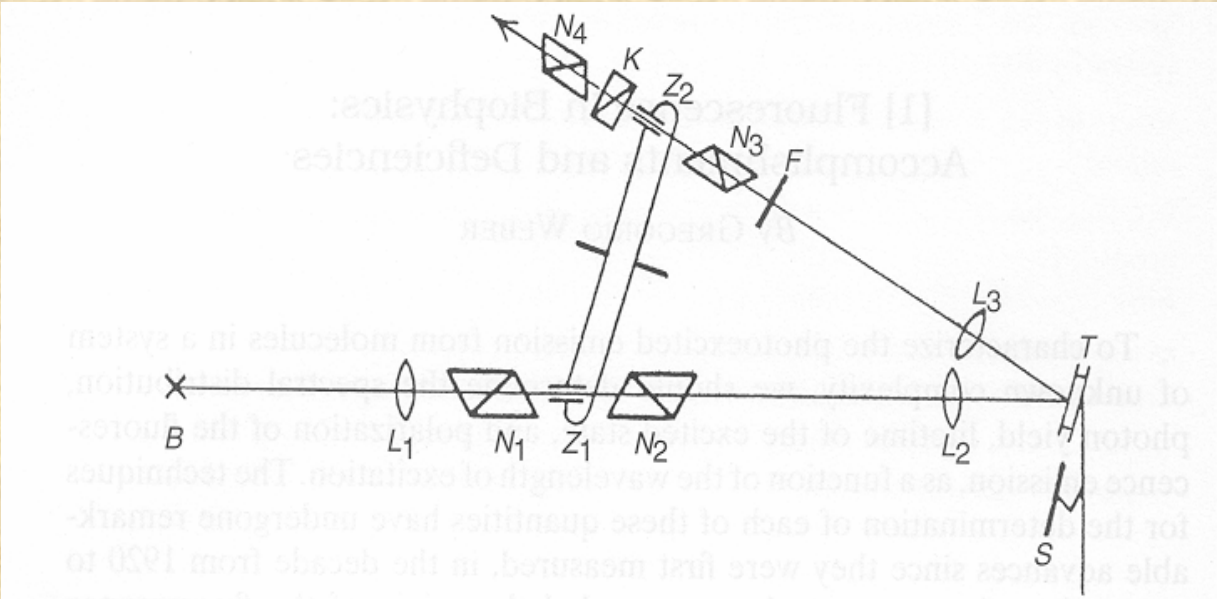

FIG. 1. Original apparatus of Gaviola[1] for the measurement of fluorescence lifetimes, described in text. *B*, Source of exciting light; *T*, cuvette containing the fluorescent solution; *S*, mirror.

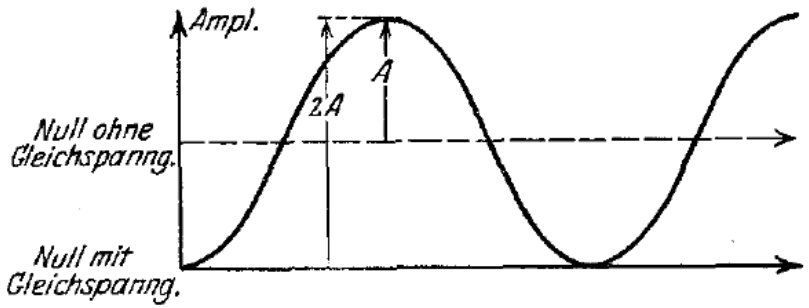

Fig. 7.

Farbstoff	Abklingungszeiten		
	in Wasser Sekunden	in Glycerin Sekunden	in Meth.-Alkohol Sekunden
Uranin	$4{,}5 \cdot 10^{-9}$	$4{,}4 \cdot 10^{-9}$	—
Fluorescein	—	—	$5{,}0 \cdot 10^{-9}$
Rhodamin B	$2{,}0 \cdot 10^{-9}$	$4{,}2 \cdot 10^{-9}$	—
Rhodulin Orange	2,7	4,3	—
Erythrosin	1,8	2,4	$2{,}6 \cdot 10^{-9}$
Tetrajodfluor. Na	1,0	2,0	2,2
Eosin 5 B	1,9	—	3,4
Uranylsulfat	—	—	1,3
Uranylsulfat in Schwefelsäure	—	—	1,9
Chinisarin in Pentan	—	—	2,9
Uranglas	—	—	$>15{,}0$
Rubinkristall	—	—	$>15{,}0$

What is meant by the “lifetime” of a fluorophore???

Although we often speak of the properties of fluorophores as if they are studied in isolation, such is not usually the case.

Absorption and emission processes are almost always studied on *populations* of molecules and the properties of the supposed typical members of the population are deduced from the macroscopic properties of the process.

In general, the behavior of an excited population of fluorophores is described by a familiar rate equation:

$$\frac{dn^*}{dt} = -n^* \Gamma + f(t)$$

where n^* is the number of excited elements at time t, Γ is the rate constant of emission and f(t) is an arbitrary function of the time, describing the time course of the excitation . The dimensions of Γ are sec^{-1} (transitions per molecule per unit time).

If excitation occurs at t = 0, the last equation, takes the form:

$$\frac{dn^*}{dt} = -n^* \Gamma$$

and describes the decrease in excited molecules at all further times. Integration gives:

$$n^*(t) = n^*(0) \exp(-\Gamma t)$$

The lifetime, τ, is equal to Γ^{-1}

If a population of fluorophores are excited, the lifetime is the time it takes for the number of excited molecules to decay to 1/e or 36.8% of the original population according to:

$$\frac{n^*(t)}{n^*(0)} = e^{-t/\tau}$$

In pictorial form:

$$\frac{n^*(t)}{n^*(0)} = e^{-t/\tau}$$

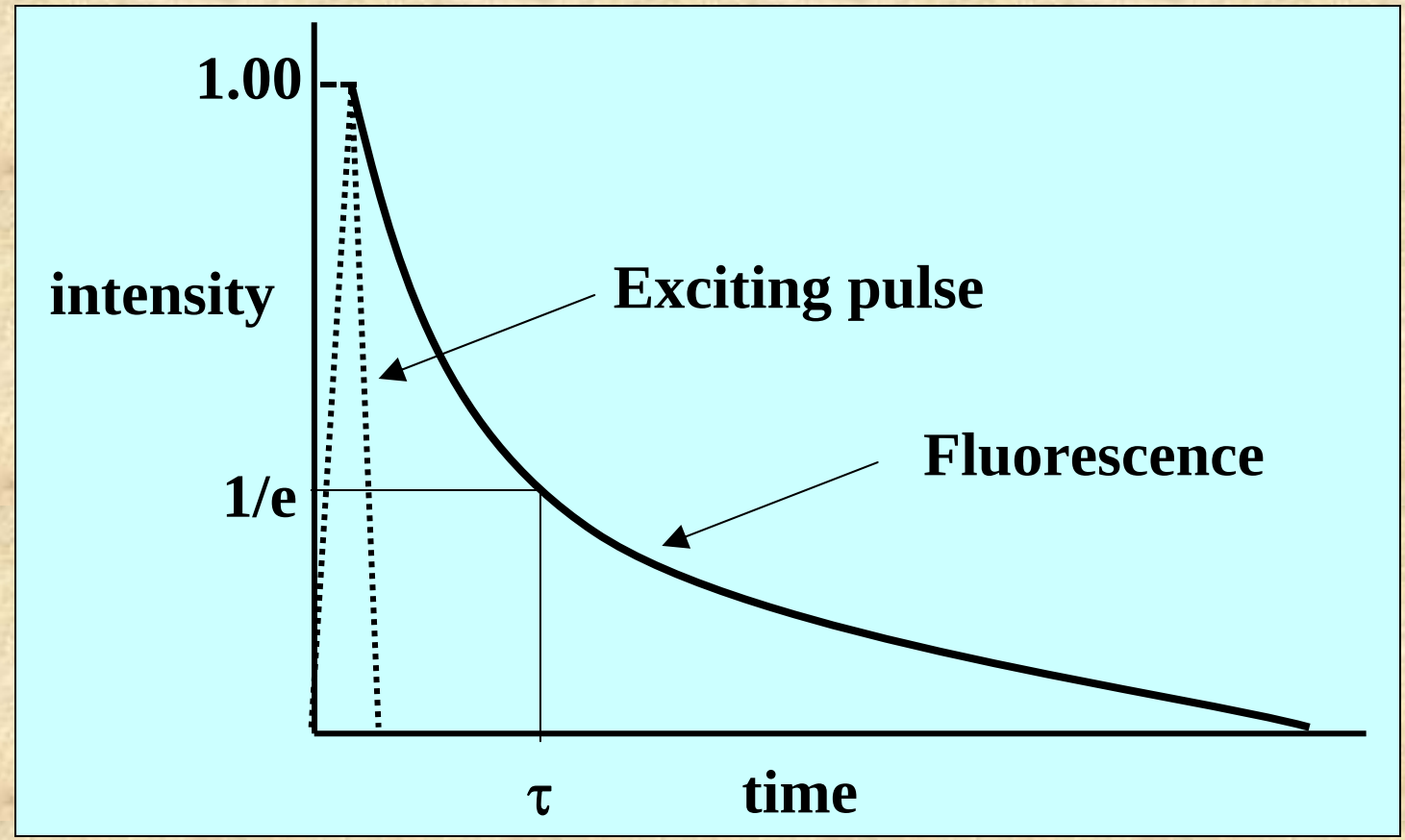

The lifetime and quantum yield for a given fluorophore is often dramatically affected by its environment.

Examples of this fact would be NADH, which in water has a lifetime of ~0.4 ns but bound to dehydrogenases can be a long as 9 ns.

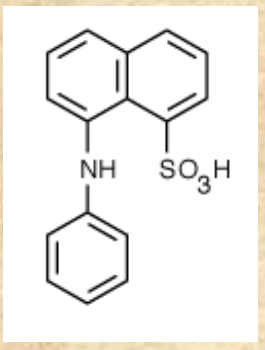

ANS in water is ~100 picoseconds but can be 8 – 10 ns bound to proteins

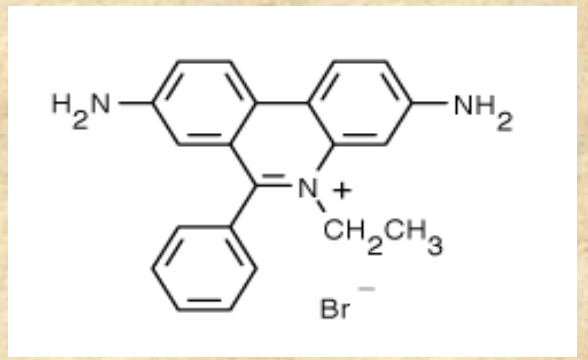

Ethidium bromide is 1.8 ns in water, 22 ns bound to DNA and 27ns bound to tRNA

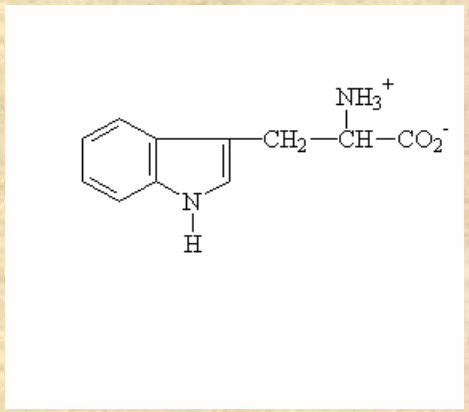

The lifetime of tryptophan in proteins ranges from ~0.1 ns up to ~8 ns

Excited state lifetimes have traditionally been measured using either the *impulse* response or the *harmonic* response method. In principle both methods have the same information content. These methods are also referred to as either the "time domain" method or the "frequency domain" method.

In the *impulse (*or pulse) method, the sample is illuminated with a short pulse of light and the intensity of the emission versus time is recorded. Originally these short light pulses were generated using *flashlamps* which had widths on the order of several nanoseconds. Modern laser sources can now routinely generate pulses with widths on the order of picoseconds or shorter.

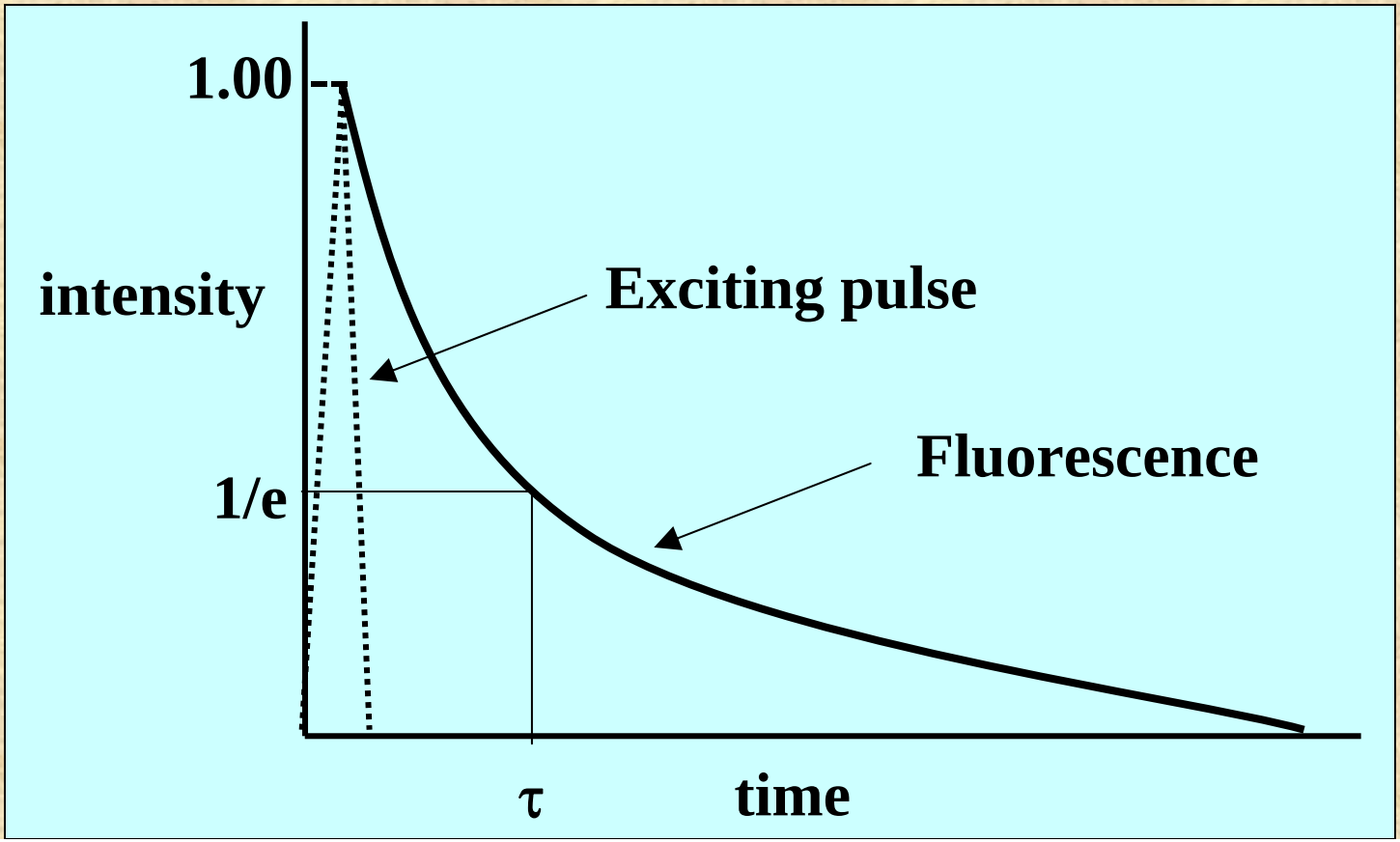

As shown in the intensity decay figure, the *fluorescence* lifetime, t , is the time at which the intensity has decayed to 1/e of the original value. The decay of the intensity with time is given by the relation:

$$I_t = \alpha e^{-t/\tau}$$

Where I_t is the intensity at time t, α is a normalization term (the pre-exponential factor) and τ is the lifetime.

It is more common to plot the fluorescence decay data using a logarithmic scale as shown here.

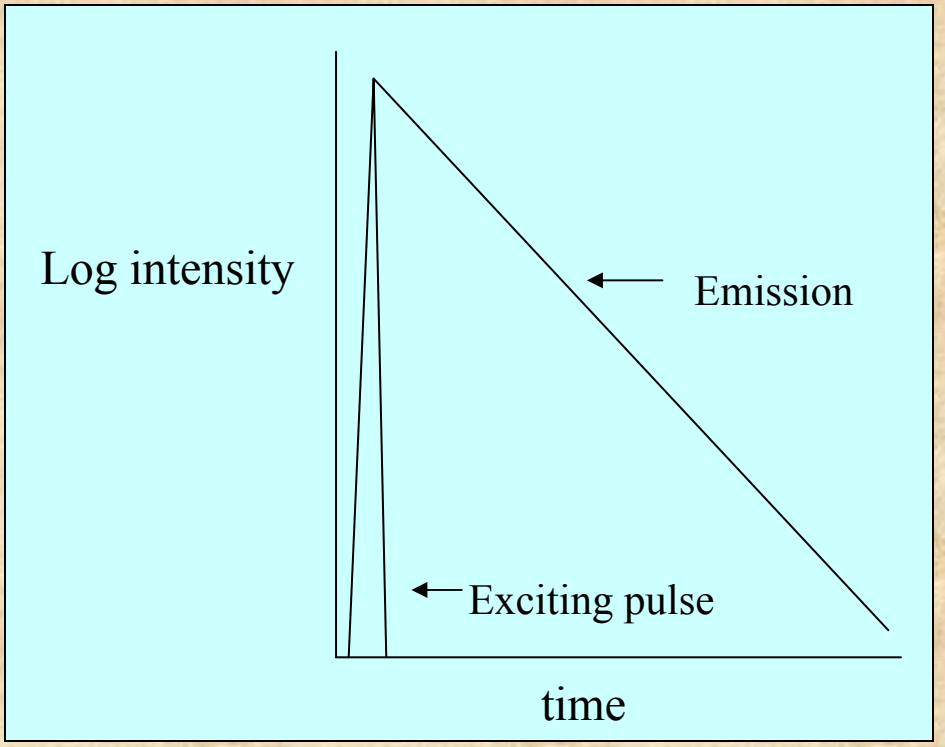

If the decay is a single exponential and if the lifetime is long compared to the exciting light then the lifetime can be determined directly from the slope of the curve.

If the lifetime and the excitation pulse width are comparable some type of *deconvolution* method must be used to extract the lifetime.

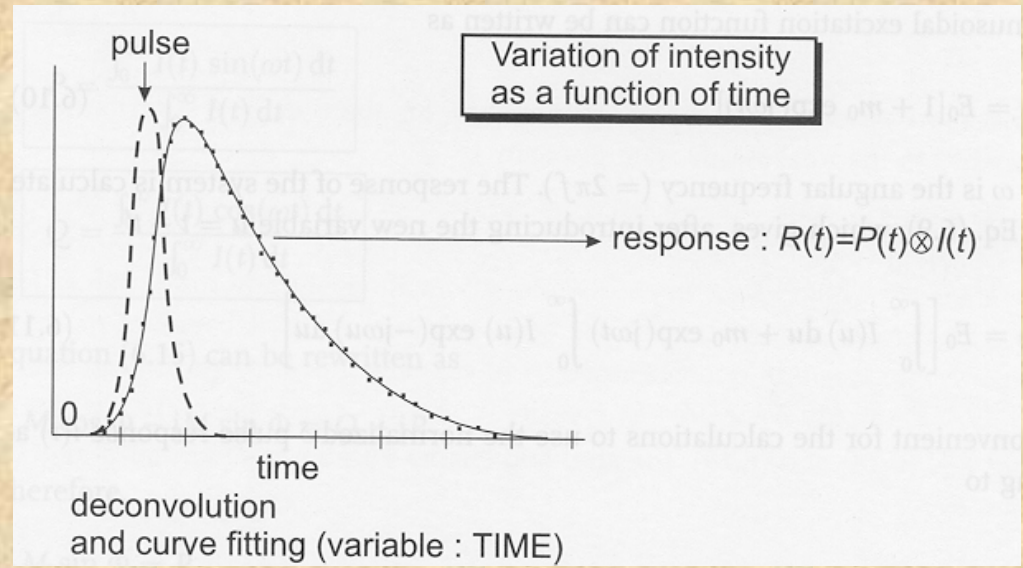

Great effort has been expended on developing mathematical methods to "deconvolve" the effect of the exciting pulse shape on the observed fluorescence decay.

With the advent of very fast laser pulses these deconvolution procedures became less important for most lifetime determinations, although they are still required whenever the lifetime is of comparable duration to the light pulse.

If the decay is multiexponential, the relation between the intensity and time after excitation is given by:

$$I(t) = \sum_i \alpha_i e^{-t/\tau_i}$$

One may then observe data such as those sketched below:

Here we can discern at least two lifetime components indicated as τ_1 and τ_2 . This presentation is oversimplified but illustrates the point.

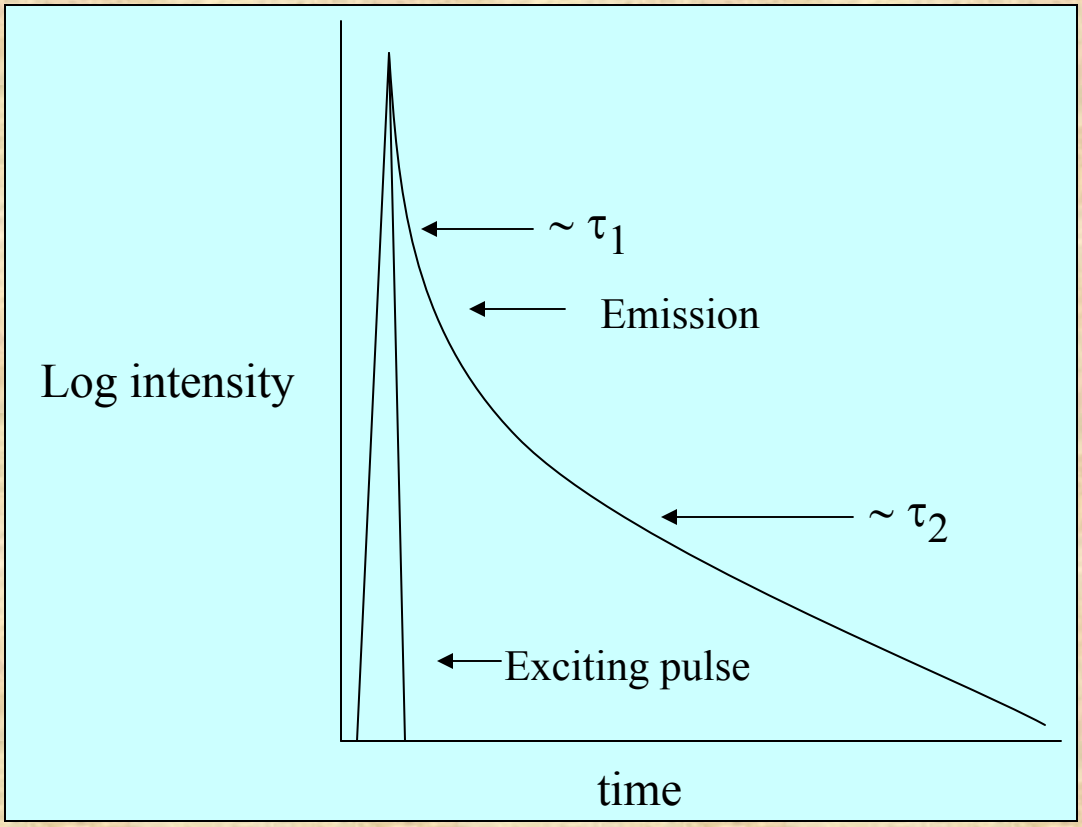

Here are pulse decay data on anthracene in cyclohexane taken on an IBH 5000U Time-correlated single photon counting instrument equipped with an LED short pulse diode excitation source.

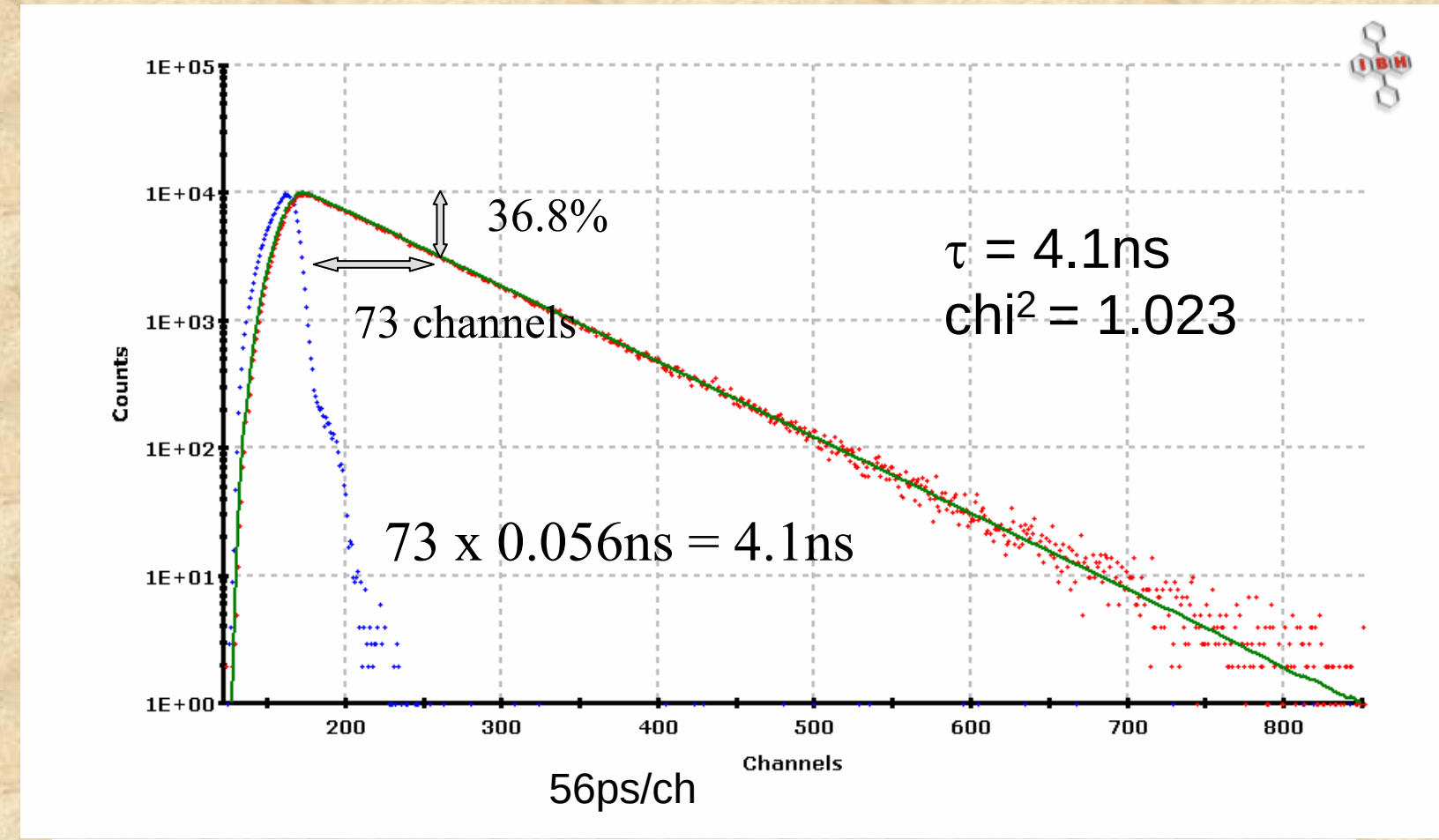

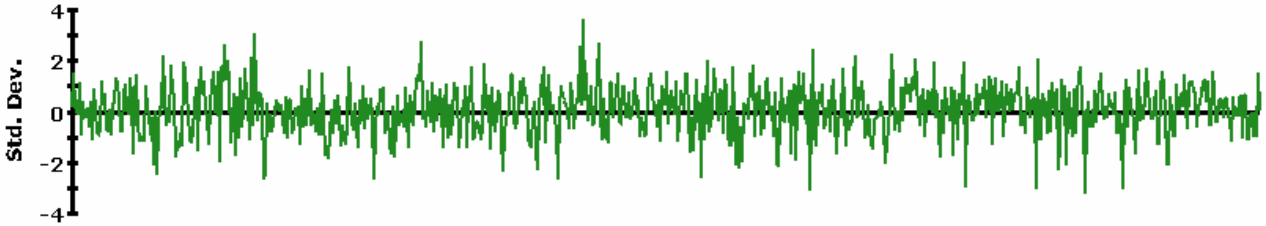

In the harmonic method (also known as the phase and modulation or frequency domain method) a continuous light source is utilized, such as a laser or xenon arc, and the intensity of this light source is modulated sinusoidally at high frequency as depicted below. Typically, an *electro-optic* device, such as a *Pockels cell* is used to modulate a continuous light source, such as a CW laser or a xenon arc lamp. Alternatively, LEDs or laser diodes can be directly modulated.

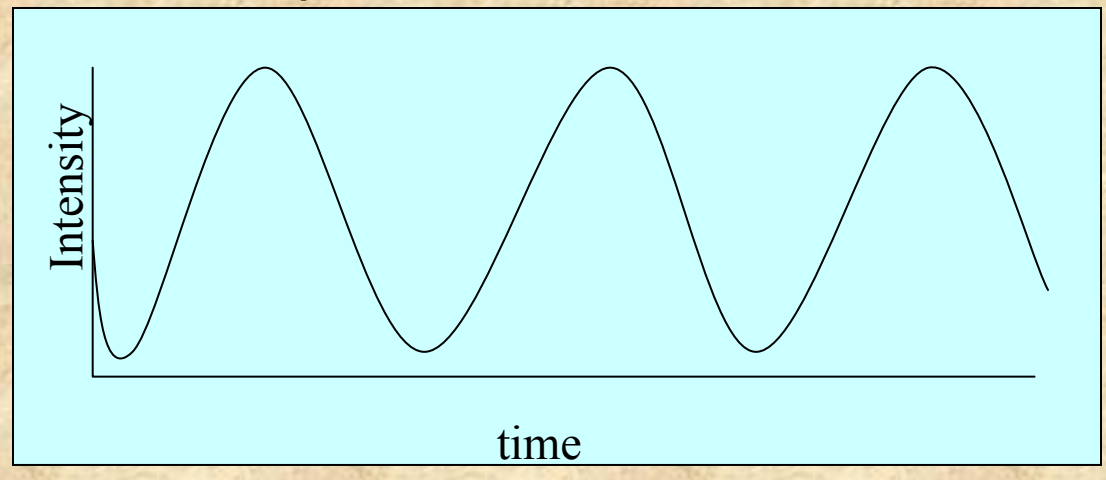

In such a case, the excitation frequency is described by:

$$E(t) = Eo\,[1 + M_E \sin \omega t]$$

E(t) and Eo are the intensities at time t and o, M_E is the modulation factor which is related to the ratio of the AC and DC parts of the signal and ω is the angular modulation frequency.

$\omega = 2\pi f$ where f is the linear modulation frequency

Due to the persistence of the excited state, fluorophores subjected to such an excitation will give rise to a modulated emission which is shifted in phase relative to the exciting light as depicted below.

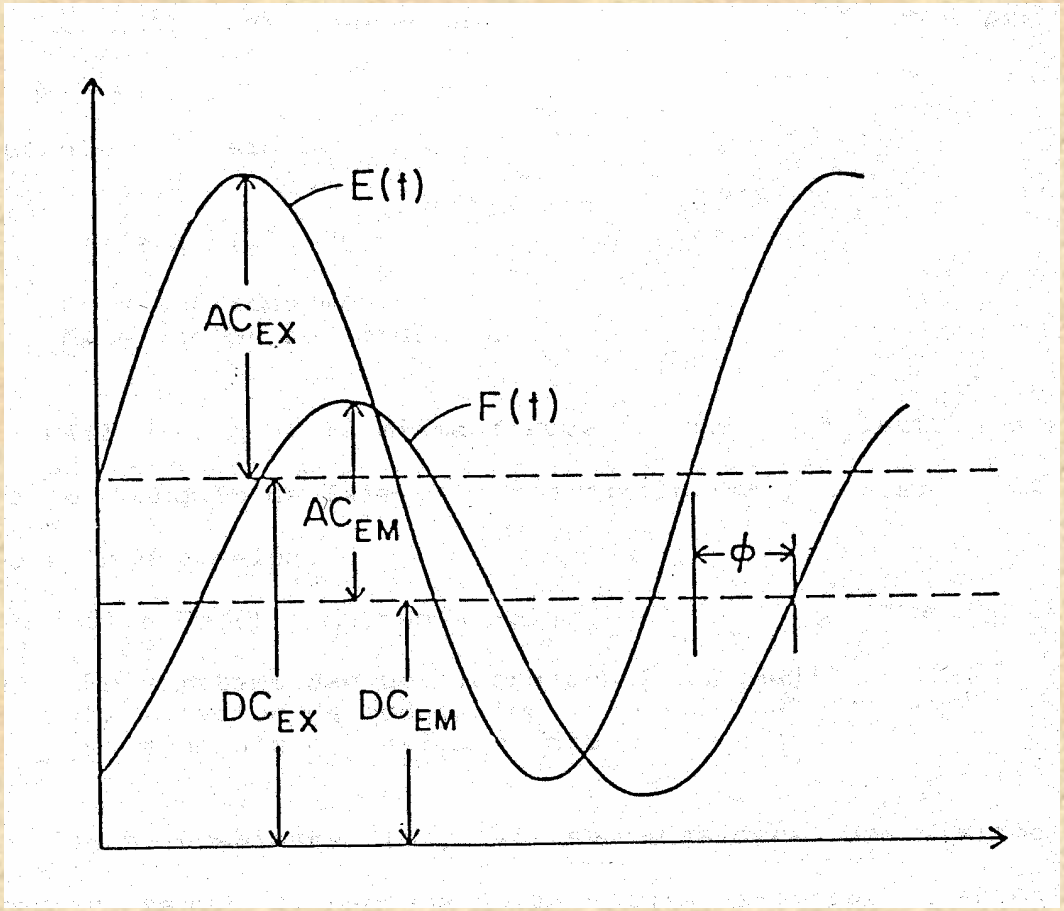

This sketch illustrates the phase delay (ϕ) between the excitation, E(t), and the emission, F(t). Also shown are the AC and DC levels associated with the excitation and emission waveforms.

One can demonstrate that:

$$\mathbf{F(t) = Fo\,[1 + M_F \sin(\omega t + \phi)]}$$

This relationship signifies that measurement of the phase delay, ϕ, forms the basis of one measurement of the lifetime, τ. In particular one can demonstrate that:

$$\mathbf{\tan \phi = \omega\tau}$$

The *modulations* of the excitation (M_E) and the emission (M_F) are given by:

$$M_E = \left(\frac{AC}{DC}\right)_E \quad \text{and} \quad M_F = \left(\frac{AC}{DC}\right)_F$$

The *relative modulation*, M, of the emission is then:

$$M = \frac{(AC/DC)_F}{(AC/DC)_E}$$

τ can also be determined from M according to the relation: $M = \dfrac{1}{\sqrt{1+(\omega\tau)^2}}$

Using the *phase shift* and *relative modulation* one can thus determine a *phase lifetime* (τ_P) and a *modulation lifetime* (τ_M).

If the fluorescence decay is a single exponential, then τ_P and τ_M will be equal at all modulation frequencies.

If, however, the fluorescence decay is multiexponential then $\tau_P < \tau_M$ and, moreover, the values of both τ_P and τ_M will depend upon the modulation frequency, i.e.,

$$\tau_P(\omega_1) < \tau_P(\omega_2) \quad \text{if} \quad \omega_1 > \omega_2$$

To get a feeling for typical phase and modulation data, consider the following data set.

Frequency (MHz)	τ_P (ns)	τ_M (ns)
5	6.76	10.24
10	6.02	9.70
30	3.17	6.87
70	1.93	4.27

These differences between τ_P and τ_M and their frequency dependence form the basis of the methods used to analyze for lifetime heterogeneity, i.e., the component lifetimes and amplitudes.

In the case just shown, the actual system being measured was a mixture of two fluorophores with lifetimes of 12.08 ns and 1.38 ns, with relative contributions to the total intensity of 53% and 47% respectively.

Here must must be careful to distinguish the term *fractional contribution to the total intensity* (usually designated as f) from α, the pre-exponential term referred to earlier. The relation between these two terms is given by:

$$f_i = \frac{\alpha_i \tau_i}{\sum_j \alpha_j \tau_j}$$

where j represents the sum of all components. In the case just given then, the ratio of the pre-exponential factors corresponding to the 12.08 ns and 1.38 ns components is approximately 1/3. In other words, there are three times as many molecules in solution with the 1.38 ns lifetime as there are molecules with the 12.08 ns lifetime.

Multifrequency phase and modulation data are usually presented as shown below:

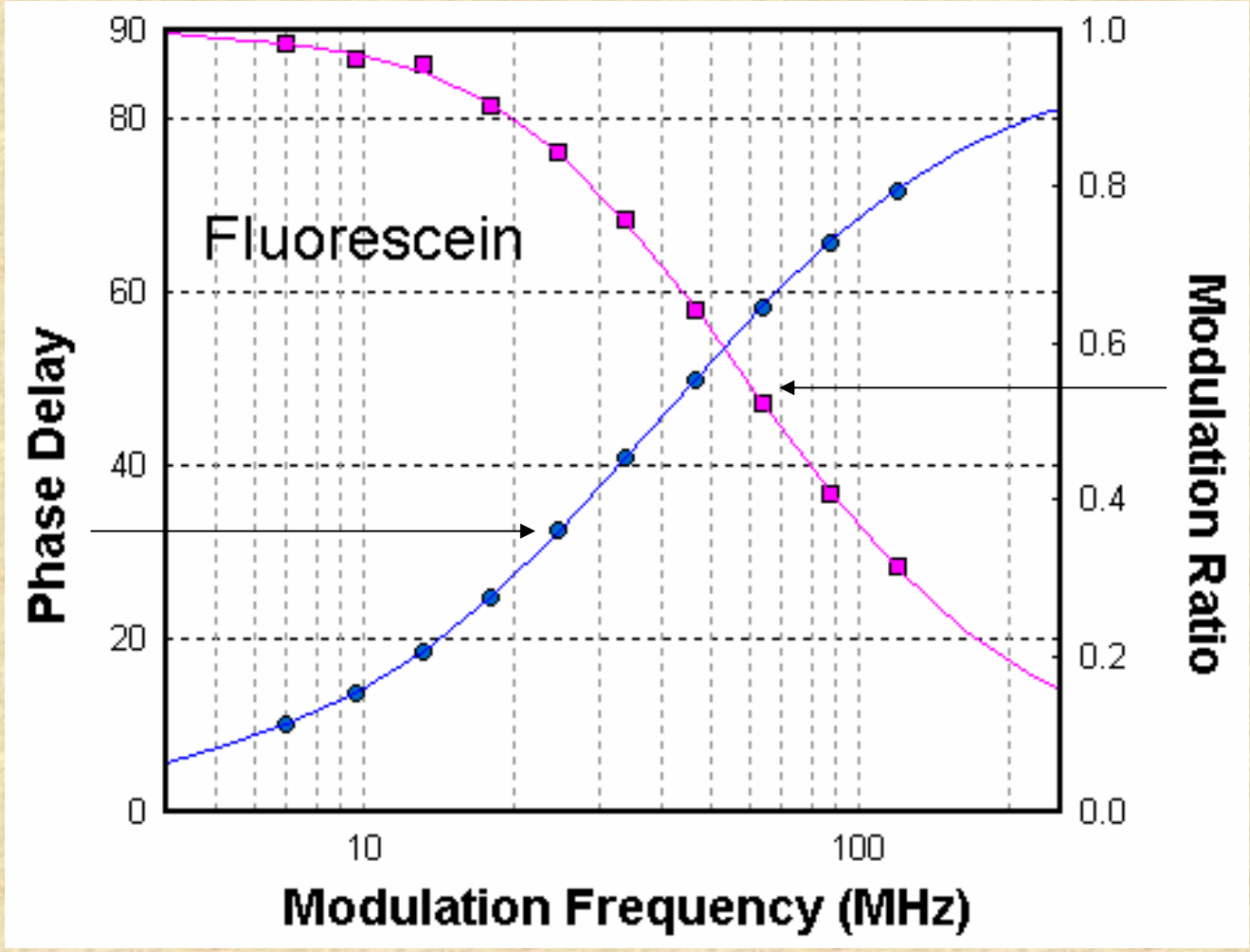

The plot shows the frequency response curve (phase and modulation) of Fluorescein in phosphate buffer pH 7.4 acquired on an ISS Chronos using a 470 nm LED. The emission was collected through a 530 high pass filter. The data is best fitted by a single exponential decay time of 4 ns.

In addition to decay analysis using discrete exponential decay models, one may also choose to fit the data to *distribution* models. In this case, it is assumed that the excited state decay characteristics of the emitting species actually results in a large number of lifetime components. Shown below is a typical lifetime distribution plot for the case of single tryptophan containing protein – human serum albumin.

The distribution shown here is Lorentzian but depending on the system different types of distributions, e.g., Gaussian or asymmetric distributions, may be utilized. This approach to lifetime analysis is described in: Alcala, J. R., E. Gratton and F. G. Prendergast. Fluorescence lifetime distributions in proteins. *Biophys. J. 51*, 597-604 (1987).

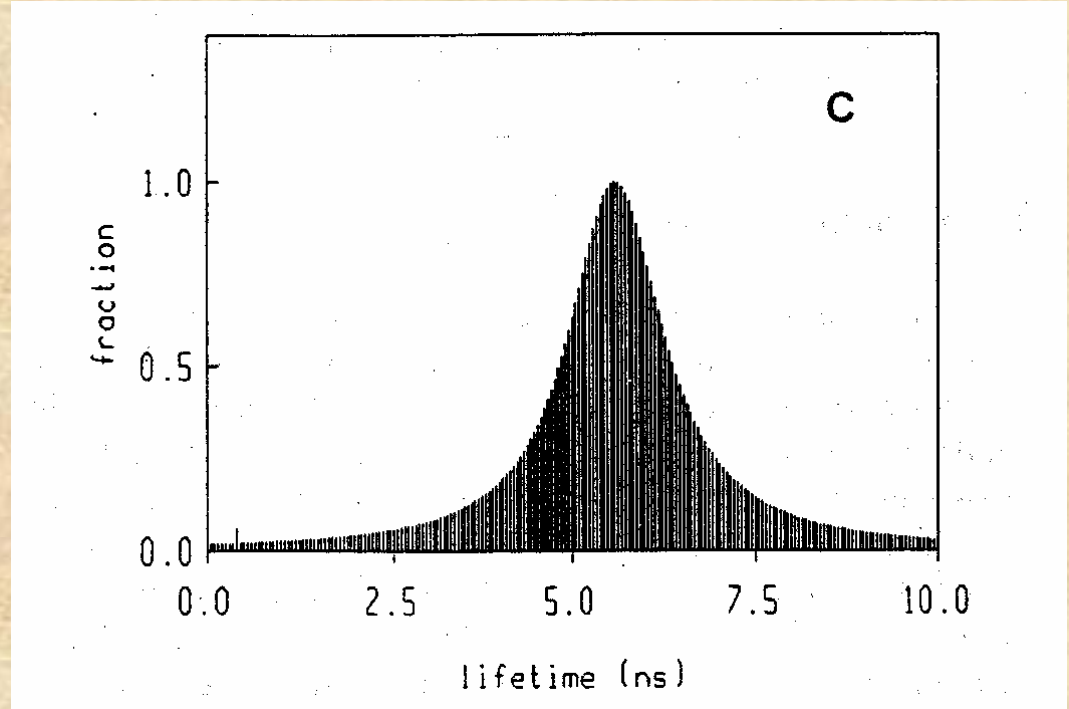

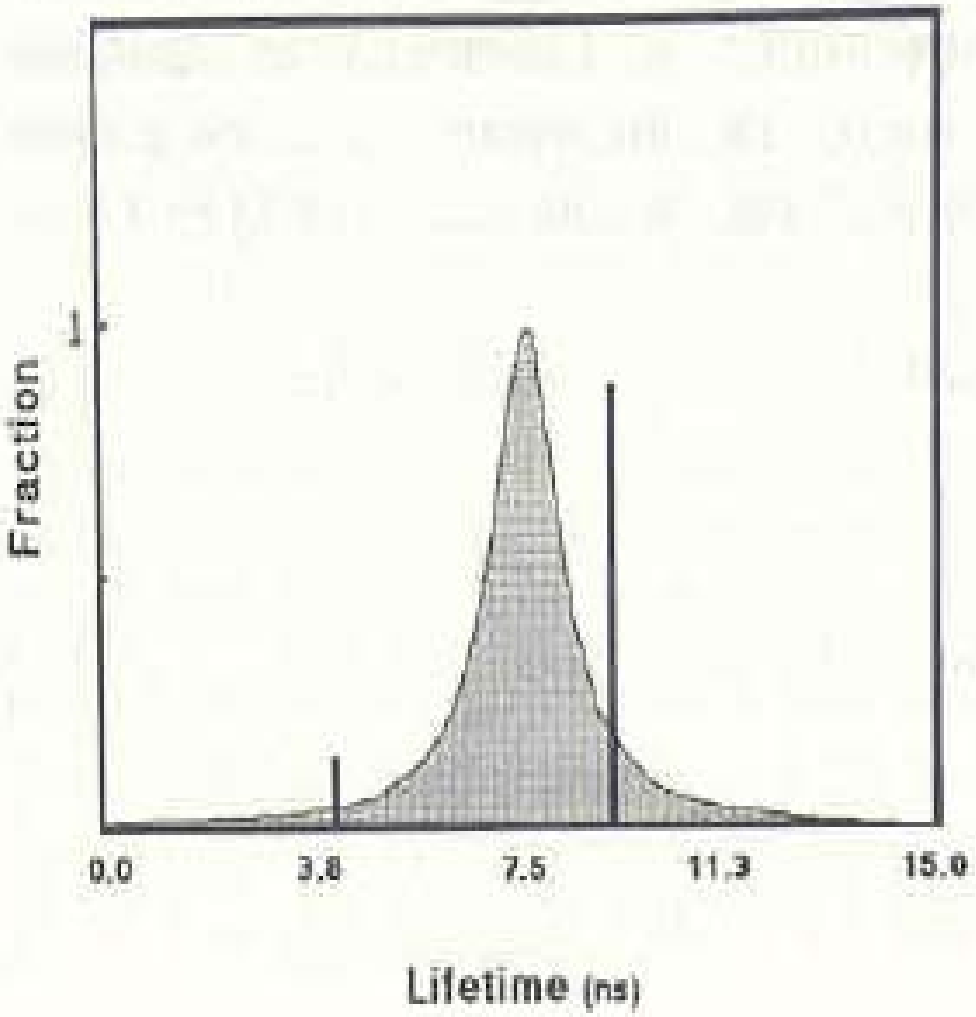

FIGURE 4. Continuous distribution (Lorentzian) lifetime analysis for methylanthraniloyl-GDP bound to the N-ras, P21 protein product (20°C). Calculated lifetime and full width at half-maximum were 7.7 and 1.1 nsec, respectively. The vertical dotted lines represent a two-component discrete lifetime fit to the same data: τ_1 = 8.5 nsec, 86% of the intensity, and τ_2 = 3.9 nsec. The χ^2 values were similar in both cases.

Another popular lifetime analysis method – based on Information Theory - is the *Maximum Entropy Method* (MEM). In this method no *a priori* intensity decay model is assumed.

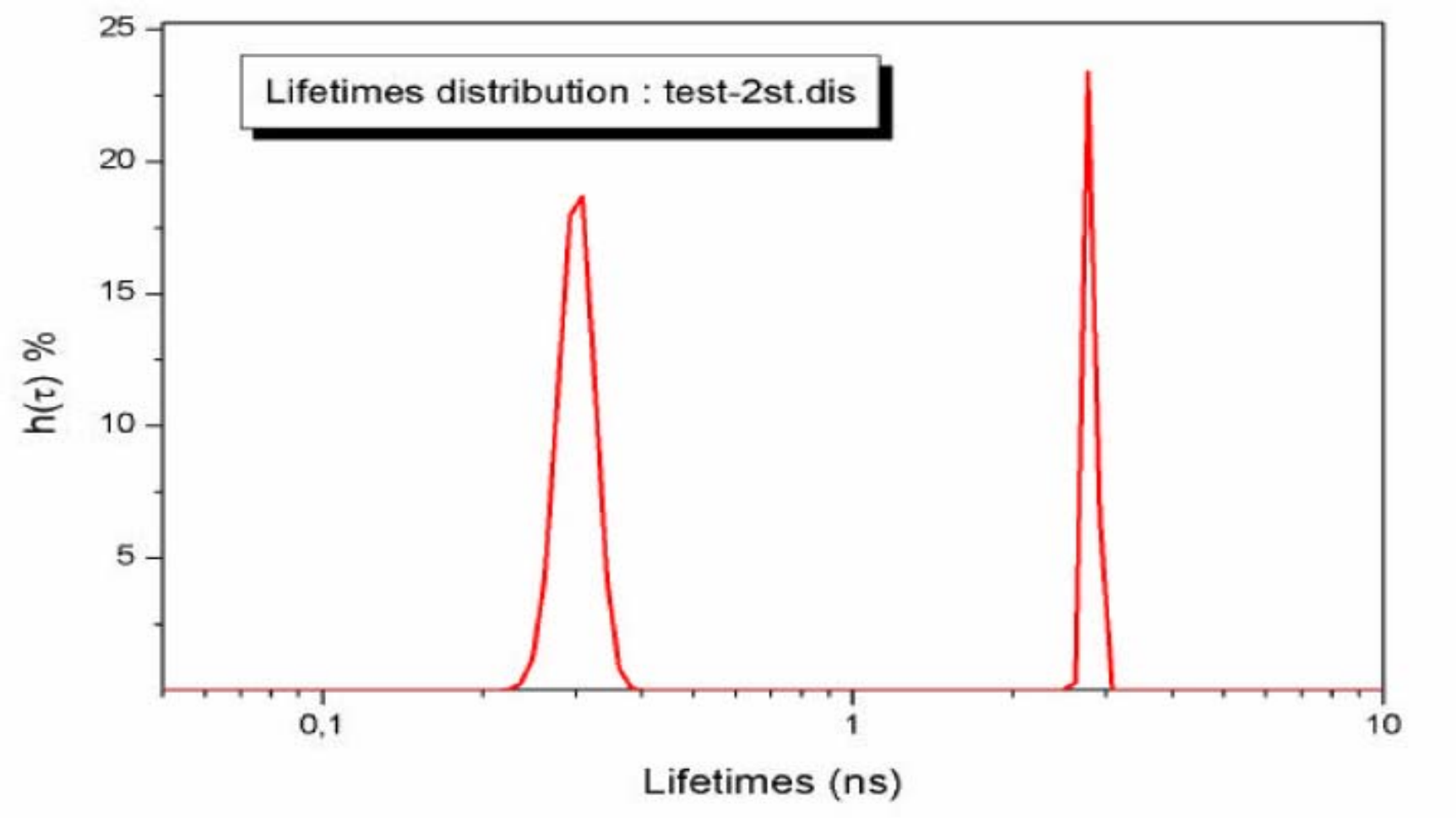

Jean-Claude Brochon
Maximum entropy method of data analysis in time-resolved spectroscopy.
Methods Enzymol. 1994;240:262-311.

Wavelength dependent lifetime data can be used to resolve individual spectra in a mixture

Gratton, E. and Jameson, D.M. (1985) *Anal. Chem. 57*:1694-1697. New Approach to Phase and Modulation Resolved Spectra.

Mixture: Lifetimes were 10.8ns, 4.3ns and 0.9ns

Spectra of individual components

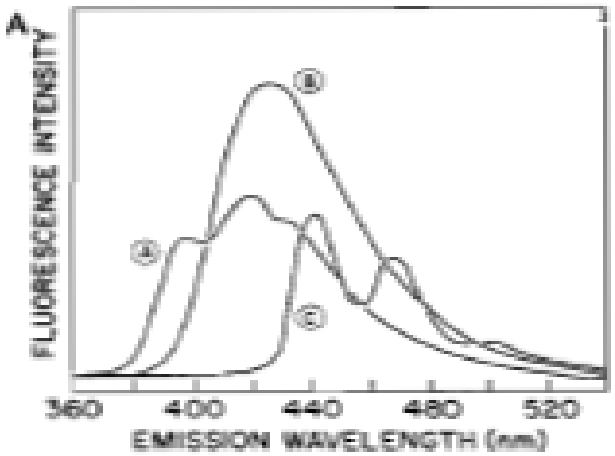

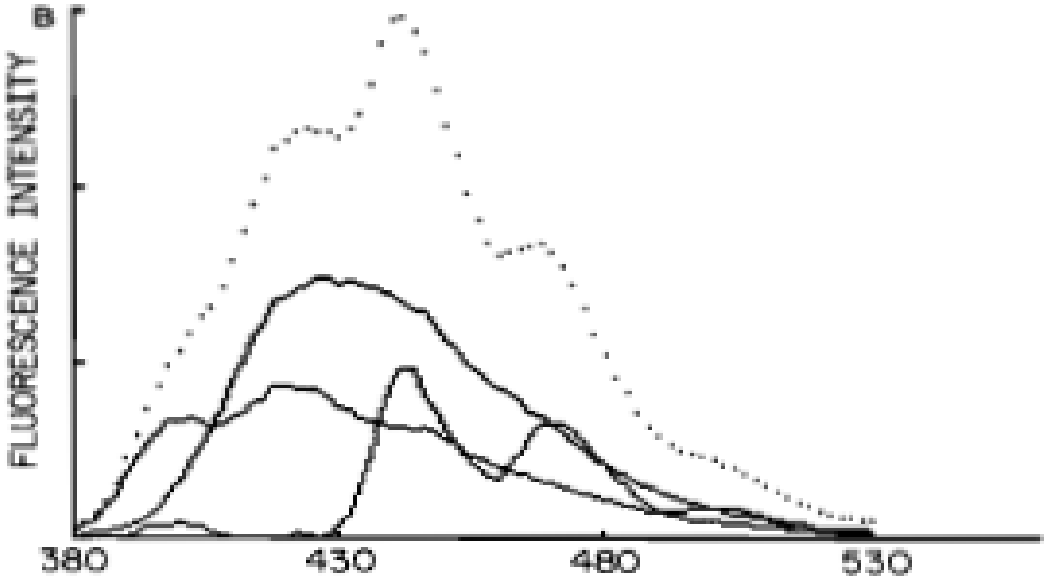

Figure 3. (A) Intensity spectra of individual components, POPOP (A), DENS (B), and perylene (C) in ethanol (not degassed). (B) Intensity (dotted line) and phase resolved spectra (solid lines) for the ternary mixture in A.

Global Analysis

In Global Analysis one can link decay parameters across many data sets which often allows for a more robust analysis

Example of the application of Global Analysis

Binding of Ethidium-Bromide to Transfer RNA

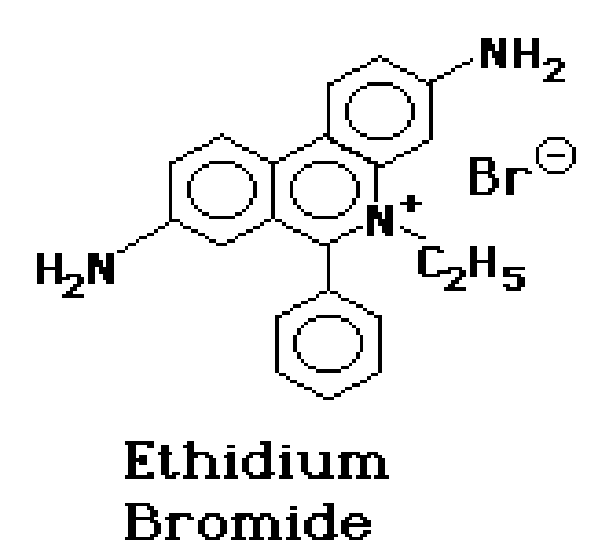

Ethidium Bromide

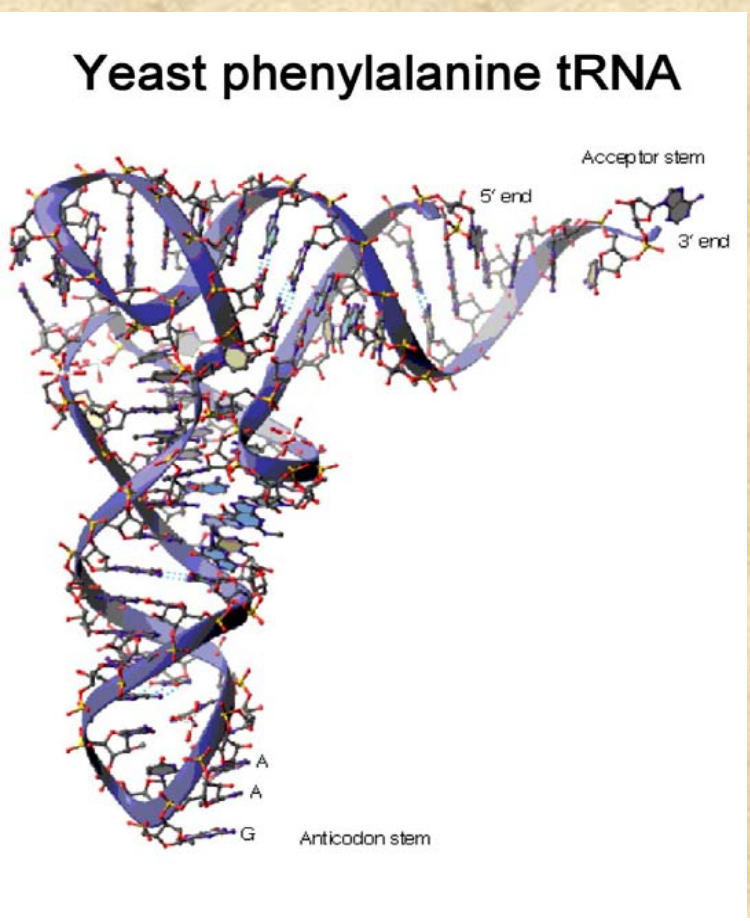

Ethidium bromide can intercalate into nucleic acid structures
It binds well to both DNA and RNA

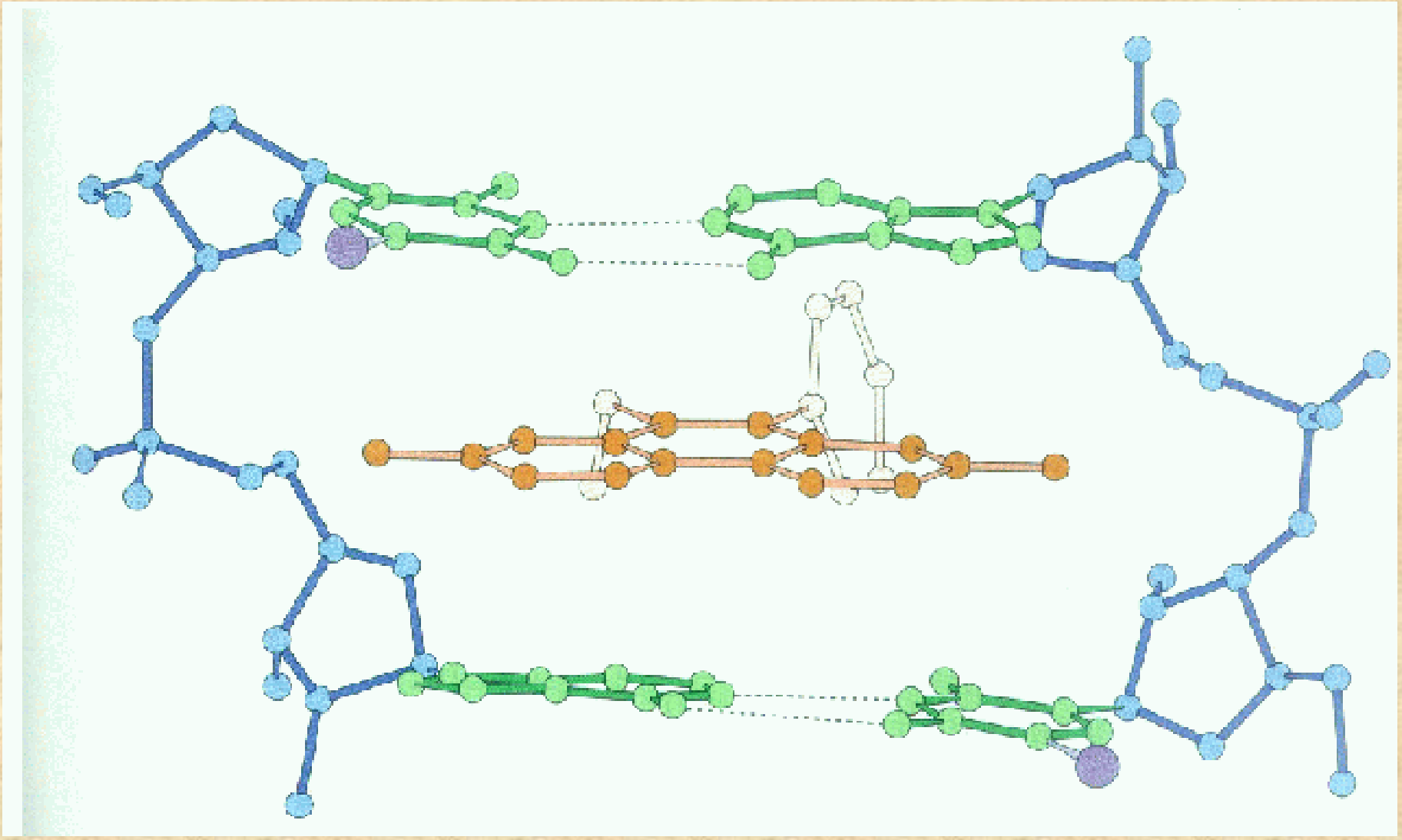

Fluorescence investigations of EB - tRNA interactions, carried out for more than 30 years, have indicated a “strong” binding site and one or more “weak, non-specific” binding sites.

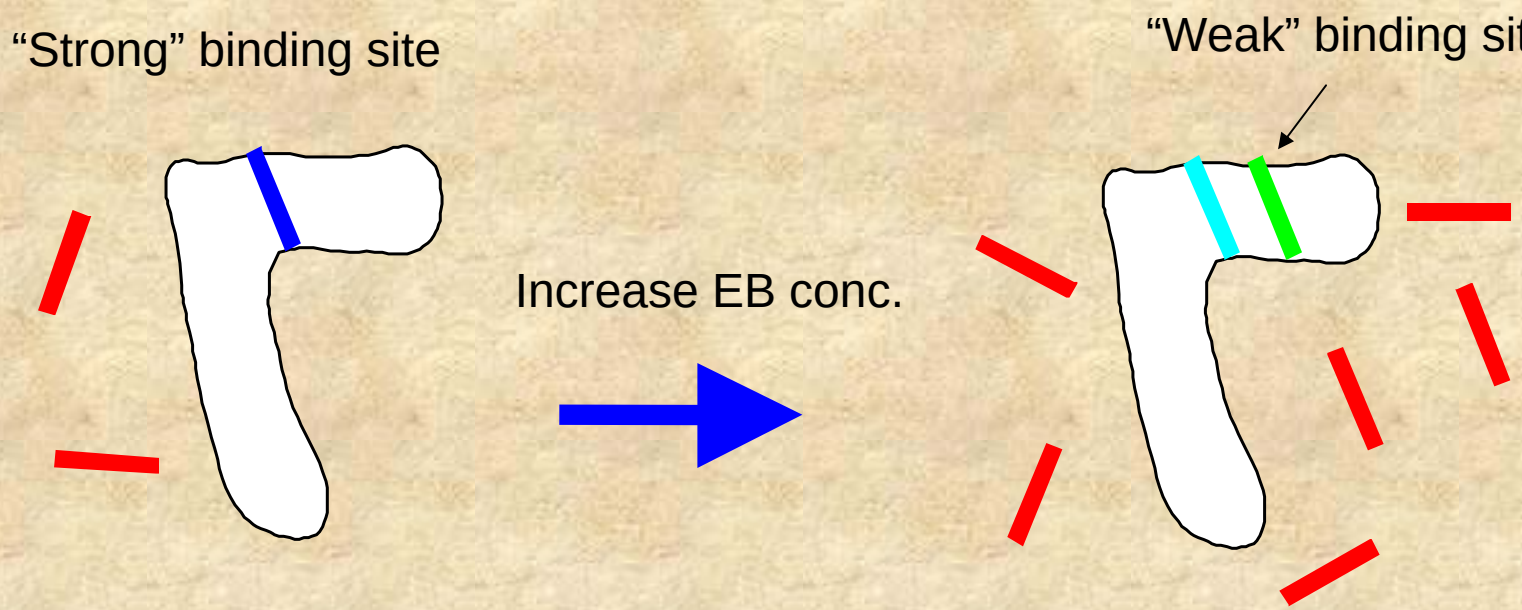

Question: What are the lifetimes of the strong and the weak binding sites???

If the tRNA is in excess only one EB will bind to the “strong” binding site which has a K_d of around 1 micromolar (under these conditions a single exponential decay of 27ns is observed). If the EB/tRNA ratio is increased, one or more additional EB’s will bind and the question is: What are the lifetimes of EB bound to different sites on tRNA?” Shown below are phase and modulation data for a solution containing 124 μM yeast $tRNA^{phe}$ and 480 μM EB

The phase and modulation data were first fit to a single exponential component shown as the solid lines in the top plot. The residuals for this fit are shown in the bottom plot.

In this case τ = 18.49 ns and the χ^2 value was 250.

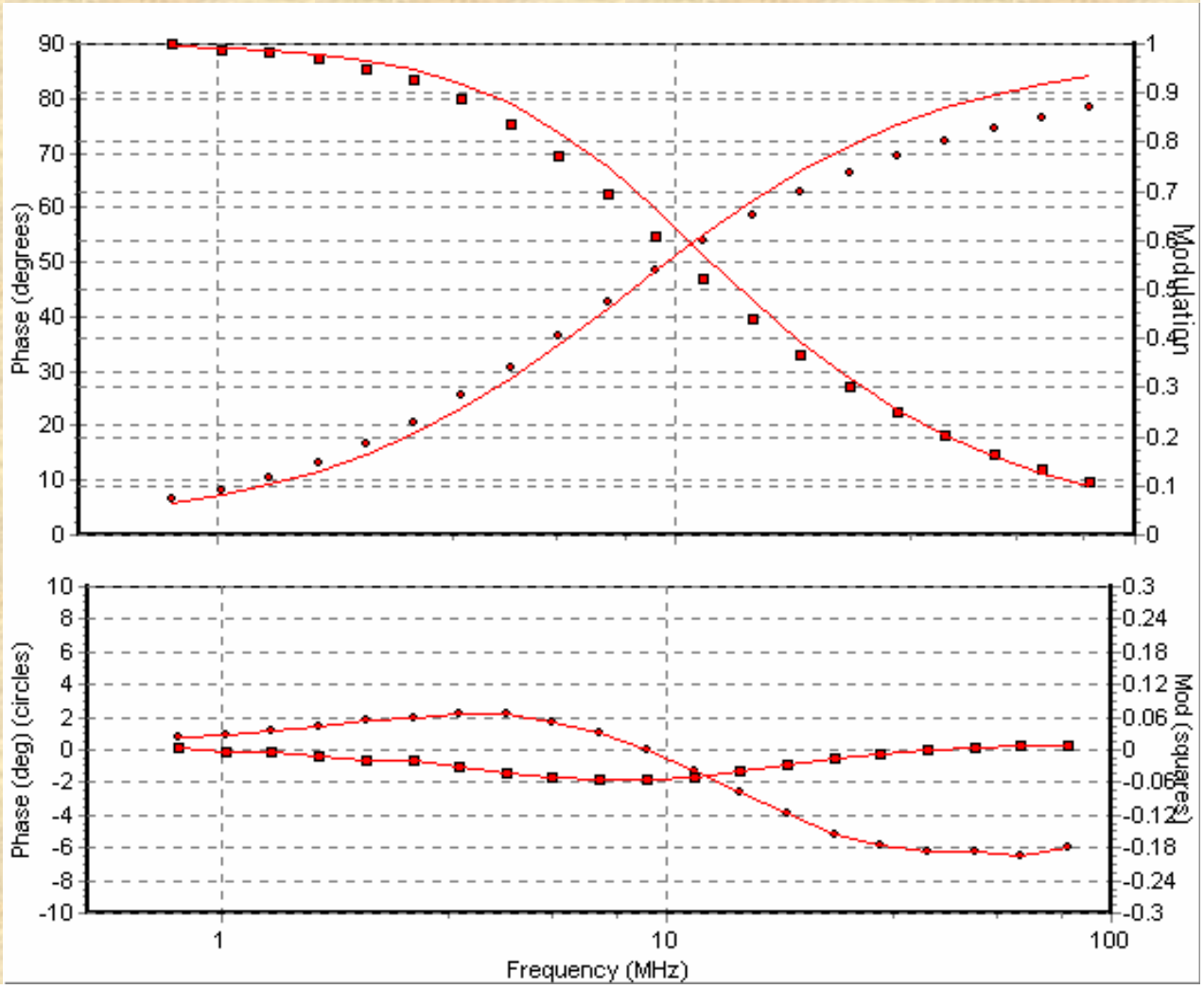

The data were then fit to a 2-component model shown here In this case the two lifetime components were 22.71 ns with a fractional intensity of 0.911 and 3.99 ns with a fractional intensity of 0.089.

The χ^2 for this fit was 3.06 (note the change in scale for the residual plot compared to the first case shown).

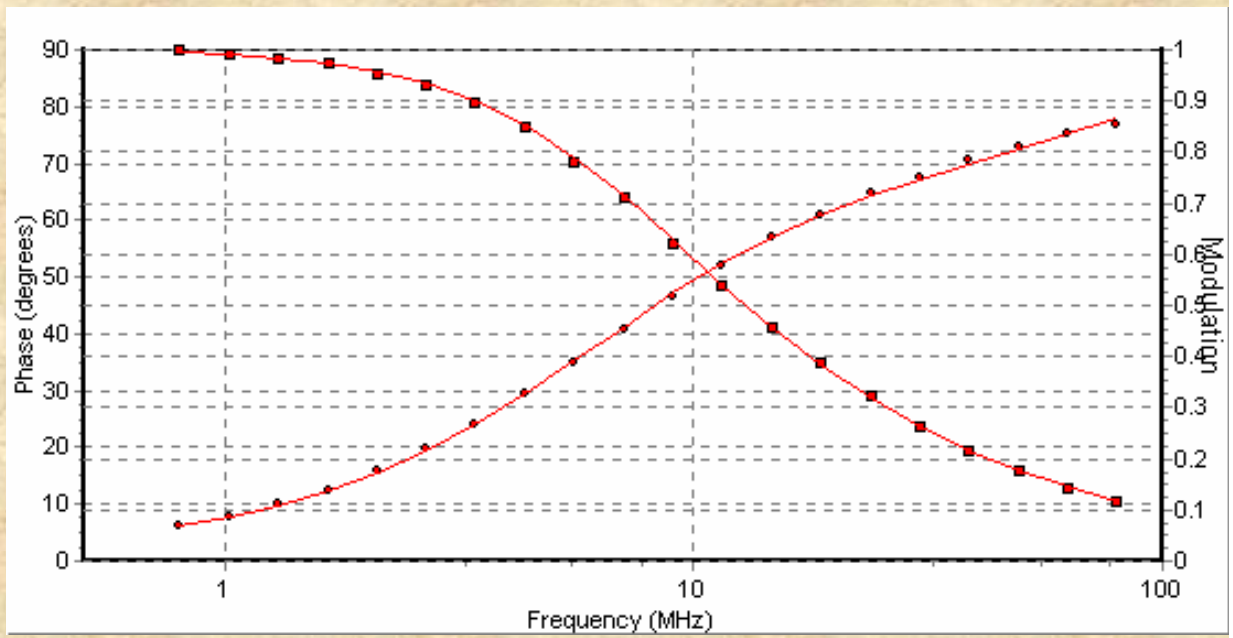

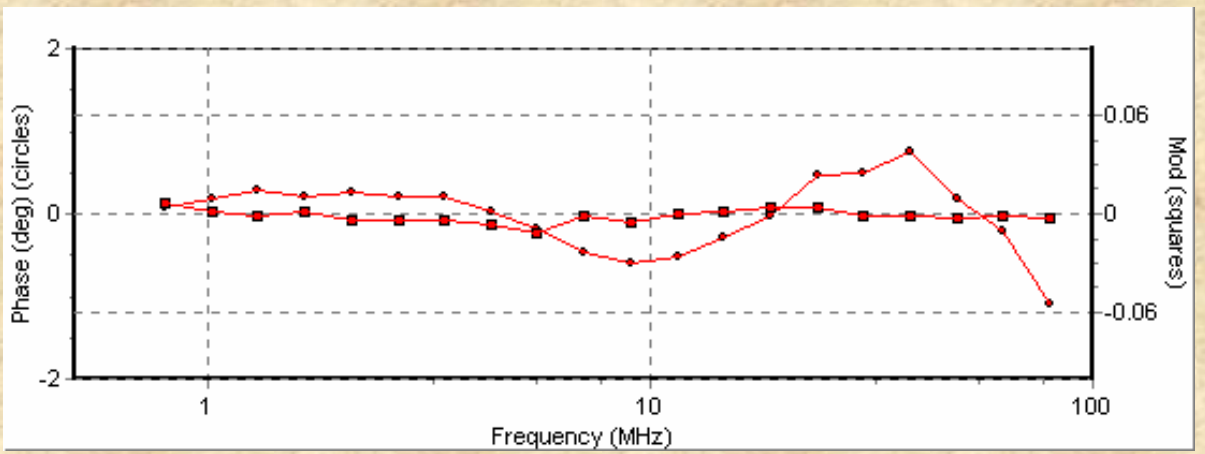

A 3-component model improves the fit still more. In this case

τ_1 = 24.25 ns, f_1 = 0.83

τ_2 = 8.79 ns, f_2 = 0.14

τ_3 = 2.09 ns, f_3 = 0.03

χ^2 = 0.39.

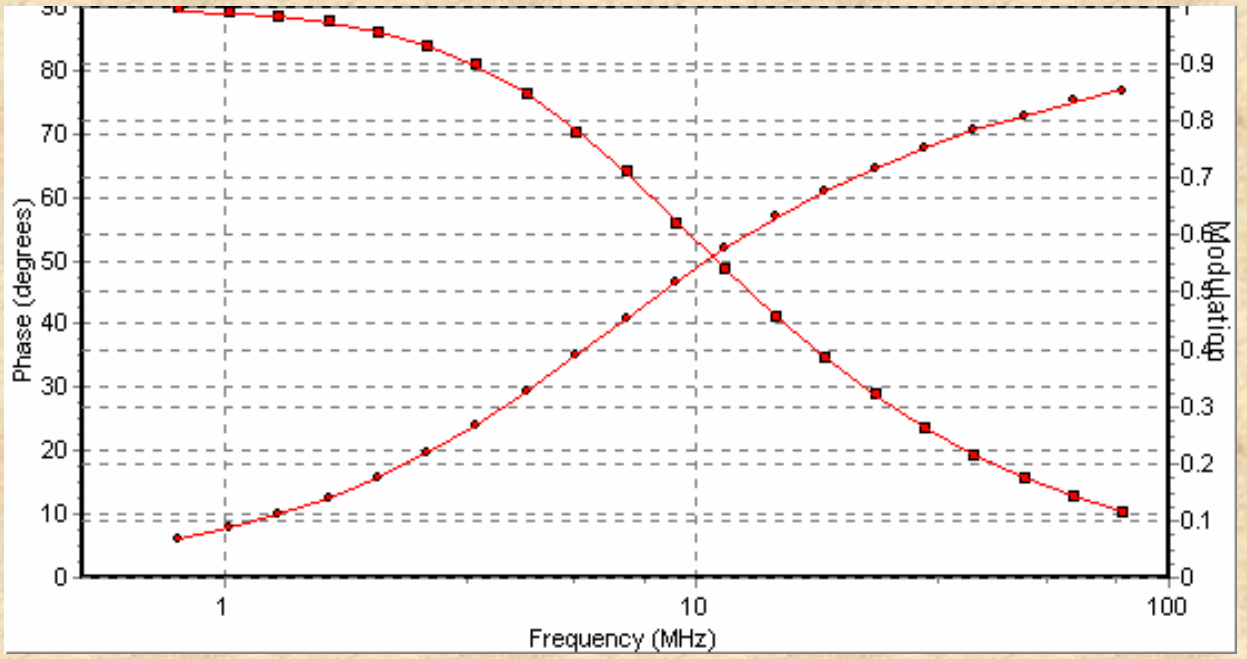

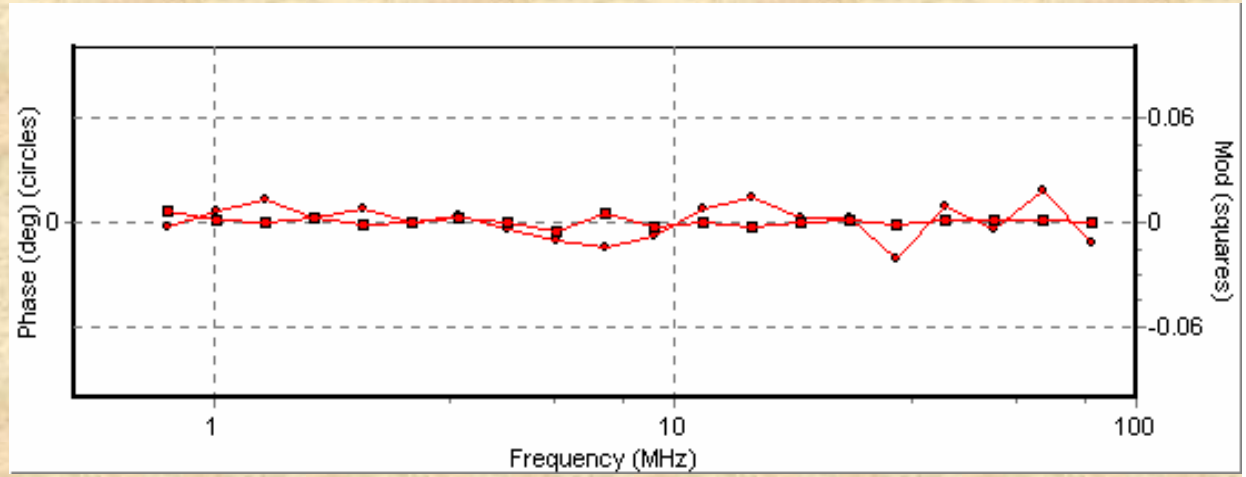

Adding a fourth component – with all parameters free to vary - does not lead to a significant improvement in the χ^2. In this case one finds 4 components of 24.80 ns (0.776), 12.13ns (0.163), 4.17 ns (0.53) and 0.88 ns (0.008).

But we are not using all of our information! We can actually fix some of the components in this case. We know that **free EB** has a lifetime of **1.84 ns** and we also know that the lifetime of **EB bound to the "strong" tRNA binding site** is **27 ns**. So we can fix these in the analysis. The results are four lifetime components of 27 ns (0.612), 18.33 ns (0.311), 5.85 ns (0.061) and 1.84 ns (0.016). The χ^2 improves to 0.16.

We can then go one step better and carry out **"Global Analysis"**.
In Global Analysis, multiple data sets are analyzed simultaneously and different parameters (such as lifetimes) can be "linked" across the data sets. The important concept in this particular experiment is that the lifetimes of the components stay the same and only their fractional contributions change as more ethidioum bromide binds.

In this system, 8 data sets, with increasing EB/tRNA ratios, were analyzed. Some of the data are shown below for EB/tRNA ratios of 0.27 (circles), 1.34 (squares), 2.41 (triangles) and 4.05 (inverted triangles).

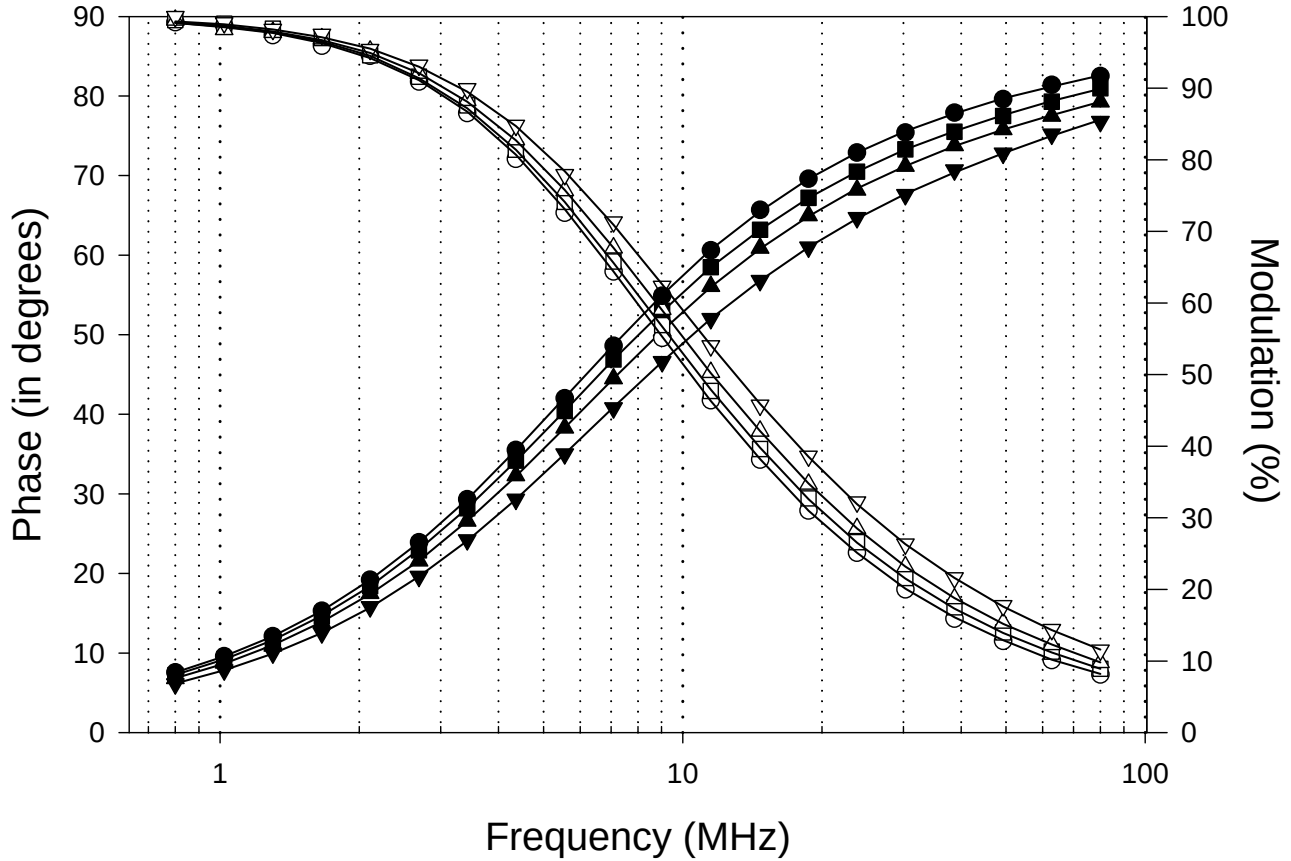

Global Analysis on seven data sets fit best to the 4 component model with two fixed components of 27ns and 1.84ns and two other components of 17.7ns and 5.4ns.

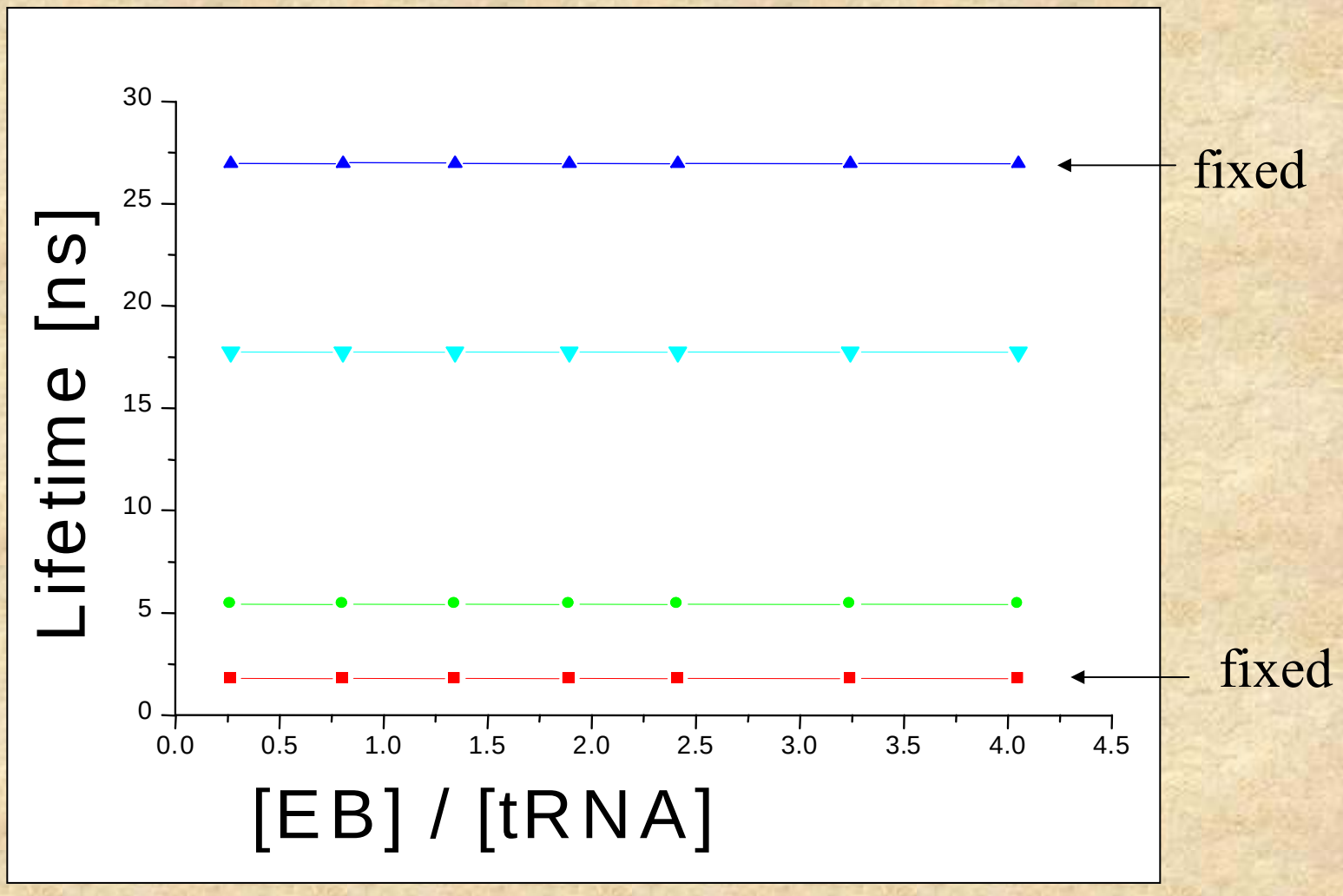

As shown in the plot below, as the EB/tRNA ratio increases the fractional contribution of the 27ns component decreases while the fractional contributions of the 17.7ns and 5.4ns components increase.

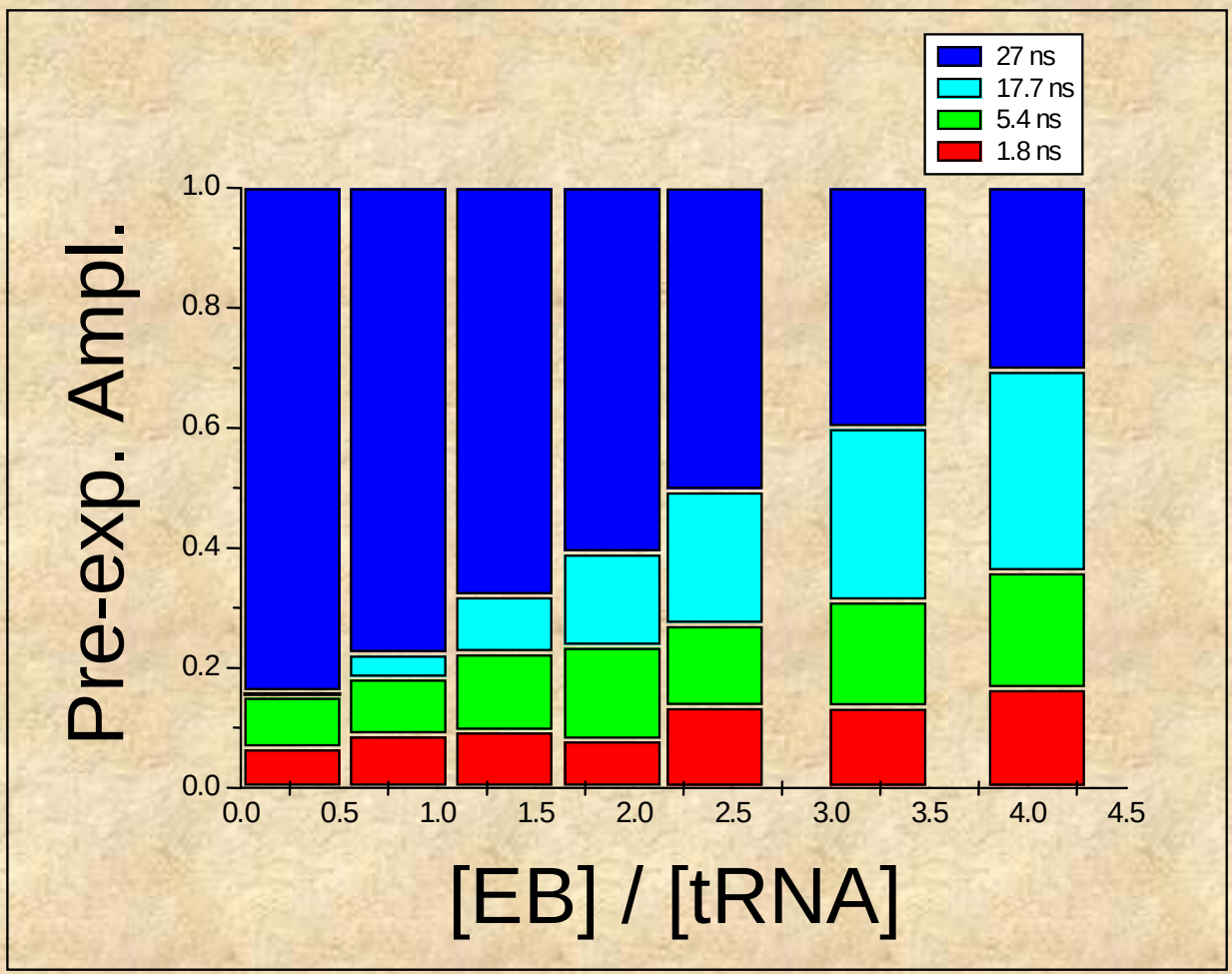

The Model

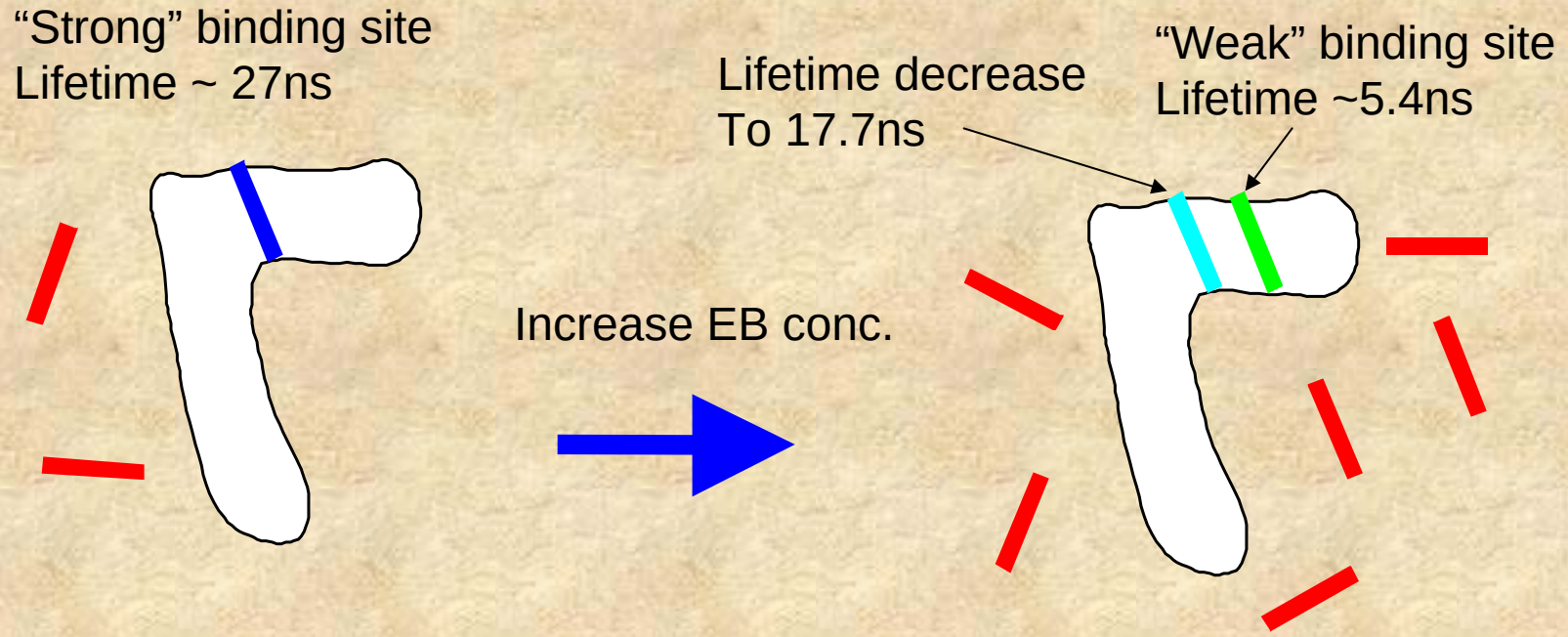

Question:
Is the drop in the lifetime of the "strong" binding site due to a change in tRNA conformation or energy transfer???

Answer: ???

Later in this workshop you'll learn about Fluorescence Lifetime Imaging or FLIM

In FLIM, lifetime data are obtained through a microscope - lifetime data is acquired at each pixel in the image

Lifetime data is more robust than intensity since it does not depend on how many fluorescent molecules are present

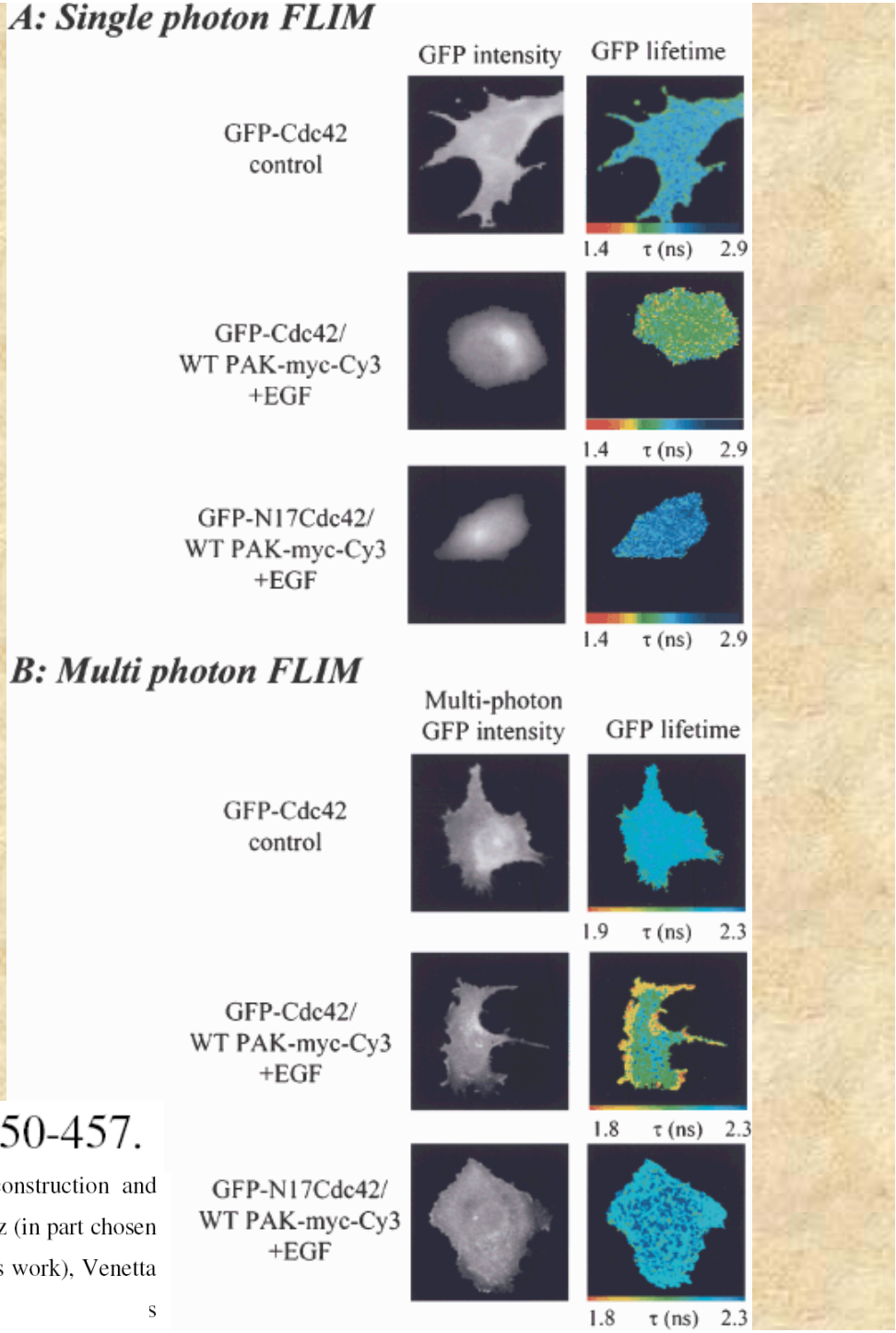

B. D. Venetta, *Rev. Sci. Instrum.*, 1959, **30**, 450-457.

In 1959 Venetta[4] described the construction and operation of a phase fluorometer coupled to a microscope. Using a frequency of 5.8 MHz (in part chosen due to the availability of FM transformers in televisions which could be salvaged for this work), Venetta was able to measure a lifetime of 2.7 ns for proflavin bound to the nuclei of tumor cells. s

Time-Resolved Anisotropy and Excited State Reactions

Many of these slides were prepared by Theodore Hazlett

Time-resolved methodologies provide information on the changes of orientation as a function of time of a system. The time-domain approach is usually termed the **anisotropy decay** method while the frequency-domain approach is known as **dynamic polarization**. In principle both methods yield the same information.

In the time-domain anisotropy method the sample is illuminated by a pulse of vertically polarized light and the decay over time of both the vertical and horizontal components of the emission are recorded. The anisotropy function is then plotted versus time as illustrated here:

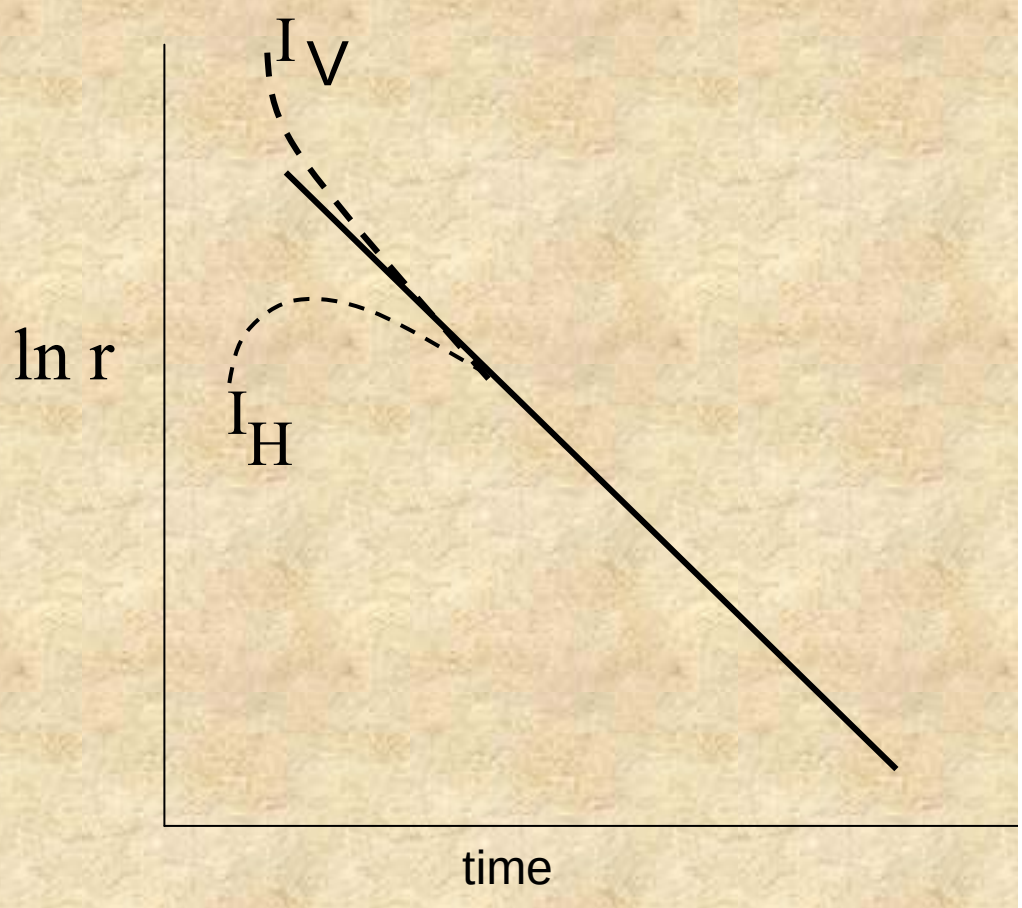

Note that the horizontal component actually increases during short times, since initially the fluorophores have not rotated significantly. As time passes though the number of horizontally oriented molecules increases

Simplest Case: Spherical Body

Fully Symmetrical

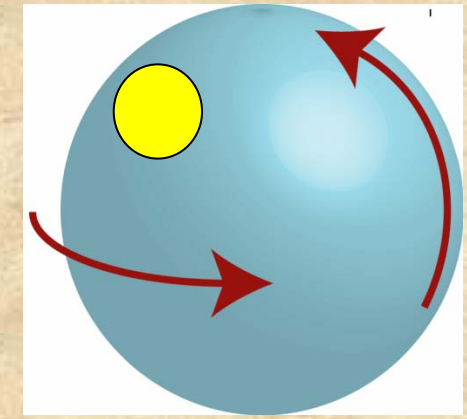

(in this case we assume that the fluorophore has no local mobility – such is the case for non-covalent interactions)

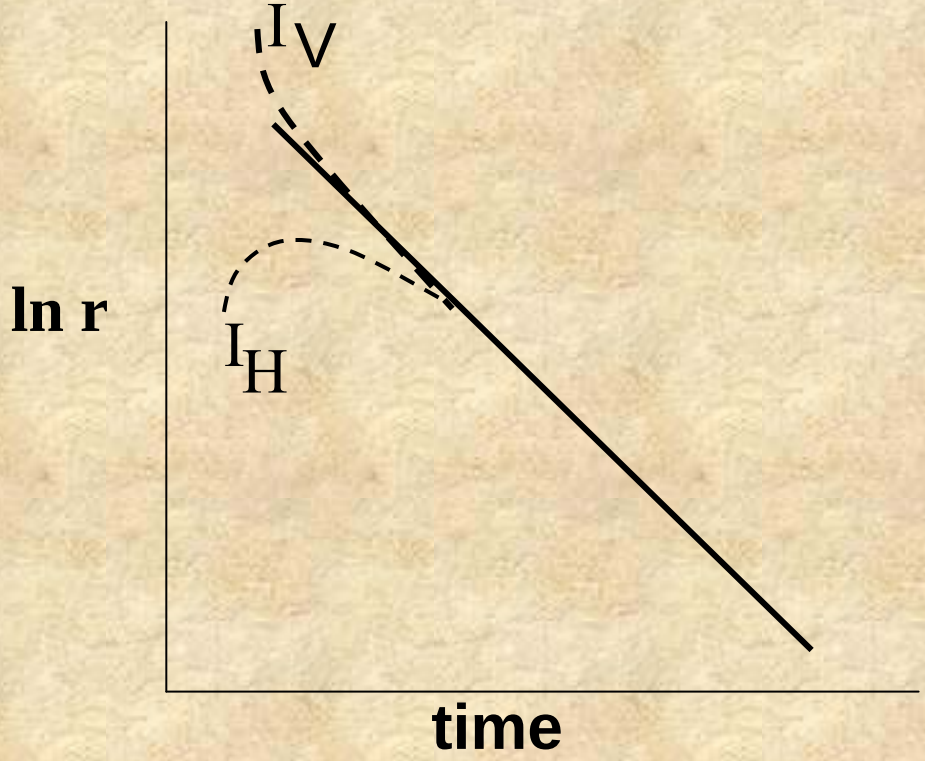

The decay of the anisotropy with time, r(t), for a sphere is given by:

$$r = \frac{Iv - Ih}{Iv + 2Ih} = r_o e^{-\left(t/\tau_c\right)}$$

τ_c is the rotational correlation time

$$\tau_c = \frac{1}{6 \cdot D_{rotation}}$$

In the case of non-spherical particles the time-decay of anisotropy function is more complicated. Mathematically simple symmetrical ellipsoids give us a sense of how changes in Shape affect the rotational diffusion rates.

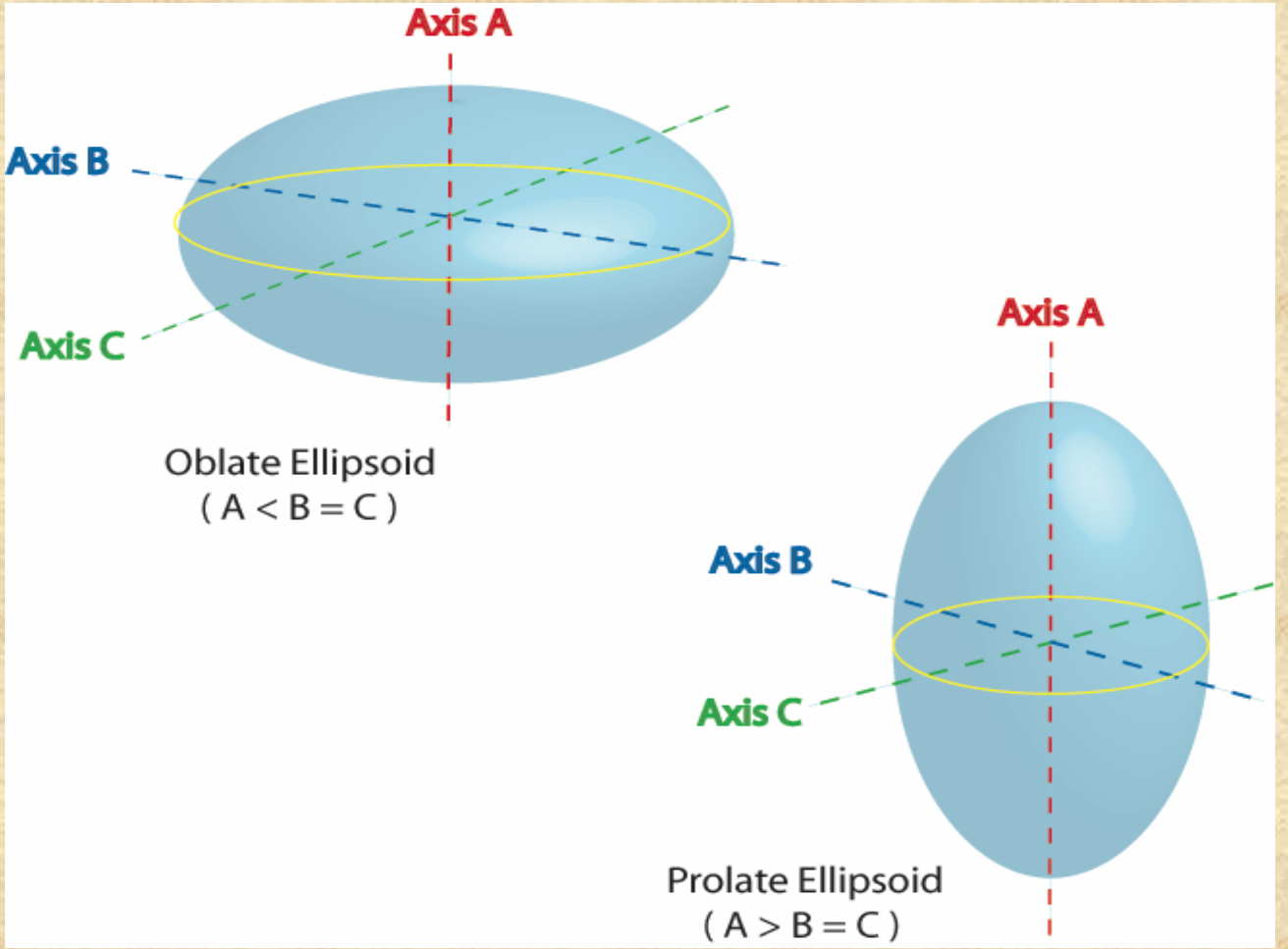

Effect of Shape on Diffusion

Translational Diffusion

20:1 Prolate

20:1 Oblate

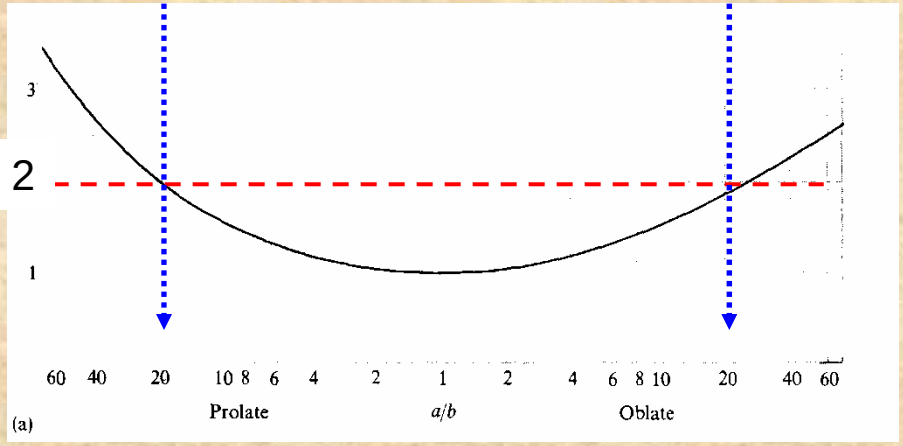

Rotational Diffusion

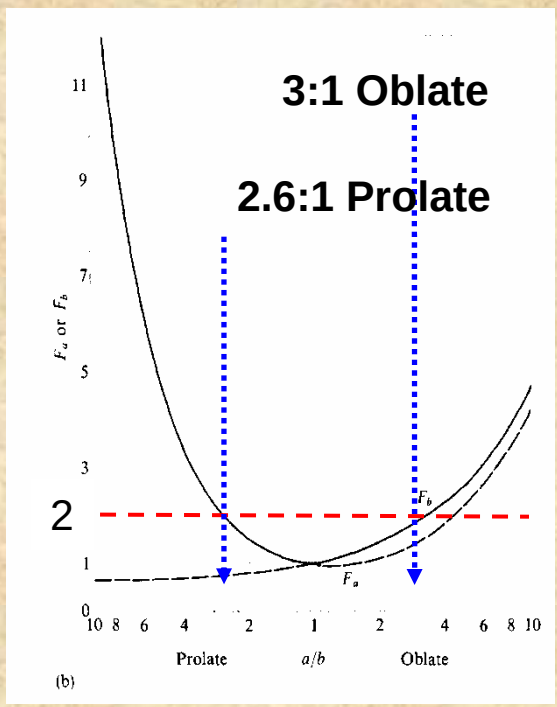

Rotational Diffusion is much more influenced by macromolecular shape than is Translational diffusion

How are these Shapes Modeled?

In the case of symmetrical ellipsoids of revolution the relevant expression is:

$$r(t) = r_1 e^{\left(\frac{-t}{\tau_{c1}}\right)} + r_2 e^{\left(\frac{-t}{\tau_{c2}}\right)} + r_3 e^{\left(\frac{-t}{\tau_{c3}}\right)}$$

where: $\tau_{c1} = 1/6D_2$

$\tau_{c2} = 1/(5D_2 + D_1)$

$\tau_{c3} = 1/(2D_2 + 4D_1)$

D_1 and D_2 are the rotational diffusion coefficients about the axes of symmetry and about either equatorial axis, respectively.

Resolution of the rotational rates is limited in practice to two rotational correlation times which differ by at least a factor of two.

What do the Anisotropy Amplitudes (r1, r2, & r3) Represent?

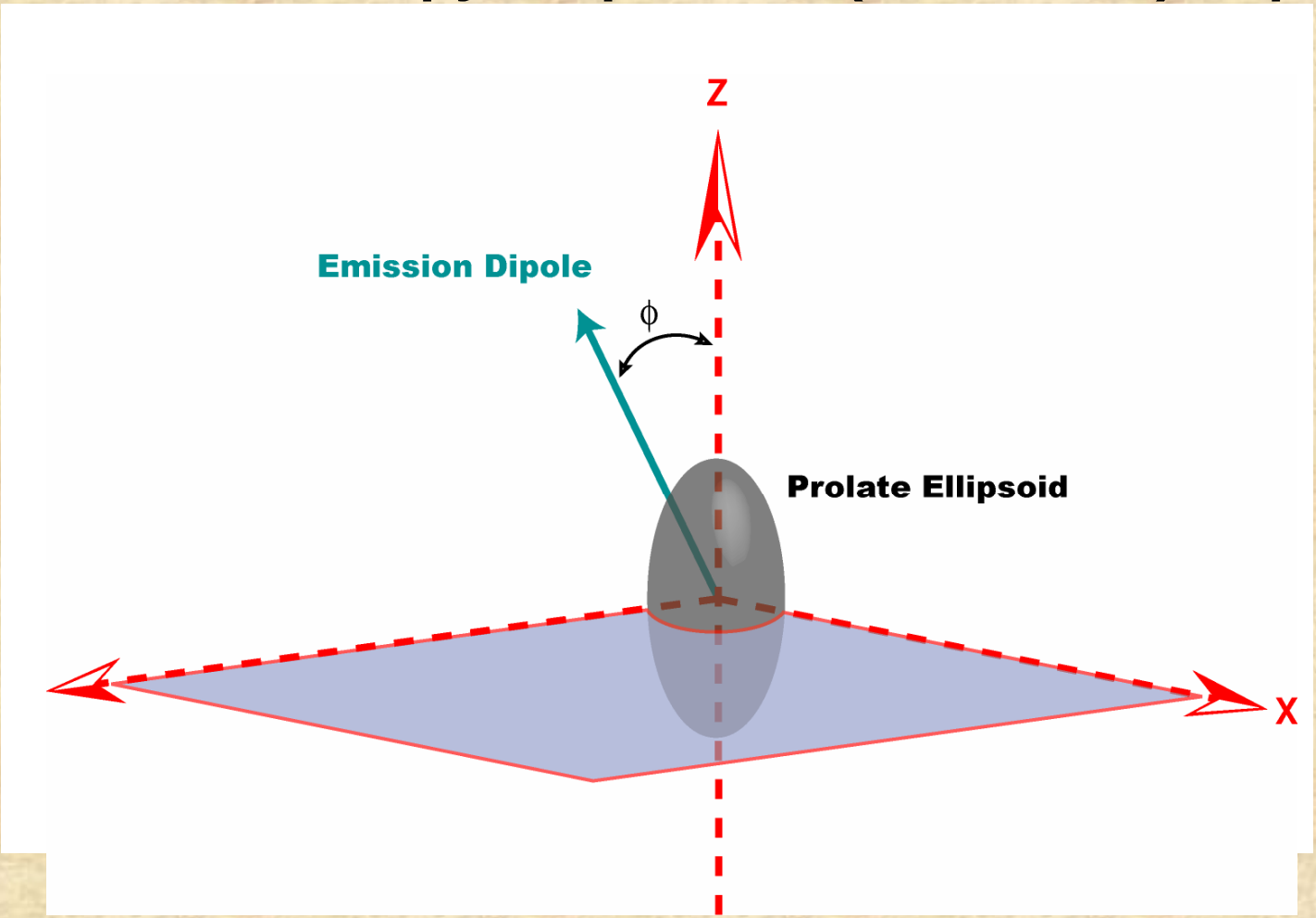

The amplitudes relate to orientation of the probe with respect to the axis of symmetry for the ellipsoid *(we are assuming colinear excitation and emission dipoles)*.

$$r_1 = 0.1(3\cos^2\phi - 1)^2$$
$$r_2 = 0.3\sin^2(2\phi)$$
$$r_3 = 0.3\sin^4(\phi)$$

Multiple Rotating Species (mixtures)

$$r(t) = r_1 e^{\left(\frac{-t}{\tau_{c1}}\right)} + r_2 e^{\left(\frac{-t}{\tau_{c2}}\right)}$$

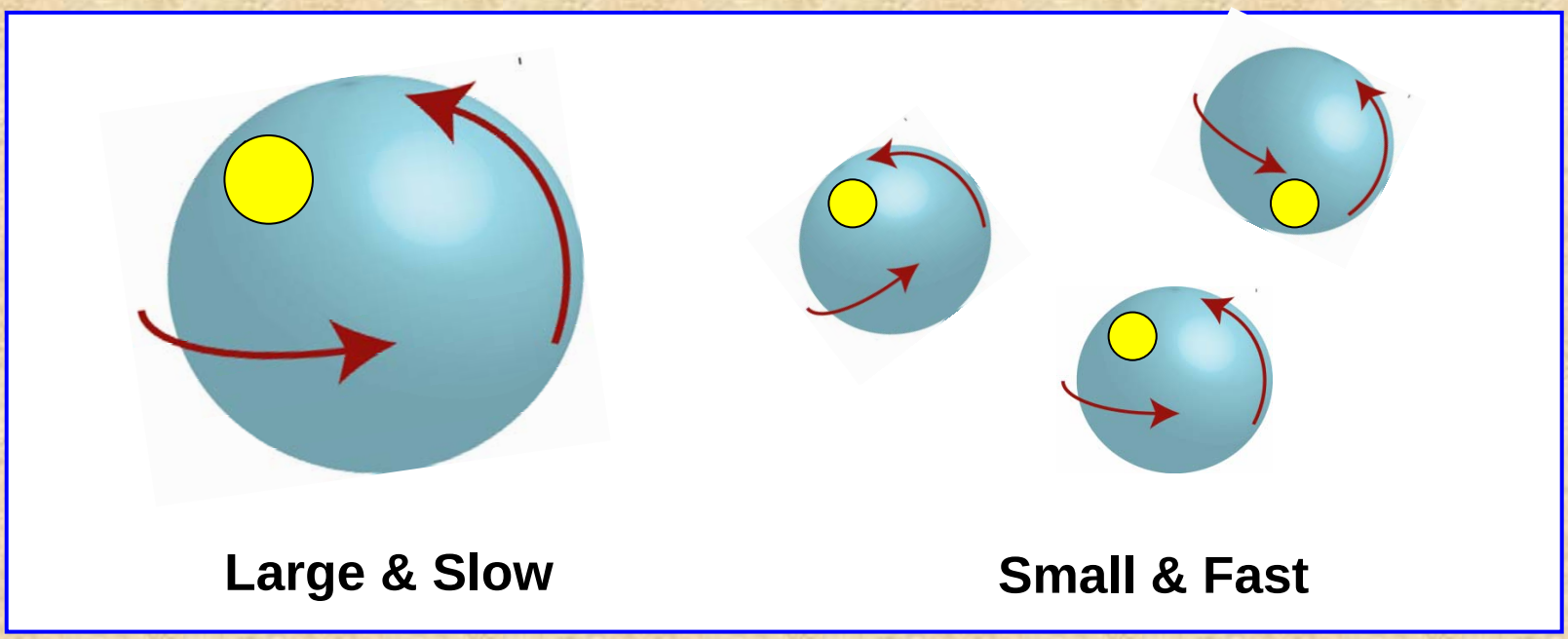

Mixed systems Show
Simple, Multi-Exponential Behavior

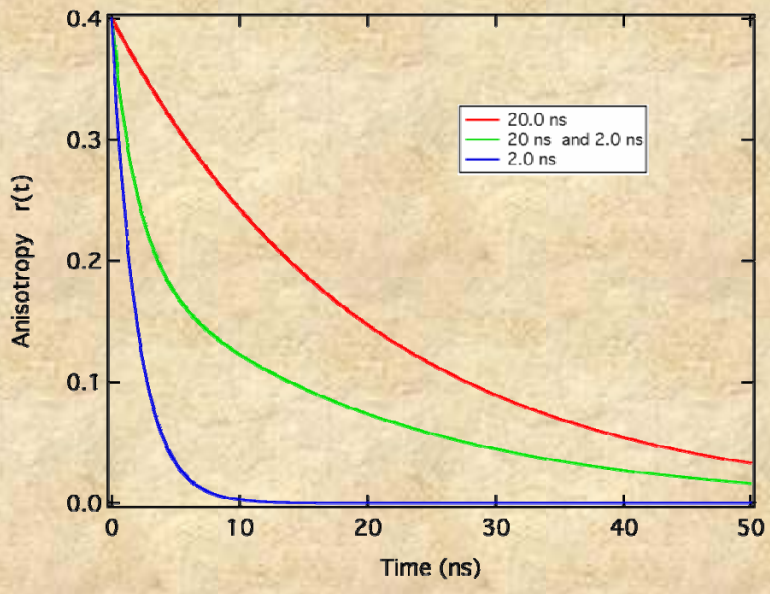

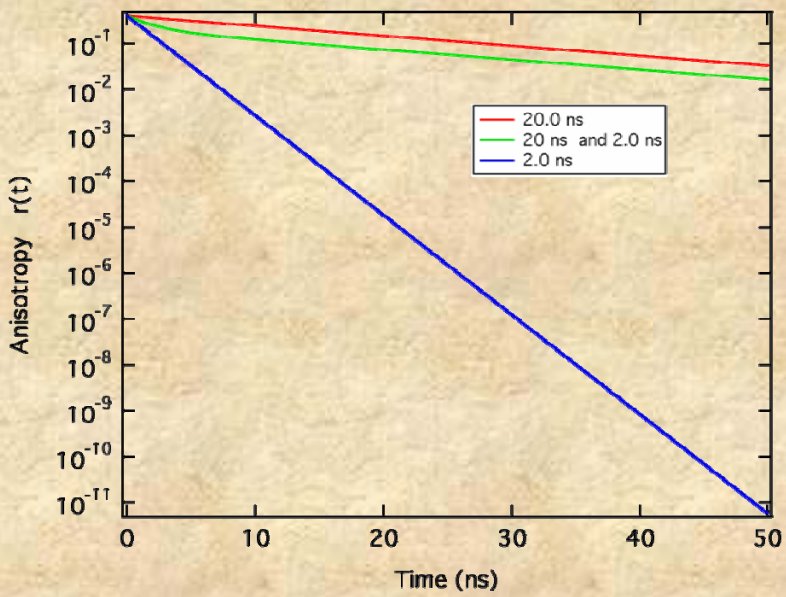

With separate species the decays reflect the sum of the exponential components present.

Multiple Rotational Modes:
Local relaxation + Global rotation

Is the case of a **“local”** rotation of a probe attached to a spherical particle any different than multiple species?

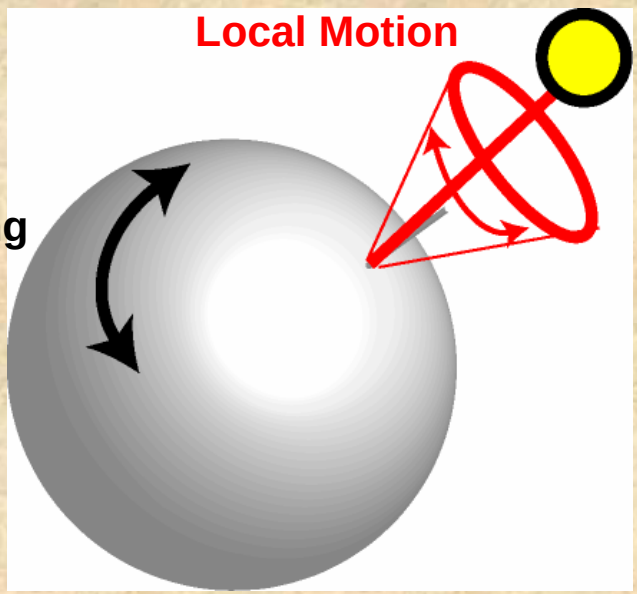

This common system represents a condition containing a hindered motion.

The expression for this case is:

$$r(t) = r_1 \cdot e^{-(t/\tau_{c1})} + r_2 \cdot e^{-\left(t/\tau_{c1} + t/\tau_{c2}\right)}$$

Where τ_{c1} represents the "Global" probe motion, τ_{c2} represents the "Local" rotation of the macromolecule.

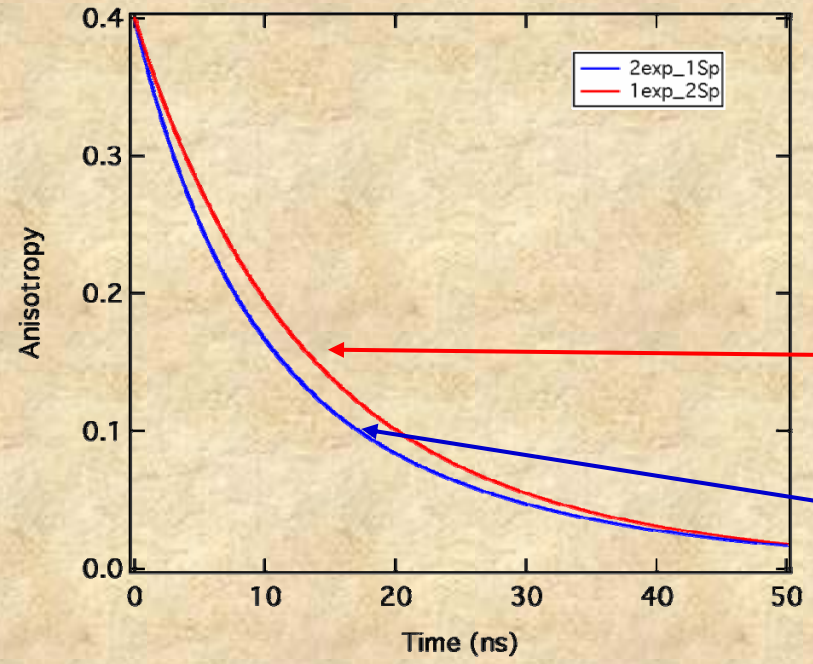

Equal pre-exponentials terms containing two rotational components of 20 ns and 10 ns

The "Mixed" case

The "Local & Global" case

Hindered Rotational Systems
Membrane Bilayers

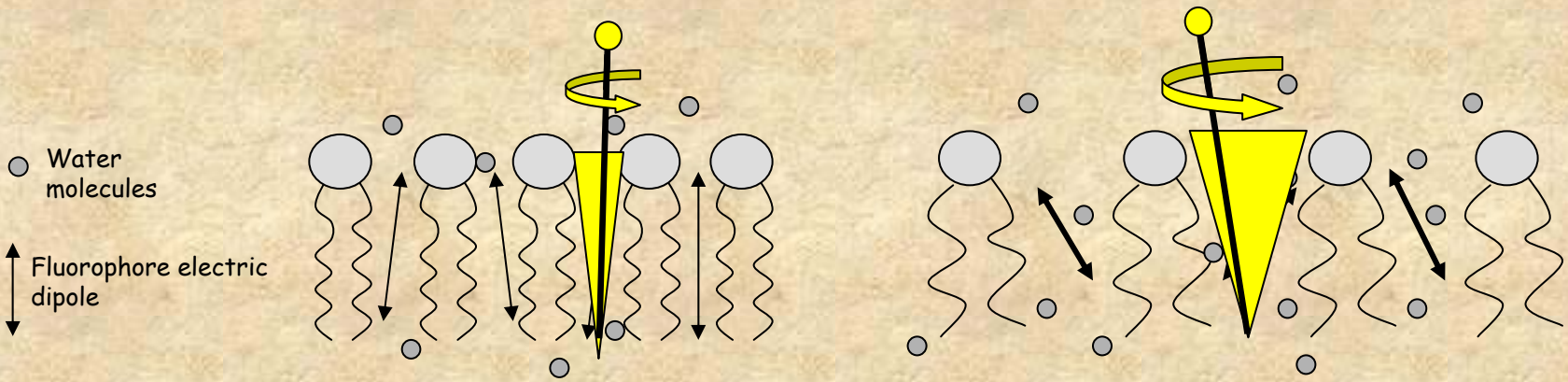

Wobble-in-a-Cone Concept

1) **Freedom of motion**
2) **The rate of motion**

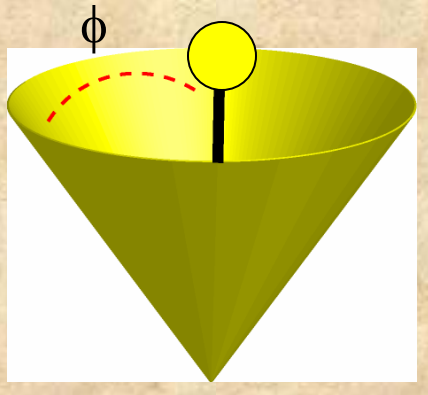

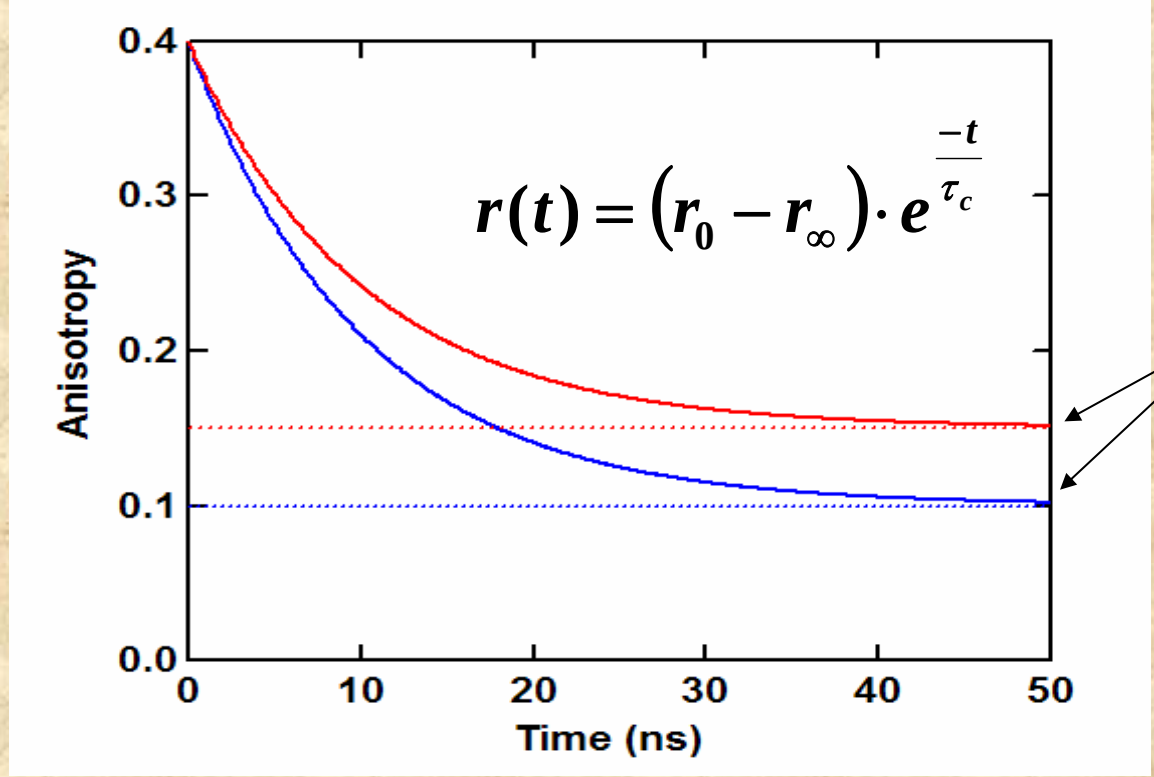

$$\frac{r_0}{r_\infty} = \left\langle \frac{3 \cdot \cos^2(\phi) - 1}{2} \right\rangle^2$$

Motion

τ_c = 20 ns

Angular Freedom

ϕ= 52 degrees

ϕ= 44 degrees

Analysis of Fluorophore Rotation in an Artificial Bilayer

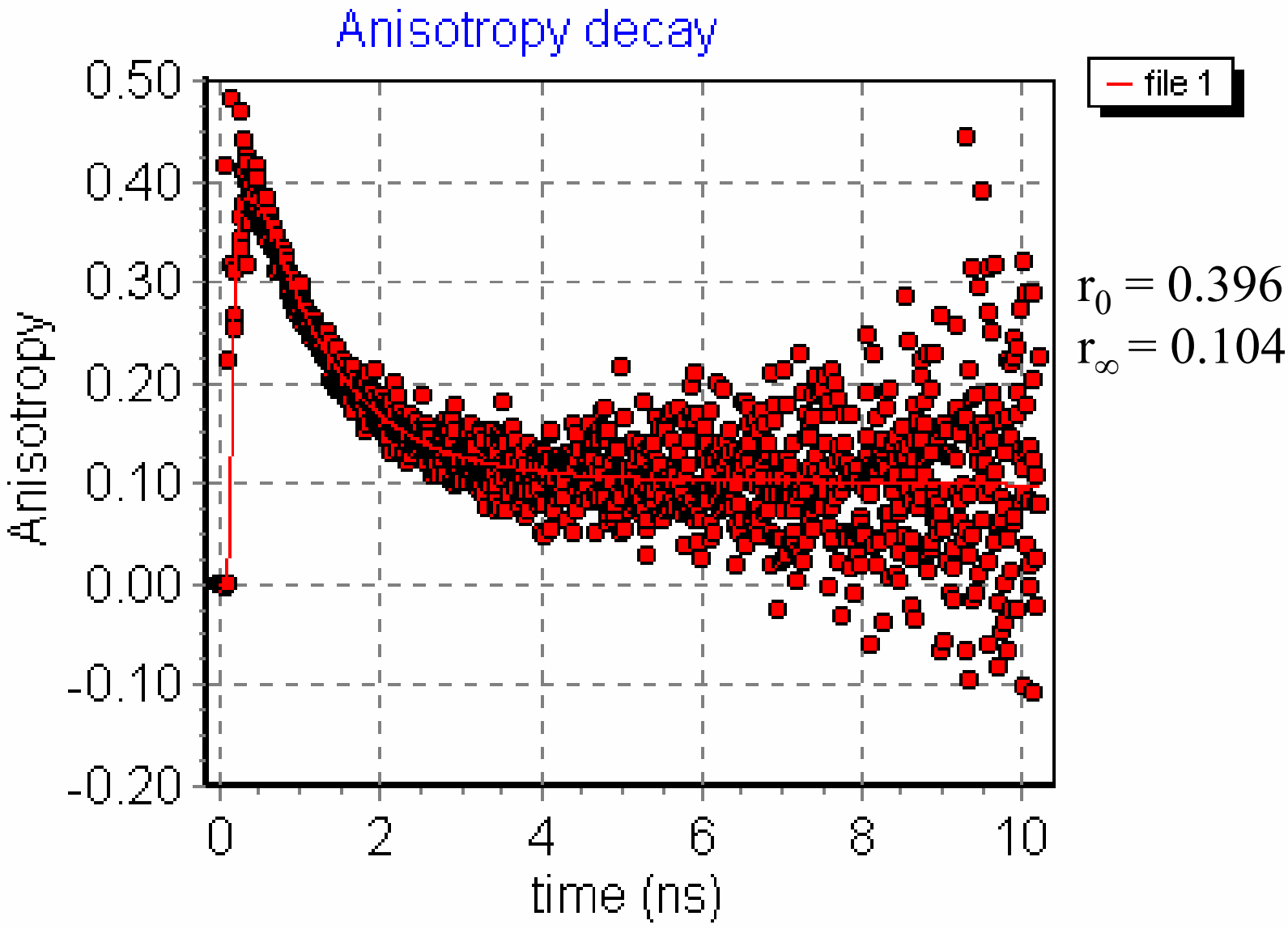

$r_0 = 0.396$

$r_\infty = 0.104$

Phase & Modulation Measurements

In dynamic polarization measurements, the sample is illuminated with vertically polarized, modulated light. The phase delay (dephasing) between the parallel and perpendicular components of the emission is measured as well as the modulation ratio of the AC contributions of these components. The expressions a spherical particle are:

$$\Delta\phi = \tan^{-1}\left[\frac{18\omega r_o R}{\left(k^2+\omega^2\right)\left(1+r_o-2r_o^2\right)+6R\left(6R+2k+kr_o\right)}\right]$$

$$Y^2 = \frac{\left(\left(1-r_o\right)k+6R\right)^2+\left(1-r_o\right)^2\omega^2}{\left[\left(1+2r_o\right)k+6R\right]^2+\left(1+2r_o\right)^2\omega^2}$$

Where $\Delta\phi$ is the phase difference, Y the modulation ratio of the AC components, ω the angular modulation frequency, r_o the limiting anisotropy, k the radiative rate constant ($1/\tau$) and R the rotational diffusion coefficient.

The illustration below depicts the $\Delta\phi$ function for the cases of spherical particles with different rotational relaxation times.

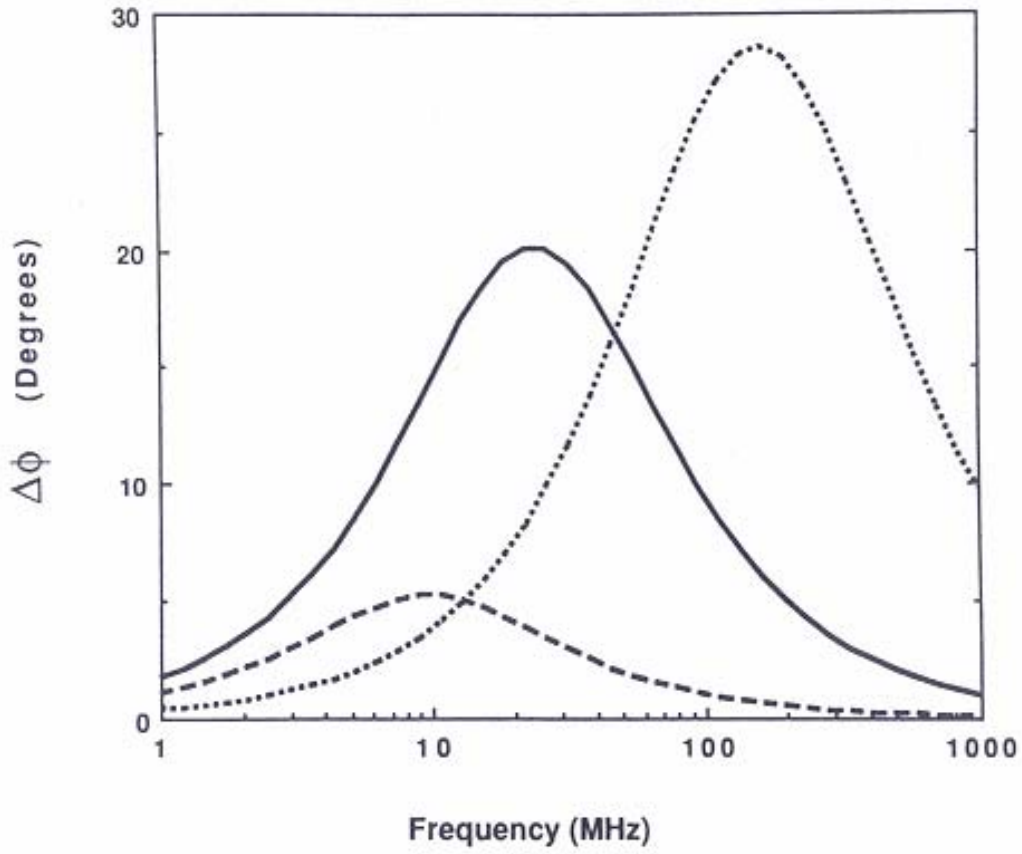

Differential phase data for an isotropic rotator with a 3-nsec (dotted line), 30-nsec (solid line), or 300-nsec (dashed line) rotational relaxation time. In each case a lifetime of 20 nsec was used and colinear excitation and emission dipoles were assumed.

The figures here show actual results for the case of ethidium bromide free and bound to tRNA - one notes that the fast rotational motion of the free ethidium results in a shift of the “bell-shaped” curve to higher frequencies relative to the bound case. The lifetimes of free and bound ethidium bromide were approximately 1.8 ns and 27 ns respectively.

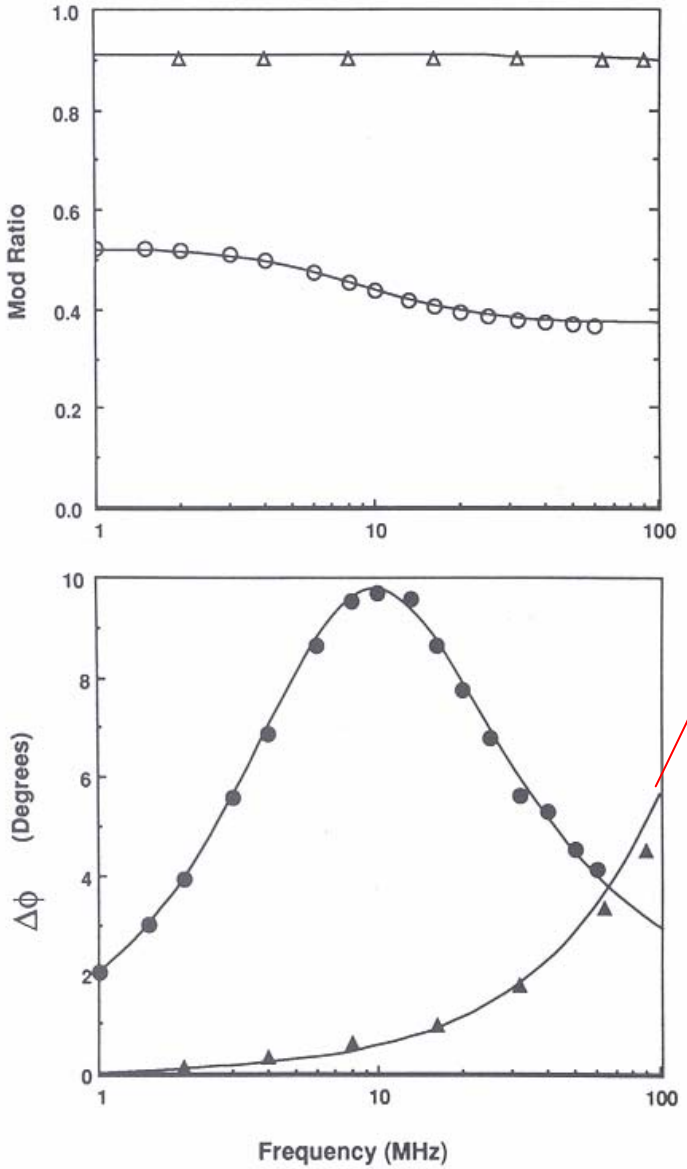

FIGURE 9. Differential phase (closed symbols) and modulation (open symbols) data for ethidium bromide in solution (triangles) and ethidium bromide bound to tRNA (circles). The resolved rotational relaxation times (5°C) were 144 and 0.5 nsec for free and bound ethidium bromide, respectively. The curves are the least-squares fit to the data.

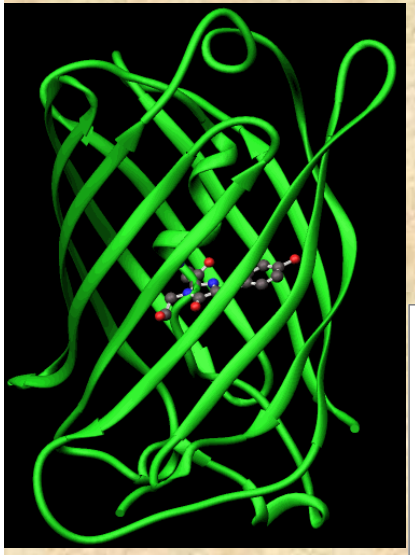

In GFP the fluorophore is rigidly attached to the protein framework

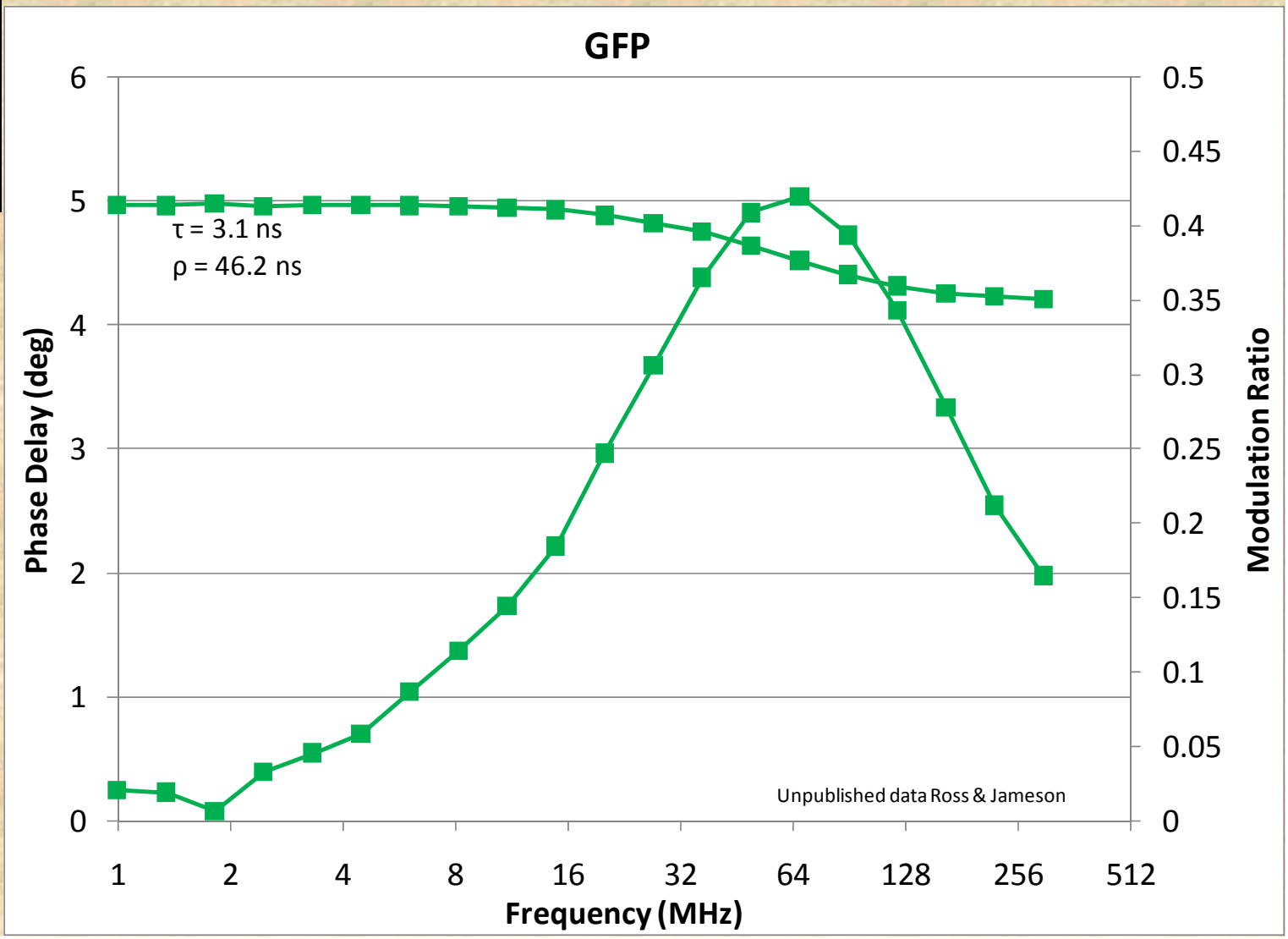

In the case of local plus global motion, the dynamic polarization curves are altered as illustrated below for the case of the single tryptophan residue in elongation factor Tu which shows a dramatic increase in its local mobility when EF-Tu is complexed with EF-Ts.

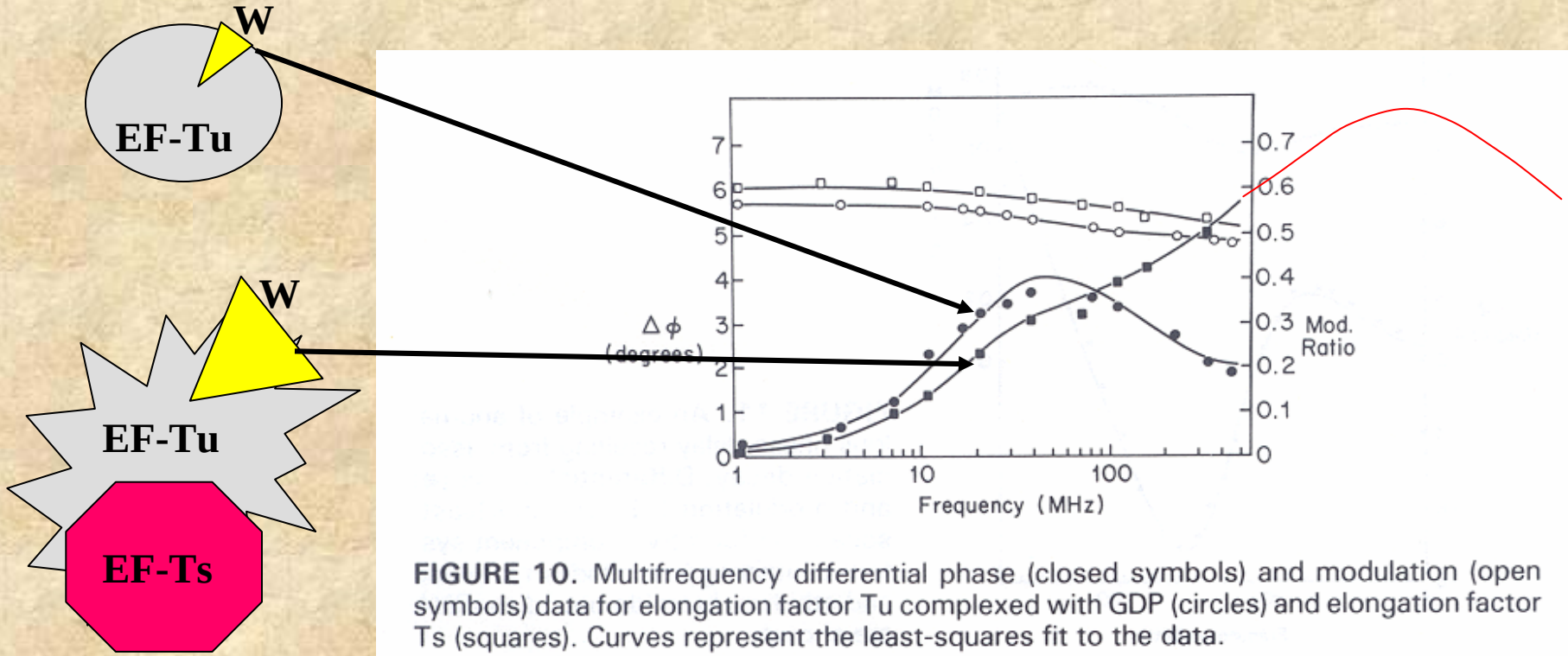

FIGURE 10. Multifrequency differential phase (closed symbols) and modulation (open symbols) data for elongation factor Tu complexed with GDP (circles) and elongation factor Ts (squares). Curves represent the least-squares fit to the data.

How about this case?

Negative phase delay?!

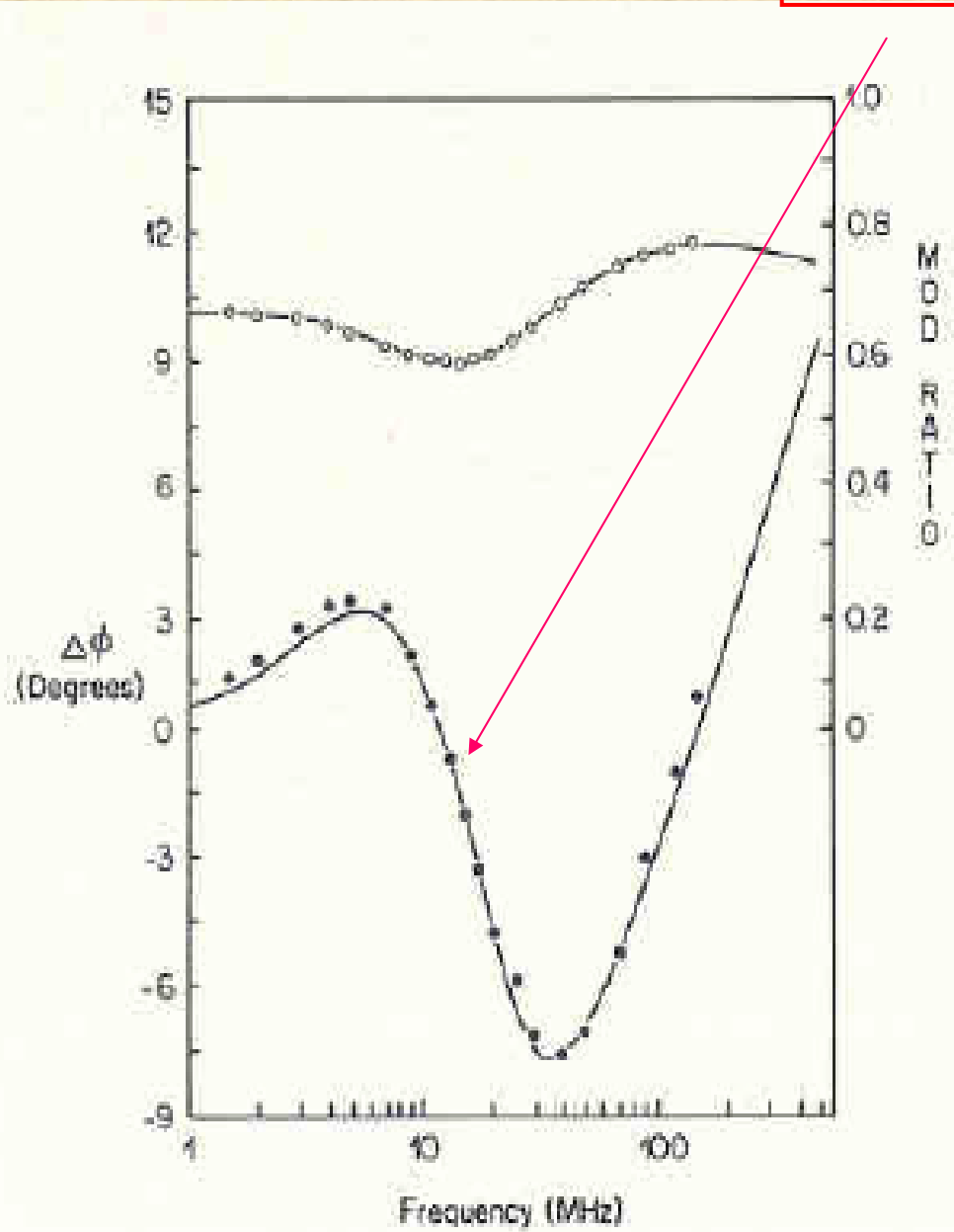

Anomalous Phase Delay (Chip Dip)

tRNA + Ethidium Bromide (equilibrium conditions)

Compare to individual species

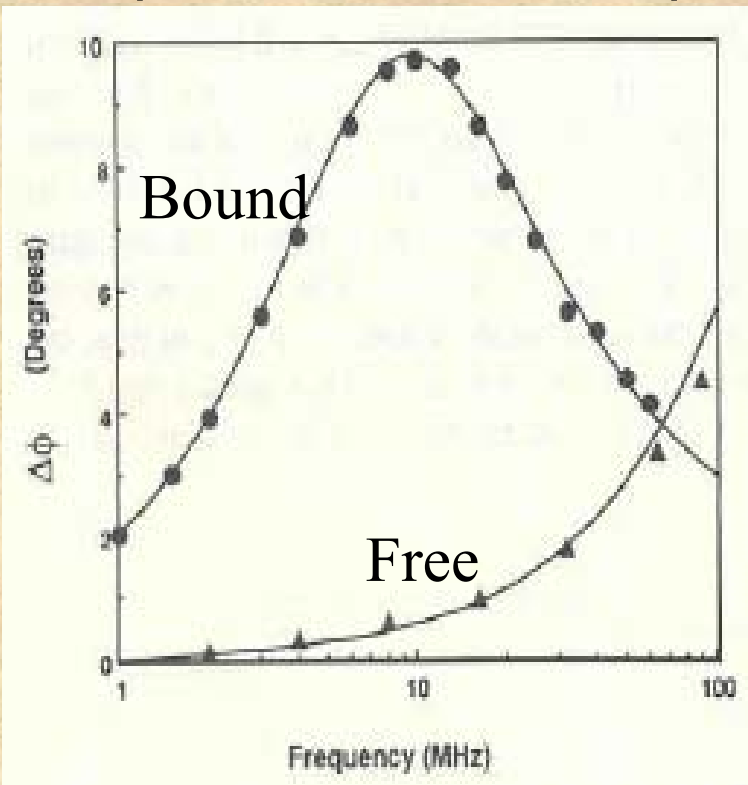

What do We have in Our Mixture?

+

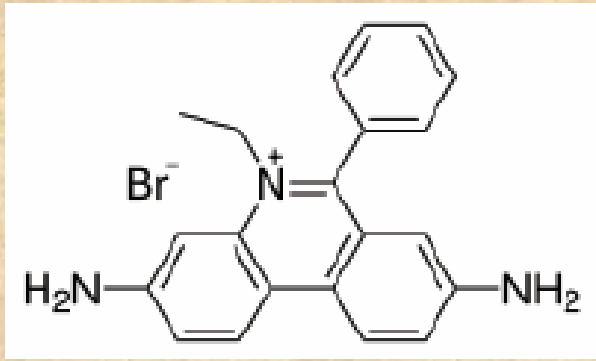

Ethidium Bromide

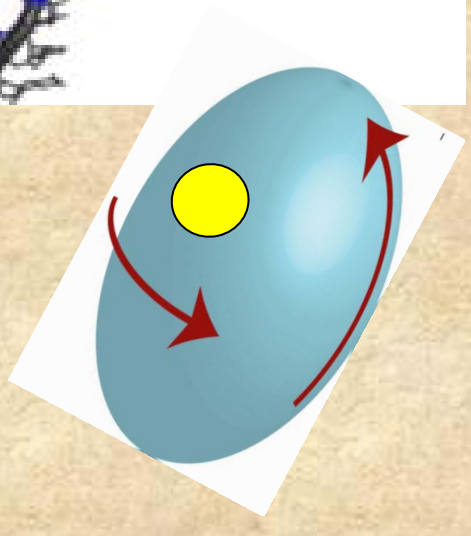

+

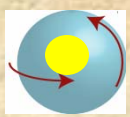

Slow rotation + long lifetime

Fast rotation + short lifetime

Time Domain Equivalent of the Anomalous Phase Delay

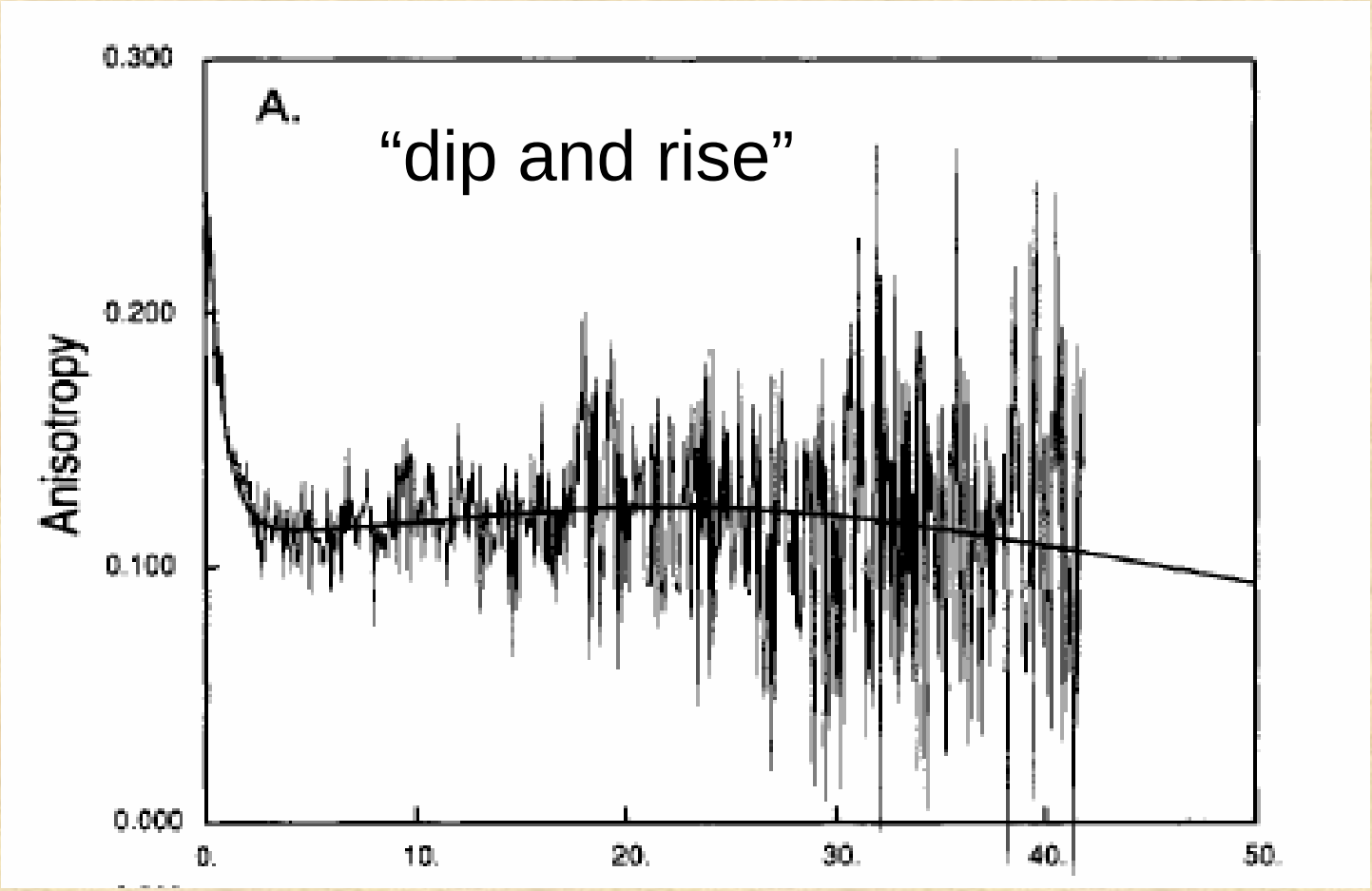

Guest et al., Interaction of DNA with the Klenow fragment of DNA polymerase I studied by time-resolved fluorescence spectroscopy. Biochemistry. 1991 Sep 10;30(36):8759-70.

Final comment: Although we have discussed analysis of rotational rates in terms of discrete components, in some cases a more realistic approach may be to use distribution functions

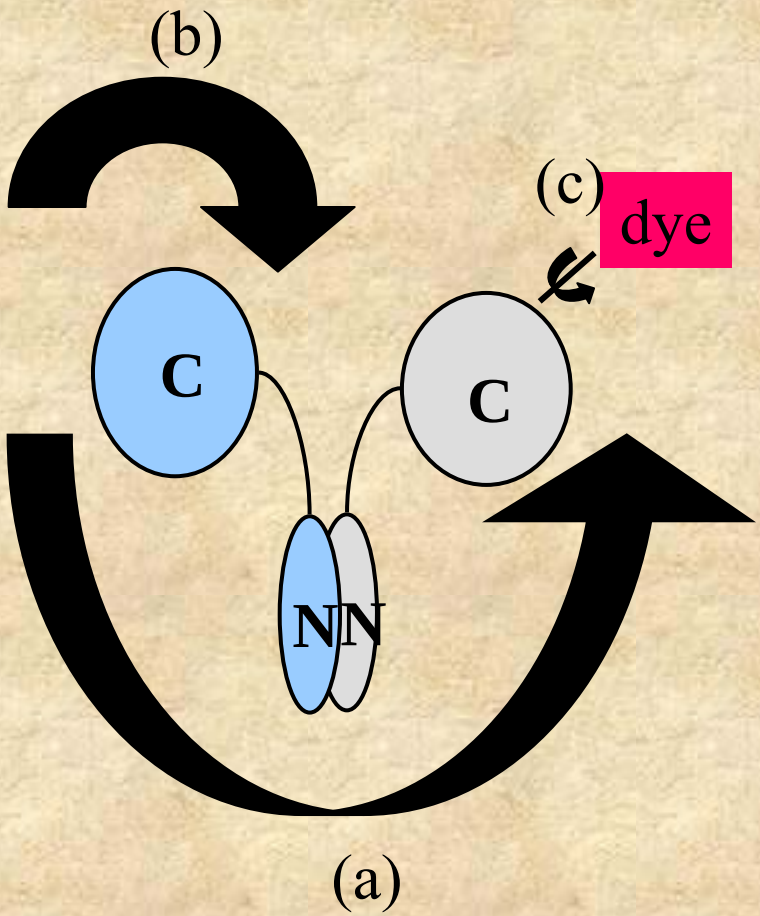

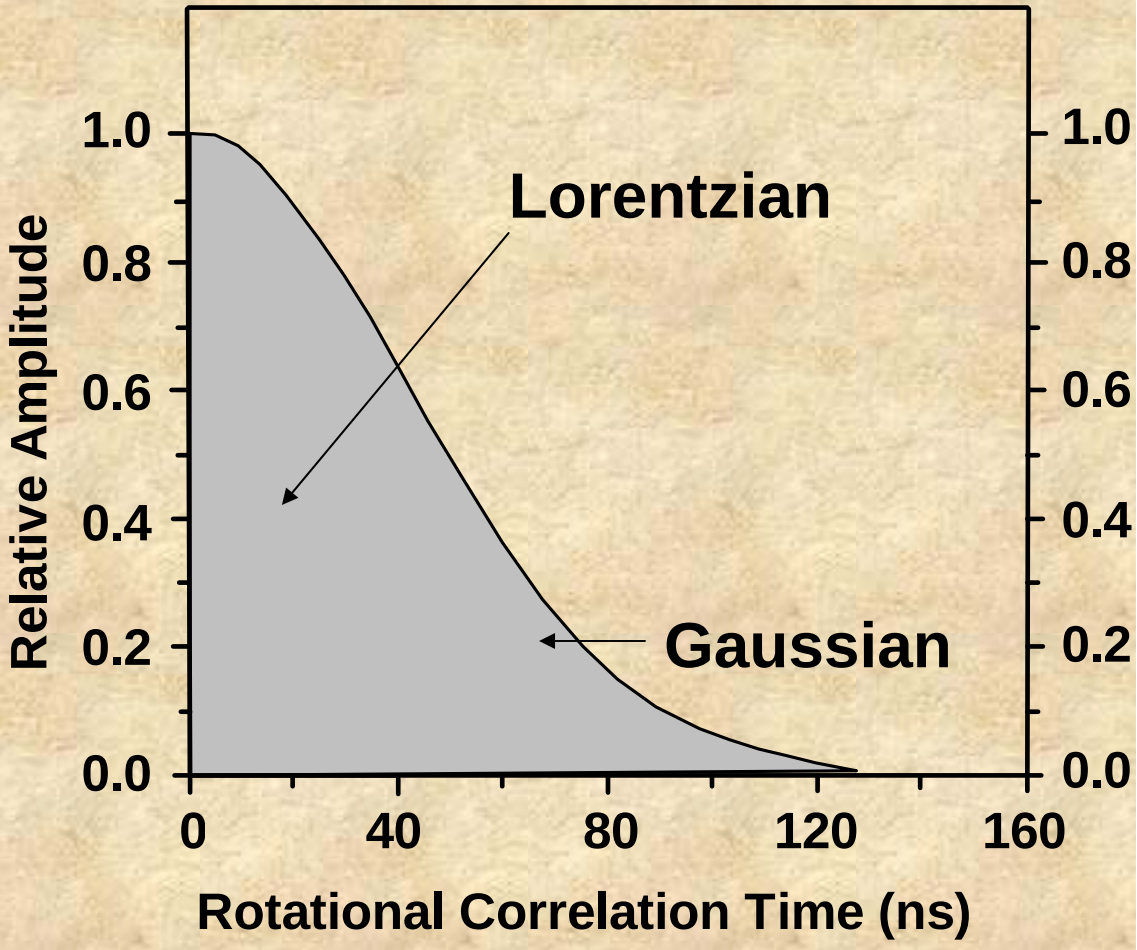

See: Analysis of anisotropy decays in terms of correlation time distributions, measured by frequency-domain fluorometry. Biophys Chem. 1994 Sep;52(1):1-13. Gryczynski I, Johnson ML, Lakowicz JR.

Förster Resonance Energy Transfer
FRET

I should note before we start that the Merriam-Webster online dictionary defines “FRET” as:

“to cause to suffer emotional strain”

Some of these slides were prepared by Pierre Moens

This sentence appears in a 2006 book!

Let's correct this mistake!

More than 50 years ago, the German scientist Förster discovered that close proximity of two chromophores changes their spectral properties in predictable ways (Förster, 1948a).

Milestones in the Theory of Resonance Energy Transfer

1922 G. Cario and J. Franck demonstrate that excitation of a mixture of mercury and thallium atomic vapors with 254nm (the mercury resonance line) also displayed thallium (sensitized) emission at 535nm.

1924 E. Gaviola and P. Pringsham observed that an increase in the concentration of fluorescein in viscous solvent was accompanied by a progressive depolarization of the emission.

1925 J. Perrin proposed the mechanism of resonance energy transfer

1928 H. Kallmann and F. London developed the quantum theory of resonance energy transfer between various atoms in the gas phase. The dipole-dipole interaction and the parameter R_0 are used for the first time

1932 F. Perrin published a quantum mechanical theory of energy transfer between molecules of the same specie in solution. Qualitative discussion of the effect of the spectral overlap between the emission spectrum of the donor and the absorption spectrum of the acceptor

1946-1949 T. Förster develop the first complete quantitative theory of molecular resonance energy transfer


André Marie Ampère

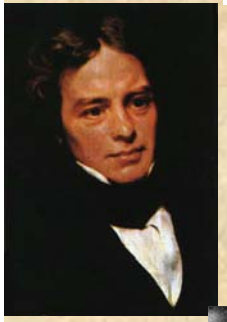


Heinrich Rudolf Hertz

π^5

From Förster's famous book
"Fluoreszenz Organischer Verbindungen";
which everyone references, but few read,

setzt, wobei n_{AB} die Häufigkeit des zwischenmolekularen Energieüberganges ist. Sie ist gleich der Zahl der Übergänge in der Zeiteinheit unter der Annahme, daß nach jedem Übergang stets wieder der ursprüngliche Zustand hergestellt wird. Aus Gl. (13,5) erhält man so, indem man gleichzeitig von der bisher benutzten Kreisfrequenz ω zur Frequenz ν selbst übergeht:

$$(13,6) \qquad n_{A,B} = \frac{\varkappa^2 e^4}{16\pi^2 n^4 m^2 R^6} \int_0^\infty f_e^{(A)}(\nu) \cdot f_a^{(B)}(\nu) \frac{d\nu}{\nu^2}.$$

Statt der Oszillatorenstärkefunktionen $f_e^{(A)}(\nu)$ und $f_a^{(B)}(\nu)$ führt man hier zweckmäßig die leichter zugänglichen Größen $f_Q^{(A)}(\nu)$ (Quantenspektrum des energieabgebenden Moleküls A) und $\varepsilon^{(B)}(\nu)$ (molarer dekadischer Extinktionskoeffizient des energieaufnehmenden Moleküls B) nach Gln. (12,46′) und (12,43′) ein. Man erhält so für die Übergangshäufigkeit

$$(13,7) \quad n_{A,B} = \frac{9 \cdot \ln 10}{128\pi^6} \frac{\varkappa^2 c^4}{n^4 N' \tau_e R^6} \int_0^\infty f_Q^{(A)}(\nu) \cdot \varepsilon^{(B)}(\nu) \frac{d\nu}{\nu^4}.$$

Diese Beziehung ist auch auf exakter quantenmechanischer Grundlage zu gewinnen [FÖRSTER (1947a)].

Die dimensionslose Konstante $\varkappa$ ist nach Gl. (13,1) durch die Feldstärkekomponente des Oszillators A am Ort und in der Richtung des Oszillators B bestimmt. Sie hängt daher von der Orientierung beider Oszillatoren zueinander und zu deren Verbindungslinie ab. Seien φ_A und φ_B die Winkel zwischen den einzelnen Oszillationsrichtungen und dieser Verbindungslinie und φ_{AB} der Winkel zwischen den Oszillationsrichtungen, so ist nach einer elementaren Formel für die Wechselwirkungsenergie zweier Dipole:

$$(13,8) \qquad \varkappa = \cos\varphi_{AB} - 3\cos\varphi_A \cdot \cos\varphi_B.$$

Wegen der Rotationsbewegung der Moleküle wechseln sämtliche Richtungen in den meisten Fällen so rasch, daß statt der Momentanwerte von $\varkappa^2$ dessen *statistischer Mittelwert* über sämtliche Orientierungen einzusetzen ist. Dieser ergibt sich am einfachsten durch

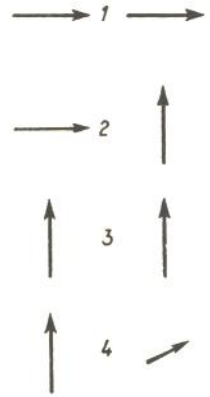

Fig. 16. Hauptlagen für die gegenseitige Orientierung zweier Oszillatoren. Der rechte Vektor zeigt in der Lage 4 nach hinten. Die nach Gl. (13,8) berechneten Werte von $\varkappa^2$ und die statistischen Gewichte der Hauptlagen sind:
$\varkappa_1^2 = 4\,(\frac{1}{9})$, $\varkappa_2^2 = 0\,(\frac{4}{9})$,
$\varkappa_3^2 = 1\,(\frac{2}{9})$, $\varkappa_4^2 = 0\,(\frac{2}{9})$.

Thanks to Bob Clegg for this slide

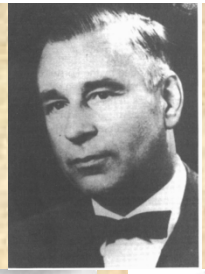

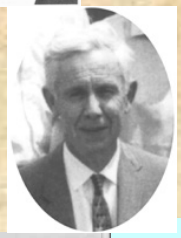

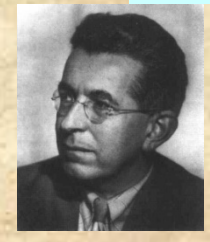

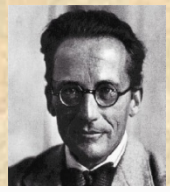


Werner Heisenberg

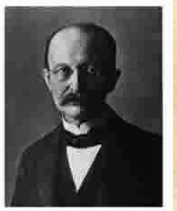
Max Planck

What is FRET ?

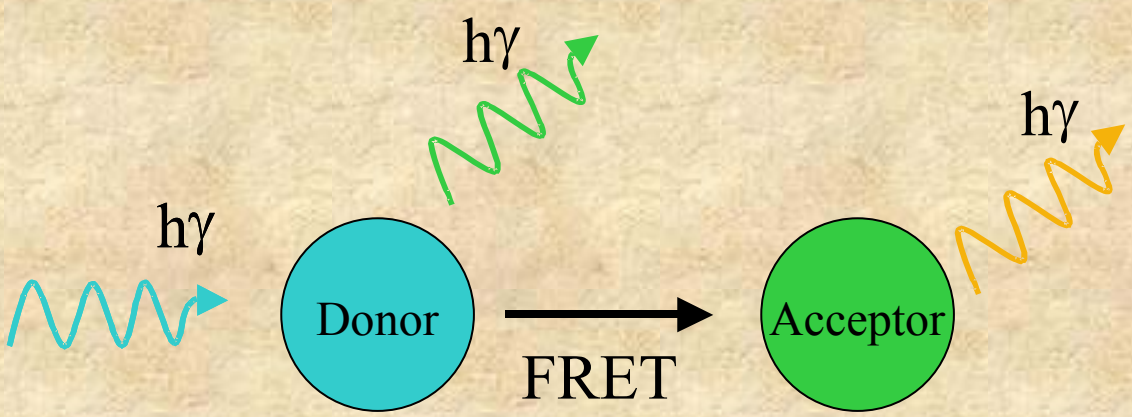

When the donor molecule absorbs a photon, and there is an acceptor molecule close to the donor molecule, radiationless energy transfer can occur from the donor to the acceptor.

FRET results in a decrease of the fluorescence intensity and lifetime of the donor probe, It enhance the fluorescence of the acceptor probe when the acceptor is fluorescent.

PM

Tuning fork analogy for resonance energy transfer

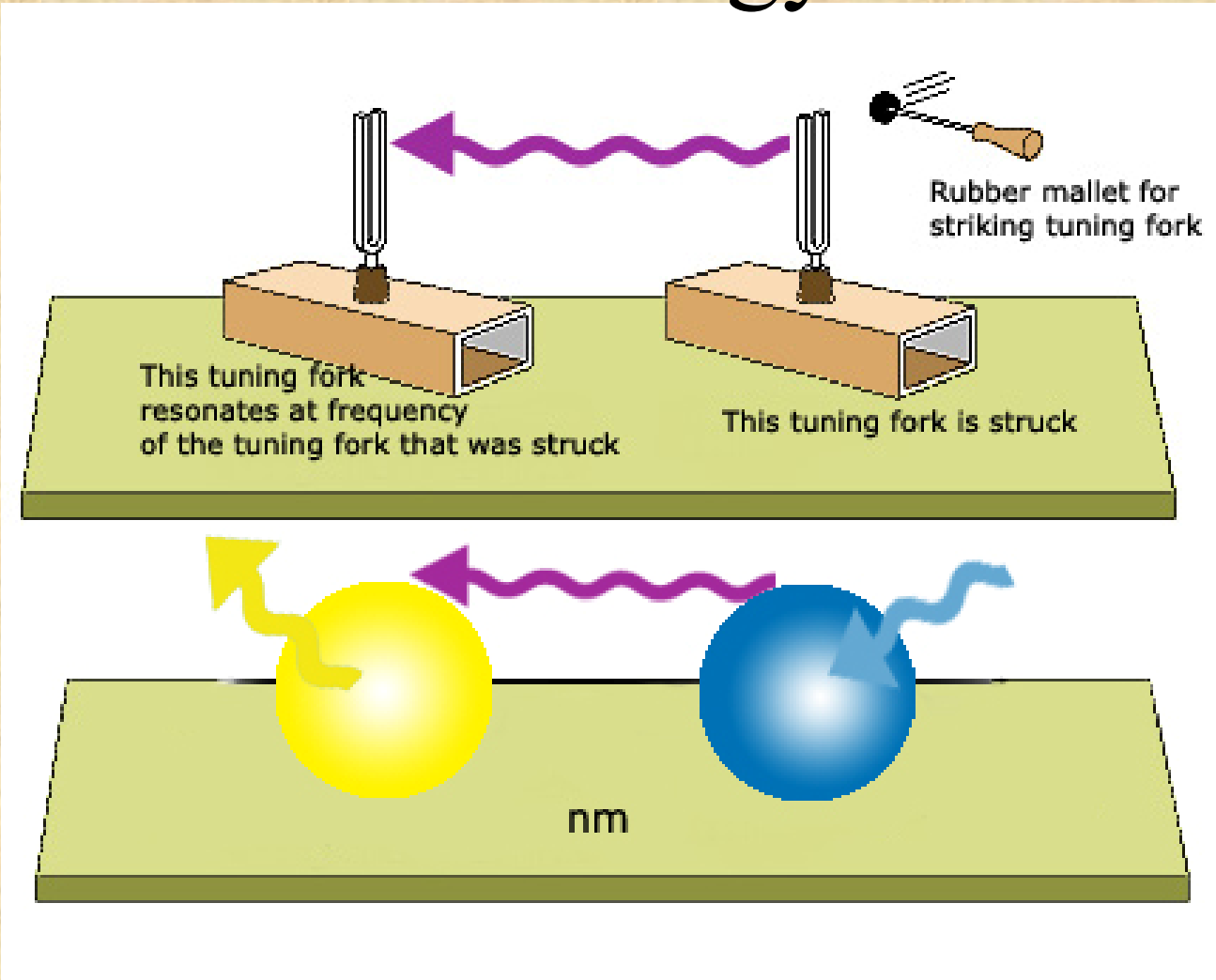

Simplified FRET Energy Diagram

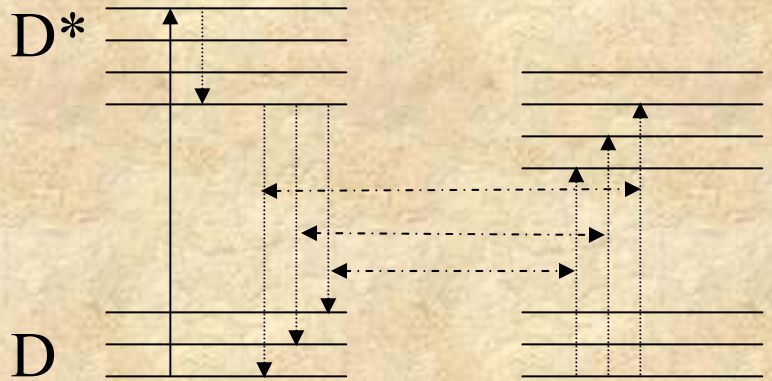

Coupled transitions

Suppose that the energy difference for one of these possible deactivation processes in the donor molecule matches that for a possible absorption transition in a nearby acceptor molecule. Then, with sufficient energetic coupling between these molecules (overlap of the emission spectrum of the donor and absorption spectrum of the acceptor), both processes may occur simultaneously, resulting in a transfer of excitation from the donor to the acceptor molecule

The interaction energy is of a dipole-dipole nature and depends on the distance between the molecules as well as the relative orientation of the dipoles

PM

Dipole-dipole interaction

The rate of transfer (k_T) of excitation energy is given by:

$$k_T = (1/\tau_d)(R_0/r)^6$$

Where τ_d is the fluorescence lifetime of the donor in the absence of acceptor, r the distance between the centers of the donor and acceptor molecules and R_0 the Förster critical distance at which 50% of the excitation energy is transferred to the acceptor and can be approximated from experiments independent of energy transfer.

Förster critical distance

$$R_0 = 0.2108\,(n^{-4} Q_d \kappa^2 J)^{1/6} \text{ Å}$$

n is the refractive index of the medium in the wavelength range where spectral overlap is significant (usually between 1.2-1.4 for biological samples)

Q_d is the fluorescence quantum yield of the donor in absence of acceptor (i.e. number of quanta emitted / number of quanta absorbed)

κ^2 (pronounced “kappa squared”) is the orientation factor for the dipole-dipole interaction

J is the normalized spectral overlap integral [$\varepsilon(\lambda)$ is in $M^{-1}\,cm^{-1}$, λ is in nm and J units are $M^{-1}\,cm^{-1}\,(nm)^4$]

The overlap integral J is defined by:

$$J = \int_0^\infty I_D(\lambda)\varepsilon_A(\lambda)\lambda^4 d\lambda$$

Where λ is the wavelength of the light, $\varepsilon_A(\lambda)$ is the molar absorption coefficient at that wavelength and $I_D(\lambda)$ is the fluorescence spectrum of the donor normalized on the wavelength scale:

$$I_D(\lambda) = \frac{F_{D\lambda}(\lambda)}{\int_0^\infty F_{D\lambda}(\lambda)d\lambda}$$

Where $F_{D\,\lambda}(\lambda)$ is the donor fluorescence per unit wavelength interval

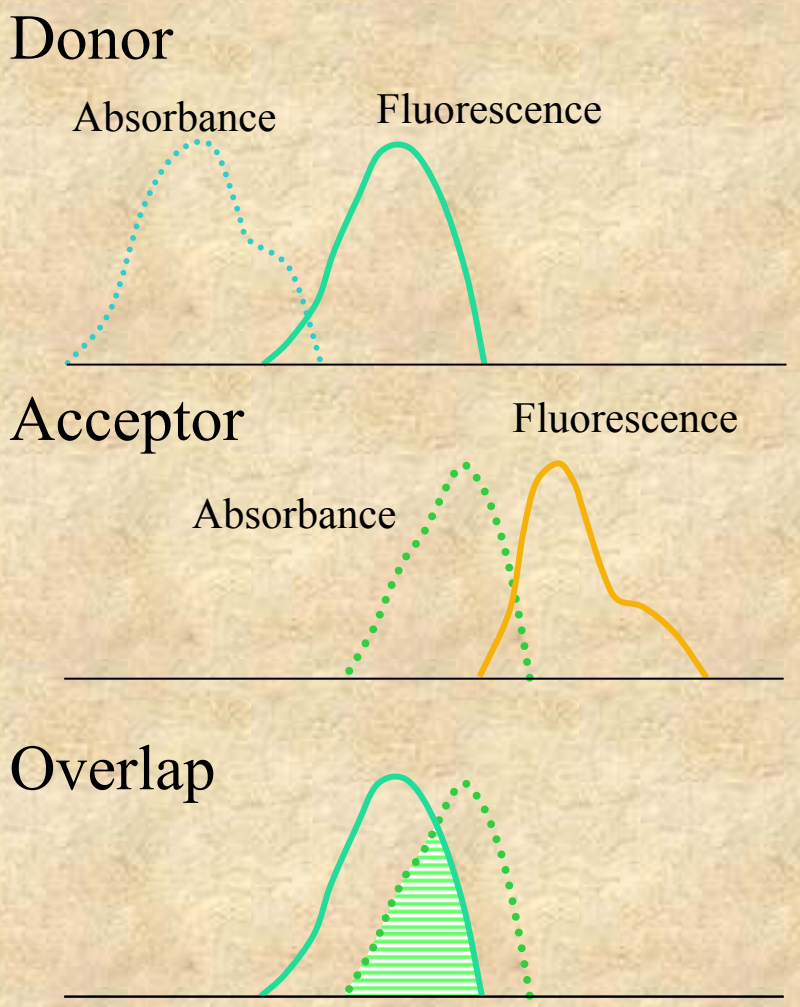

Determination of the efficiency of energy transfer (E)

Steady state method: *Decrease in donor fluorescence.* the fluorescence intensity of the donor is determined in absence and presence of the acceptor.

$$E = 1 - \frac{F_{da}}{F_d}$$

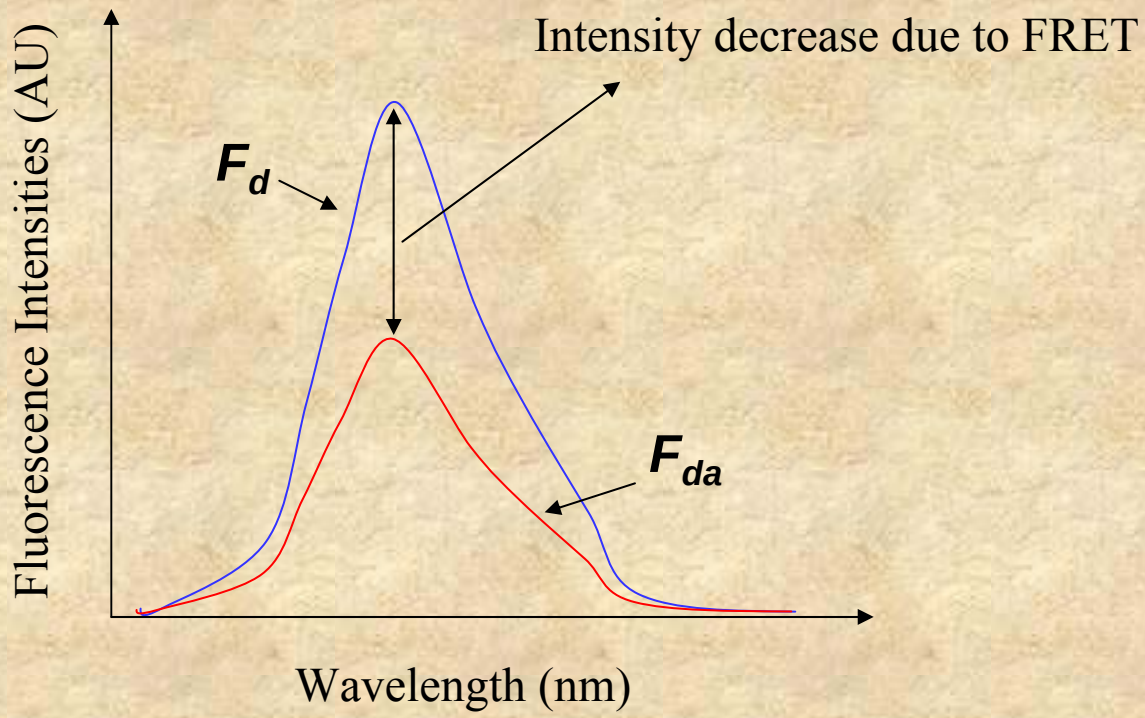

Determination of the efficiency of energy transfer (E)

Time-resolved method: Decrease in the lifetime of the donor

If the fluorescence decay of the donor is a single exponential then:

$$E = 1 - \frac{\tau_D}{\tau_D^0}$$

Where τ_D and τ_D^0 are the lifetime of the donor in the presence and absence of acceptor, respectively

Determination of the efficiency of energy transfer (E)

If the donor fluorescence decay in absence of acceptor is not a single exponential (probably resulting from heterogeneity of the probe's microenvironment) , then it may be modeled as a sum of exponential and the transfer efficiency can be calculated using the average decay times of the donor in absence and presence of acceptor:

$$E = 1 - \frac{\langle \tau_D \rangle}{\langle \tau_D^0 \rangle}$$

Where $<\tau>$ is the amplitude-average decay time and is defined as:

$$\langle \tau \rangle = \frac{\sum_i \alpha_i \tau_i}{\sum_i \alpha_i}$$

The distance dependence of the energy transfer efficiency (E)

$$r = \left(\frac{1}{E} - 1 \right)^{1/6} R_0$$

Where r is the distance separating the donor and acceptor fluorophores, R_0 is the Förster distance.

Many equivalent forms of this equation is found in the literature, such as:

$$E = R_0^6 / (R_0^6 + r^6) \text{ or } E = 1 / \left[1 + \left(r/R_0 \right)^6 \right]$$

The distance dependence of the energy transfer efficiency (E)

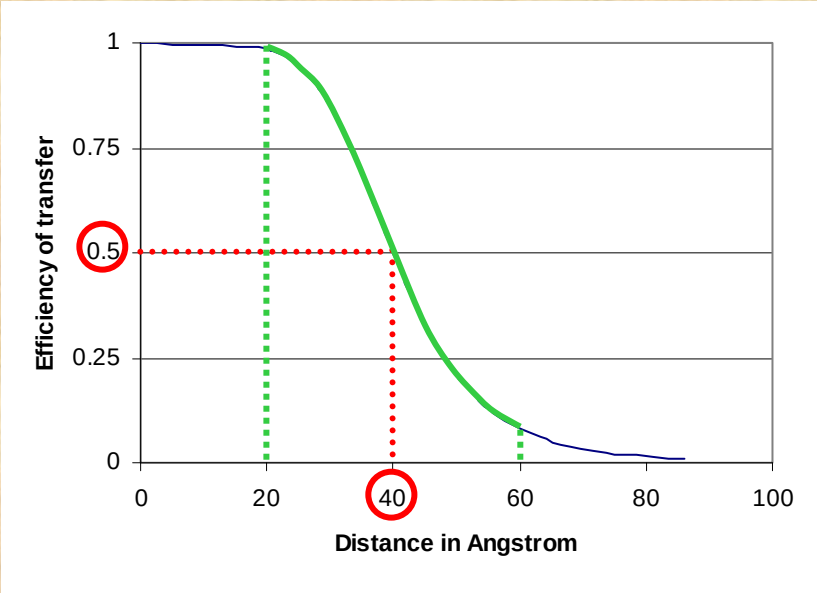

The efficiency of transfer varies with the inverse sixth power of the distance.

R_0 in this example was set to 40 Å. When the E is 50%, $R=R_0$

Distances can usually be measured between 0.5 R_0 and ~1.5R_0. Beyond these limits, we can often only say that the distance is smaller than 0.5 R_0 or greater than 1.5R_0. If accurate distance measurement is required then a probe pair with a different R_0 is necessary.

How was FRET theory tested experimentally?

Energy Transfer. A System with Relatively Fixed Donor–Acceptor Separation

JACS 87:995(1965)

S. A. Latt, H. T. Cheung, and E. R. Blout

Contribution from the Department of Biological Chemistry, Harvard Medical School, Boston, Massachusetts. *Received August 24, 1964*

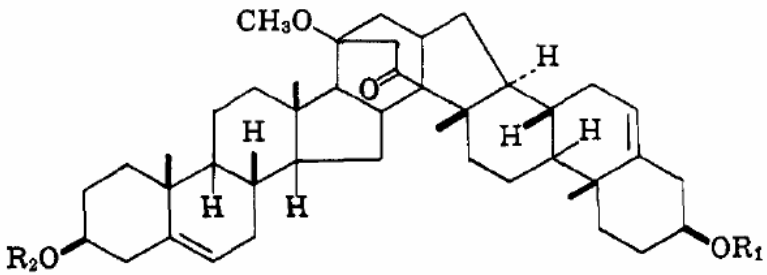

XIb, R_1 = *p*-methoxyphenylacetyl; R_2 = 1-naphthoyl
XIIb, R_1 = 1-naphthoyl; R_2 = anthracene-9-carbonyl

Table III

Compound	$\overline{K^2}$	R_{calcd}, Å.	R_{measd} (from Dreiding models), Å.
XI	$^2/_3$	21.3 ± 1.6	21.8 ± 2.0 (linear av.)
			19.2 ± 2.0 ($[\overline{1/R^6}]^{-6}$)
XII	$^2/_3$	16.7 ± 1.4	21.5 ± 2.0 (linear av.)
			19.4 ± 2.0 ($[\overline{1/R^6}]^{-6}$)

The most likely explanation for this discrepancy between the predicted and observed transfer in compound XII is that the value of the average orientation factor is greater than the estimate of $^2/_3$ which was used to calculate the predicted separation.

*DEPENDENCE OF THE KINETICS OF SINGLET-SINGLET ENERGY TRANSFER ON SPECTRAL OVERLAP**

BY RICHARD P. HAUGLAND,† JUAN YGUERABIDE,‡ AND LUBERT STRYER‡

DEPARTMENT OF CHEMISTRY, STANFORD UNIVERSITY, AND
DEPARTMENT OF BIOCHEMISTRY, STANFORD UNIVERSITY SCHOOL OF MEDICINE

Communicated by Harden M. McConnell, February 19, 1969

PNAS

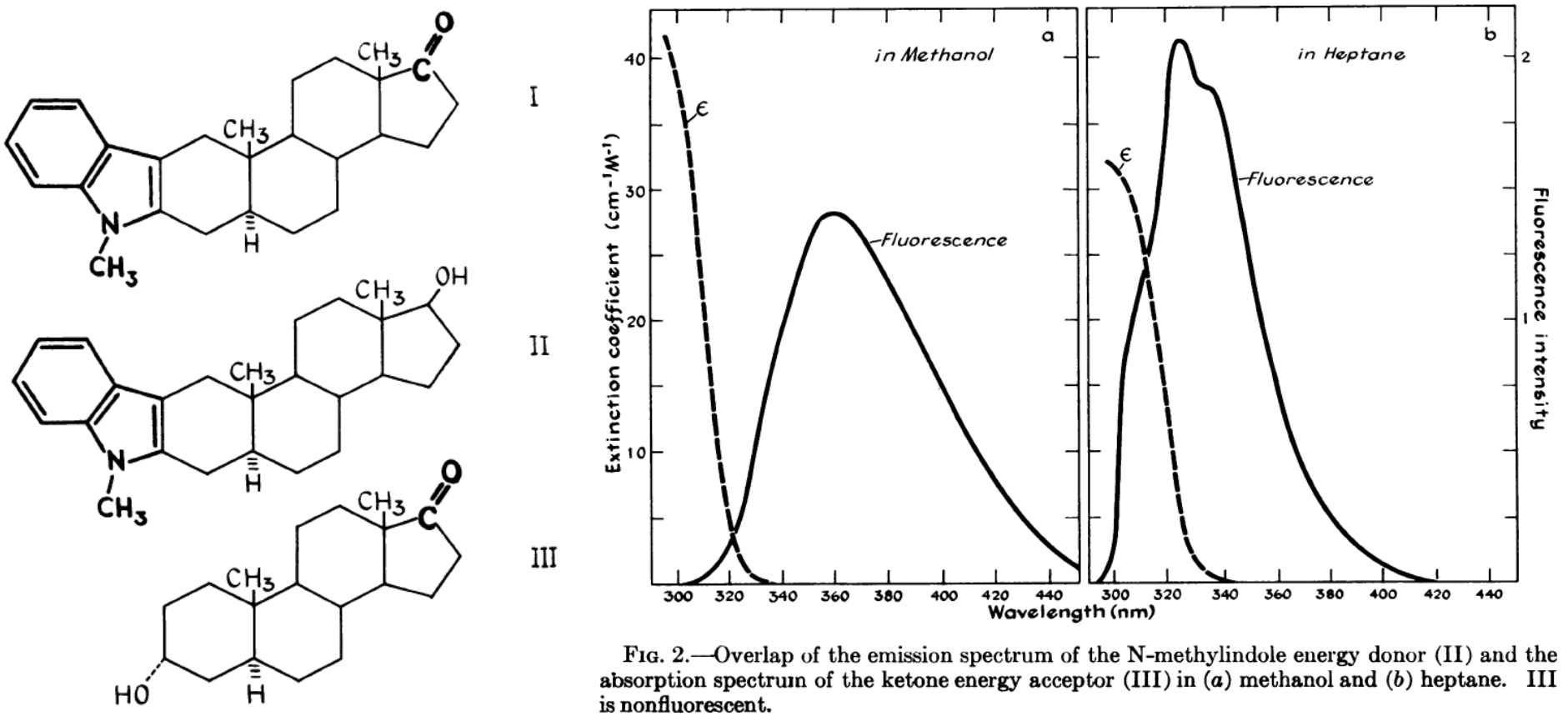

FIG. 2.—Overlap of the emission spectrum of the N-methylindole energy donor (II) and the absorption spectrum of the ketone energy acceptor (III) in (*a*) methanol and (*b*) heptane. III is nonfluorescent.

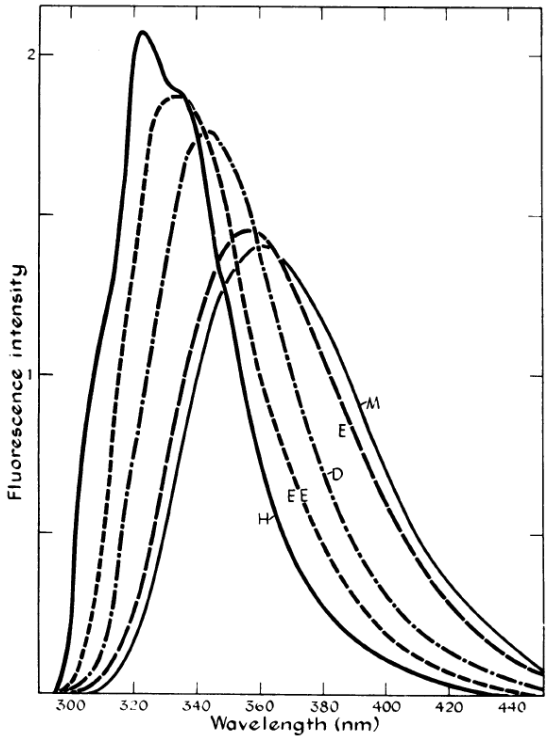

FIG. 3.—Fluorescence emission spectra of II in n-heptane (*H*), ethyl ether (*EE*), p-dioxane (*D*), ethanol (*E*), and methanol (*M*). The spectrum of II in ethyl acetate is virtually identical to that obtained in dioxane. The intensities have been normalized so that the areas under the curves are equal. The excitation wavelength was 290 nm.

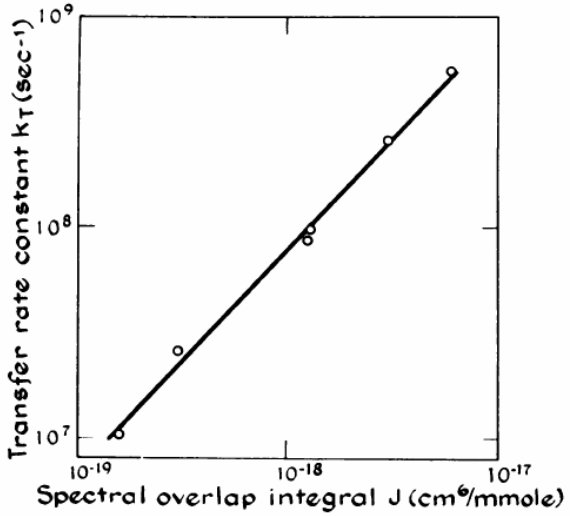

TABLE I. *Fluorescence properties of I and II in a series of solvents.*

Solvent	τ_I (nsec)	τ_{II} (nsec)	Fluorescence Quantum Yield Q_I	Q_{II}	Transfer Efficiency E_K	E_{SS}
Methanol	5.3	5.6	0.397	0.420	0.053	0.055
Ethanol	5.6	6.5	0.440	0.510	0.14	0.138
Dioxane	3.6	5.4	0.360	0.535	0.33	0.328
Ethyl acetate	3.3	4.7	0.286	0.418	0.30	0.315
Ethyl ether	2.1	4.5	0.247	0.515	0.53	0.52
Heptane	1.1	2.8	0.136	0.346	0.606	0.608

TABLE 2. *Transfer kinetics and spectral overlap integral of I in a series of solvents.*

Solvent	Transfer rate, k_T(sec^{-1}) $\times 10^{-7}$	Spectral overlap integral, J(cm^6 mmole^{-1}) $\times 10^{19}$	k_F (sec^{-1}) $\times 10^{-7}$	n_D	k_T/J $\times 10^{-26}$	$k_T/(Jk_F)$ $\times 10^{-18}$
Methanol	1.0	1.5	7.50	1.331	0.67	0.89
Ethanol	2.5	3.0	7.85	1.362	0.83	1.06
Dioxane	9.6	13.0	9.9	1.423	0.74	0.75
Ethyl acetate	11.3	12.8	8.9	1.372	0.88	0.99
Ethyl ether	25.5	30.0	11.5	1.349	0.83	0.72
Heptane	55.2	60.3	12.4	1.387	0.92	0.74

r^{-6} distance dependence?

$$k_T = (1/\tau_d)(R_0/r)^6$$

*ENERGY TRANSFER: A SPECTROSCOPIC RULER**

By Lubert Stryer and Richard P. Haugland†

Department of Biochemistry, Stanford University School of Medicine, Palo Alto, and the Department of Chemistry, Stanford University

Communicated by Arthur Kornberg, May 29, 1967 PNAS

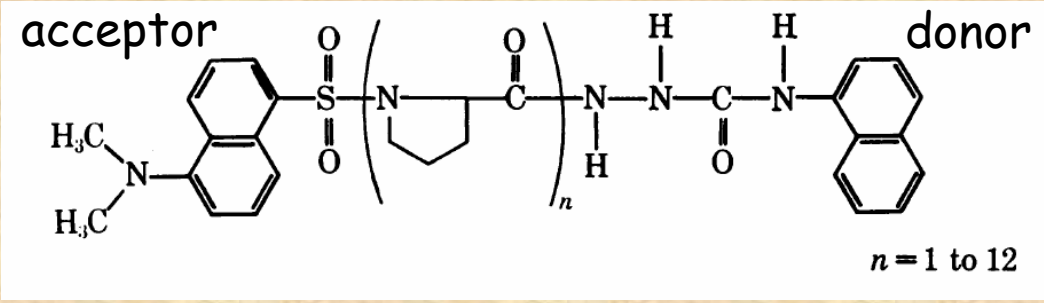

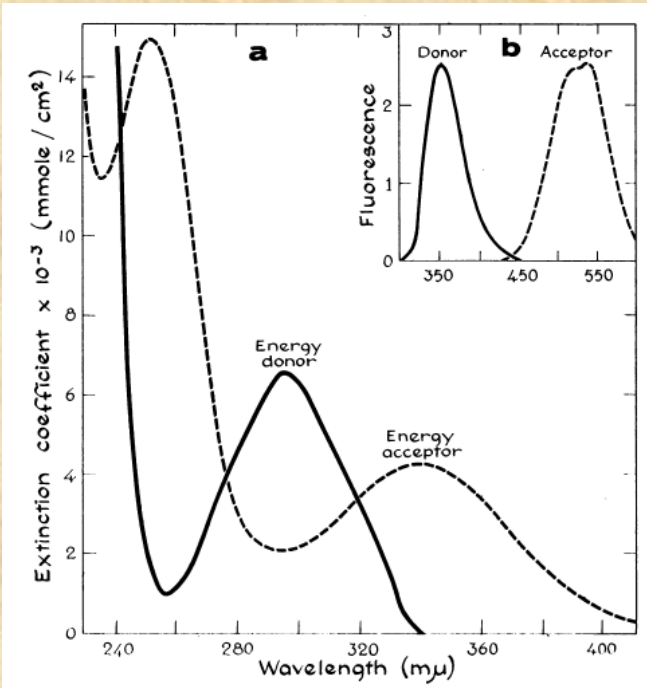

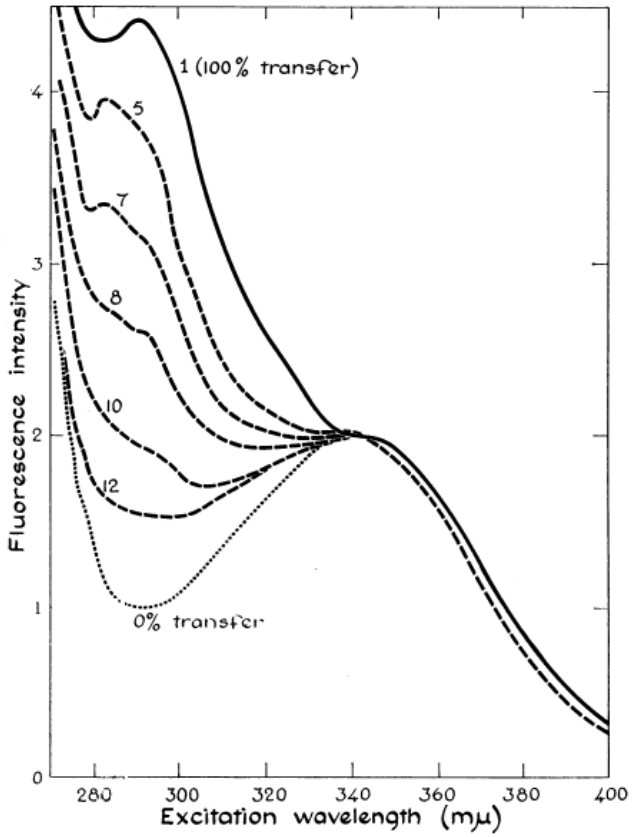

FIG. 3.—Excitation spectrum of dansyl-L-prolyl-hydrazide (·····, 0% transfer), dansyl-L-prolyl-α-naphthyl (———, 100% transfer), and dansyl-(L-prolyl)$_n$-α-naphthyl (- - - -, n = 5, 7, 8, 10, 12) in ethanol.

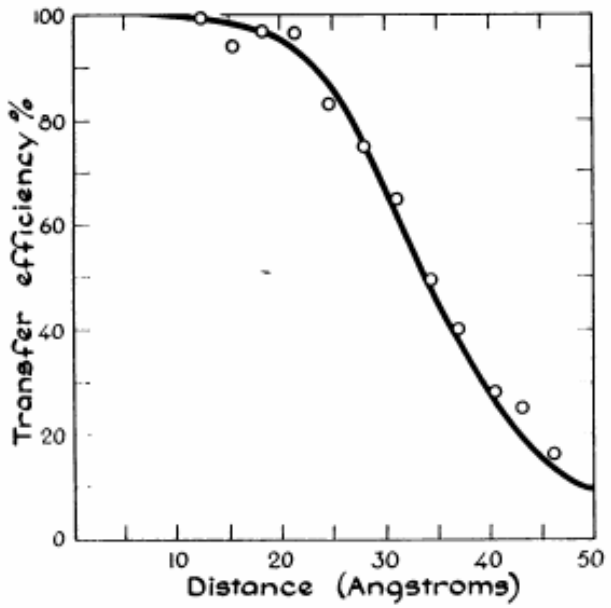

FIG. 4.—Efficiency of energy transfer as a function of distance in dansyl-(L-prolyl)$_n$-α-naphthyl, n = 1 to 12. The α-naphthyl and dansyl groups were separated by defined distances ranging from 12 to 46 Å. The energy transfer is 50% efficient at 34.6 Å. The solid line corresponds to an r^{-6} distance dependence.

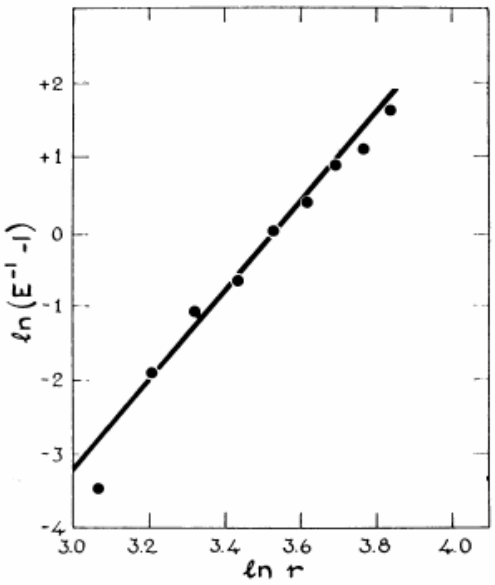

FIG. 5.—The dependence of the efficiency of energy transfer on distance is given by the slope in this plot of ln (E^{-1} − 1) versus ln r. The slope is 5.9, in excellent agreement with the r^{-6} dependence predicted by Förster.

For these parameters, R_0 is calculated to be 27.2 Å, *while the observed value is* 34.6 Å (Figs. 4 and 5). A rigorous comparison of the observed and calculated R_0 distances should be deferred until the value of K^2 is better defined. It would also be desirable to have independent confirmation of the estimated distances between the energy donor and acceptor groups.

Richard P. Haugland (left) Lubert Stryer (right) receiving the 2002 Molecular Bioanalytic award, sponsored by Roche Diagnostics GmbH, in association with the German Society for Biochemistry and Molecular Biology (GBM), in recognition of their achievements in the field of FRET. Photo retrieved on July 26, 2009 from http://probes.invitrogen.com/resources/whatsnew/pressrelease/051302.html.

More to the story???

Effect of flexibility and *cis* residues in single-molecule FRET studies of polyproline

Robert B. Best*†, Kusai A. Merchant*, Irina V. Gopich*, Benjamin Schuler*‡, Ad Bax*, and William A. Eaton*§

18964–18969 | PNAS | November 27, 2007 | vol. 104 | no. 48

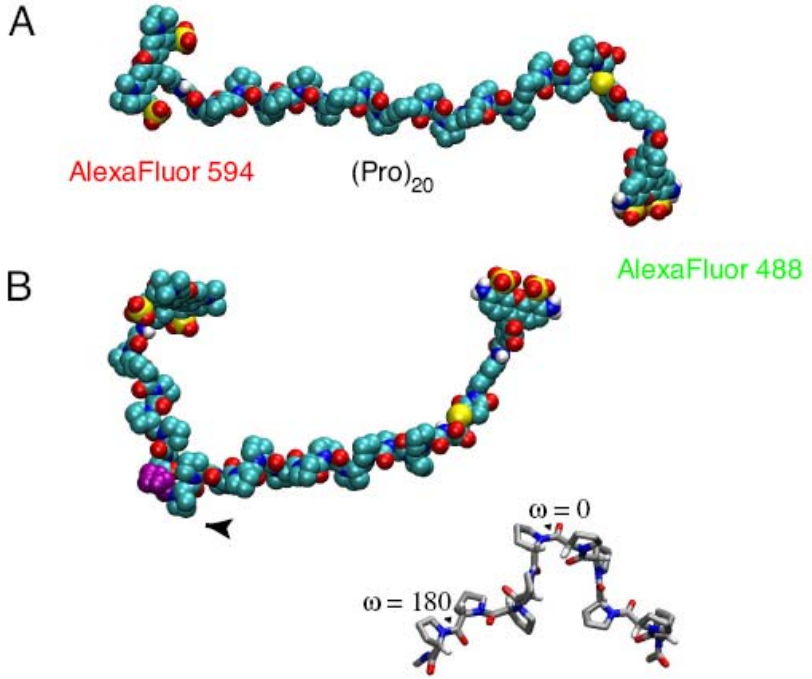

Fig. 1. Polyproline structures. Space-filling representation of polyproline-20 labeled with Alexa Fluor 488 (FRET donor) at the C-terminal cysteine and Alexa Fluor 594 (FRET acceptor) at the N-terminal glycine in the *all-trans* conformation (*A*) and with residue 8 (purple) in the *cis* conformation (*B*). (*B Inset*) A polyproline fragment with one *cis* peptide bond (shown as "$\omega = 0$"). One of the remaining *trans* peptide bonds is also indicated ("$\omega = 180$").

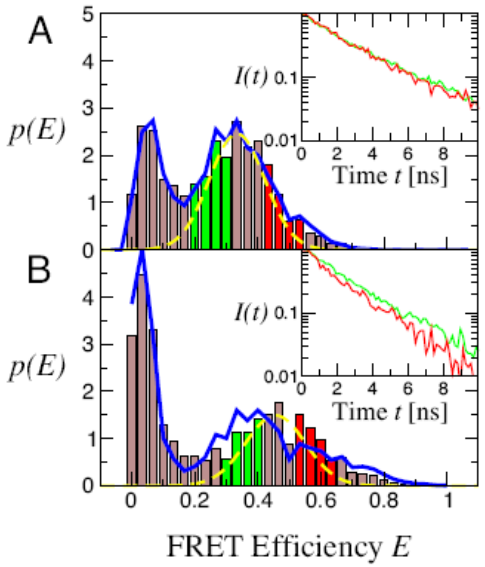

Fig. 3. Distributions of FRET efficiency for polyproline-20. The efficiency of each molecule $E = n_A/(n_A + n_D)$ was calculated from the (γ-corrected) n_A acceptor and n_D donor photons detected as it passes through the observation volume, in TFE (*A*) and water (*B*) (solid bars). Broken yellow lines indicate the shot-noise-limited width of the distribution (24, 19). Solid blue line in *A* gives a maximum likelihood fit of the data a multistate model. Solid blue line in *B* gives the expected efficiency distribution for a heterogeneous mixture of species containing *cis* proline, taking the relative populations from NMR and the efficiencies from simulation. (*Insets*) The donor fluorescence decays for donor photons from the subpopulations with corresponding colors in the efficiency histograms.

More to the story???

Polyproline has recently been used as a spacer between donor and acceptor chromophores to help establish the accuracy of distances determined from single-molecule Förster resonance energy transfer (FRET) measurements. This work showed that the FRET efficiency in water is higher than expected for a rigid spacer and was attributed to the flexibility of the polypeptide. Here, we investigate this issue further, using a combination of single-molecule fluorescence intensity and lifetime measurements, NMR, theory, and molecular dynamics simulations of polyproline-20 that include the dyes and their linkers to the polypeptide. NMR shows that in water ≈30% of the molecules contain internal *cis* prolines, whereas none are detectable in trifluoroethanol. Simulations suggest that the *all-trans* form of polyproline is relatively stiff, with persistence lengths of 9–13 nm using different established force fields, and that the kinks arising from internal *cis* prolines are primarily responsible for the higher mean FRET efficiency in water. We show that the observed efficiency histograms and distributions of donor fluorescence lifetimes are explained by the presence of multiple species with efficiencies consistent with the simulations and populations determined by NMR. In calculating FRET efficiencies from the simulation, we find that the fluctuations of the chromophores, attached to long flexible linkers, also play an important role. A similar simulation approach suggests that the flexibility of the chromophore linkers is largely responsible for the previously unexplained high value of R_0 required to fit the data in the classic study of Stryer and Haugland.

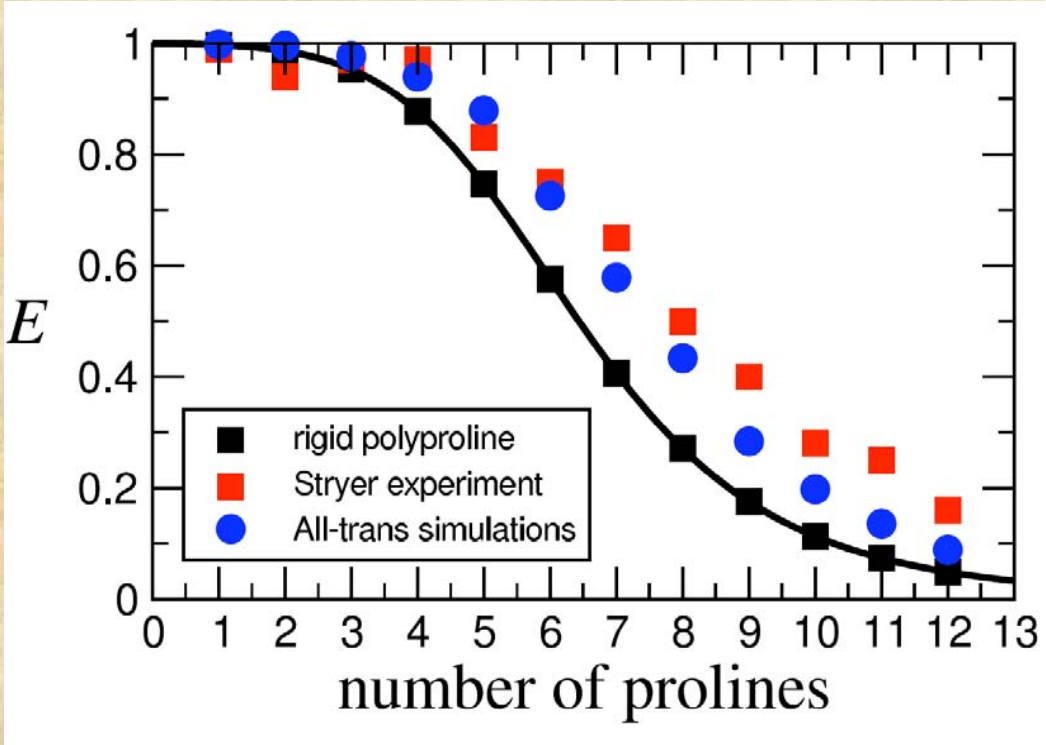

A related question that arose in the course of this work was whether donor/acceptor dynamics might explain the discrepancy mentioned earlier concerning the R_0 in the classic study of Stryer and Haugland (1). We found that simulations that included the dynamics of a naphthyl donor and dansyl acceptor resulted in increased FRET efficiency, explaining a large part of the difference between the calculated curves using the experimentally determined R_0 and the fitted R_0 (see SI Fig. 11).

Distributions

Proc. Nat. Acad. Sci. USA
Vol. 68, No. 9, pp. 2099–2101, September 1971

Determination of Distance Distribution Functions by Singlet-Singlet Energy Transfer

(flexibility/Förster theory/fluorescence/molecular structure)

CHARLES R. CANTOR AND PHILIP PECHUKAS

Proc. Nat. Acad. Sci. USA
Vol. 69, No. 8, pp. 2273–2277, August 1972

Evaluation of the Distribution of Distances Between Energy Donors and Acceptors by Fluorescence Decay

(energy transfer/fluorescence/decay/conformation/polymers)

A. GRINVALD, E. HAAS, AND I. Z. STEINBERG

$$E(R_0) = \int_0^\infty dR\, f(R)\, \frac{R_0^6}{R_0^6 + R^6}$$

Distributions

Proc. Nat. Acad. Sci. USA
Vol. 72, No. 5, pp. 1807–1811, May 1975

Distribution of End-to-End Distances of Oligopeptides in Solution as Estimated by Energy Transfer

(fluorescence decay/conformation)

ELISHA HAAS, MEIR WILCHEK, EPHRAIM KATCHALSKI-KATZIR, AND IZCHAK Z. STEINBERG

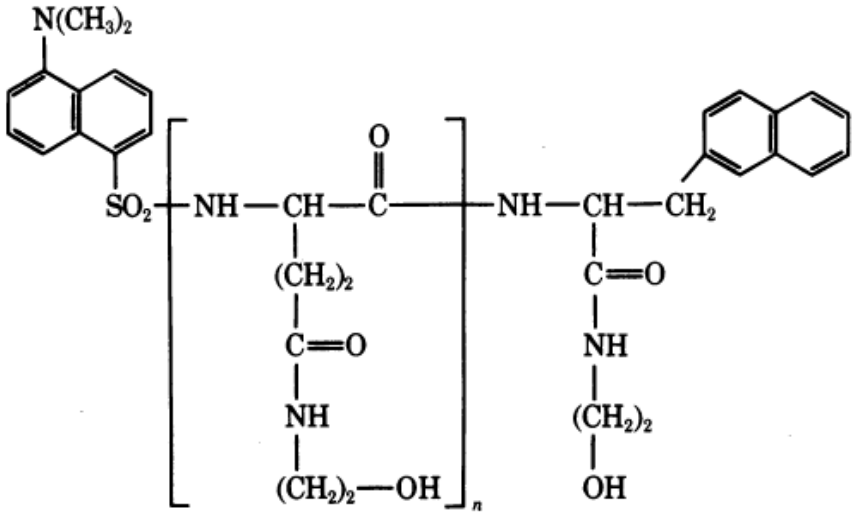

[I]

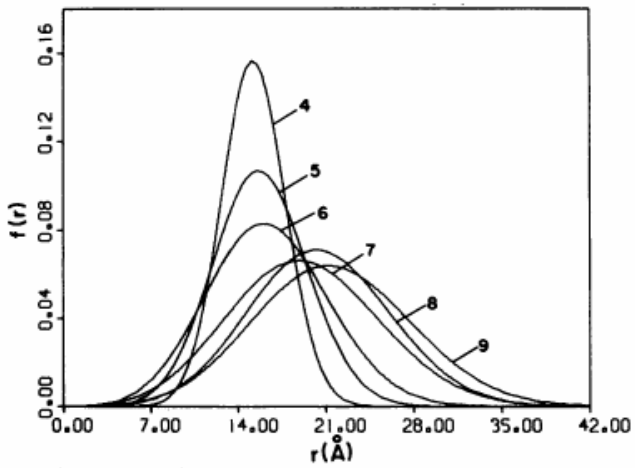

FIG. 4. The distribution function of the distances between donor and acceptor for the series of oligopeptides I, n = 4, 5, 6, 7, 8, and 9. The numbers in the figure refer to the values of n.

Distributions

Biochemistry **1988**, *27*, 9149–9160

Distance Distributions in Proteins Recovered by Using Frequency-Domain Fluorometry. Applications to Troponin I and Its Complex with Troponin C†

Joseph R. Lakowicz,*,‡ Ignacy Gryczynski,‡,§ Herbert C. Cheung,∥ Chien-Kao Wang,∥ Michael L. Johnson,⊥ and Nanda Joshi‡

 Biochemistry **1991**, *30*, 5238–5247

Distance Distributions and Anisotropy Decays of Troponin C and Its Complex with Troponin I†

Herbert C. Cheung,*,‡ Chien-Kao Wang,‡,§ Ignacy Gryczynski,∥ Wieslaw Wiczk,∥ Gabor Laczko,∥ Michael L. Johnson,⊥ and Joseph R. Lakowicz∥

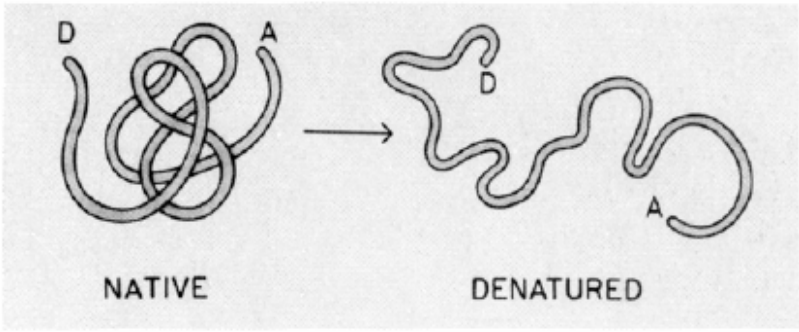

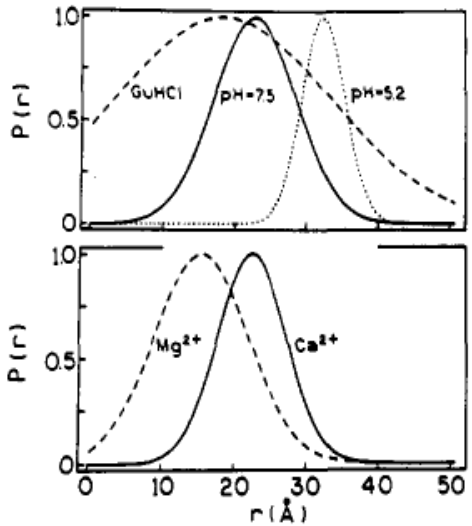

FIGURE 4: Distance distributions for TnC–DNZ–IAE in the absence of cations (top) and in the presence of Mg^{2+} and Ca^{2+} (pH 7.5, bottom). The pH for guanidine hydrochloride (GuHCl) was 7.5.

Proc. Natl. Acad. Sci. USA
Vol. 88, pp. 9355–9359, October 1991
Biochemistry

Differential flexibilities in three branches of an N-linked triantennary glycopeptide

(resonance energy transfer/oligosaccharides)

PENGGUANG WU, KEVIN G. RICE*, L. BRAND†, AND Y. C. LEE

Department of Biology, The Johns Hopkins University, Baltimore, MD 21218

ABSTRACT **The solution conformation behavior of complex oligosaccharides was studied by resonance energy transfer, as measured by the time-resolved fluorescence method, to determine the conformational heterogeneity of a triantennary glycopeptide at various temperatures. Groups that acted as a fluorescence donor (naphthyl-2-acetyl, Nap) or acceptor (dansylethylenediamine, Dan) were selectively attached to the N terminus of the peptide and a Gal residue [either 6′ (shown below), 6, or 8] of the oligosaccharide, respectively.**

(6′) Dan-Galβ4GlcNAcβ2Manα6 ↘
Manβ4GlcNAcβ4GlcNAcβ-Asn-Ala-NH-Nap
(6) Galβ4GlcNAcβ2Manα3 ↗
(8) Galβ4GlcNAcβ4 ↗

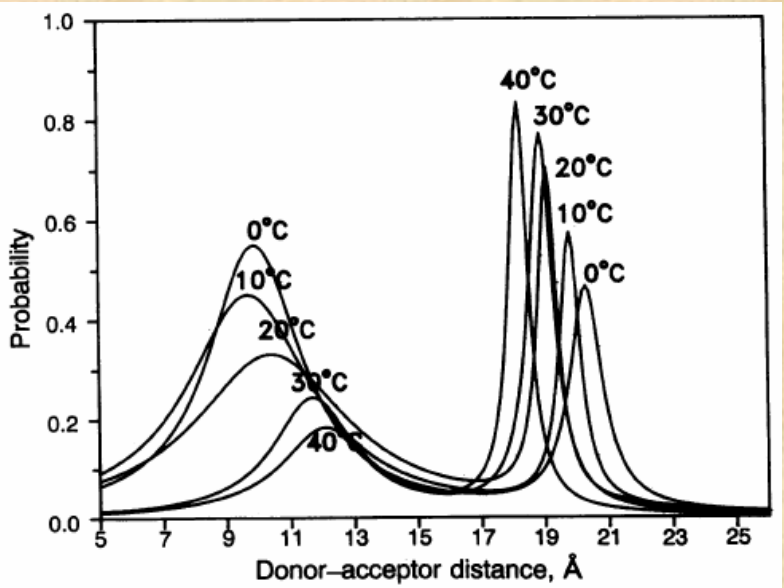

FIG. 6. Distance distribution of GP-6′-DanNap at various temperatures. Two distance populations were used to fit the data. The data were plotted to show the relative concentrations of each population by the peak at each temperature and for the same population (extended or folded) at different temperatures.

An impressive example of the use of FRET methodologies to study protein systems is given by the work of Lillo et al. ("Design and characterization of a multisite fluorescence energy-transfer system for protein folding studies: a steady-state and time-resolved study of yeast phosphoglycerate kinase" Biochemistry. 1997 Sep 16;36(37):11261-72 and "Real-time measurement of multiple intramolecular distances during protein folding reactions: a multisite stopped-flow fluorescence energy-transfer study of yeast phosphoglycerate kinase" Biochemistry. 1997 Sep 16;36(37):11273-81)

Site-directed mutagenesis was used to introduce pairs of cysteine residues in the protein at the positions shown

The pairs studied were:

135 – 290; 75 – 290

290 – 412; 412 – 202

135 – 412; 412 - 75

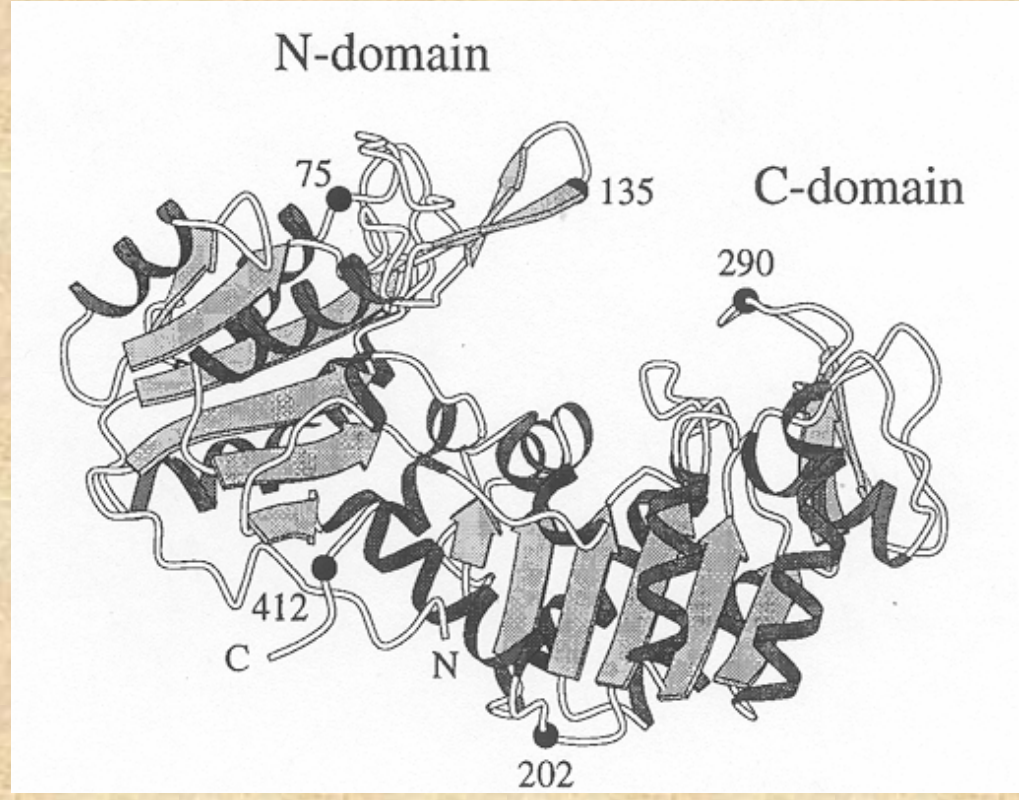

The donor was IAEDANS and the acceptor was IAF (iodoacetamindo-fluorescein). The various labeled protein products were separated by chromatography!

Table 1: Summary of the Labeled Proteins Examined for the Photophysical Characterization of Each Energy-Transfer Pair Cys*i* → Cys*j*

sample	name	Cys*i* → Cys*j*	no. of cysteines	fluorophore
donor only (D-PGK)	*i*-single cysteine	D- - -	1 (*i*)	AEDANS (*i*)
	j-single cysteine	- - -D	1 (*j*)	AEDANS (*j*)
	i-two cysteines	D- - -Cys	2 (*i*, *j*)	AEDANS (*i*)
	j-two cysteines	Cys- - -D	2 (*i*, *j*)	AEDANS (*j*)
	(*i*, *j*)-two cysteine average	D- - -Cys + Cys- - -D	2 (*i*, *j*)	AEDANS (*i*) + AEDANS (*j*)
	(*i*, *j*)-two cysteine "double donor"	D- - -D	2 (*i*, *j*)	AEDANS (*i*, *j*)
acceptor only	*i*-single cysteine	A- - -	1 (*i*)	AF (*i*)
	j-single cysteine	- - -A	1 (*j*)	AF (*j*)
donor-acceptor (D-PGK-A)	*i*, *j* specific label	D → A	2 (*i*, *j*)	AEDANS (*i*) and AF (*j*)
	j, *i* specific label	A ← D	2 (*i*, *j*)	AEDANS (*j*) and AF (*i*)
	i, *j* average label	D → A + A ← D	2 (*i*, *j*)	AEDANS (*i*) and AF (*j*) and + AEDANS (*j*) and AF (*i*)

Lifetime measurements were carried out on all samples

Table 5: Comparison of the Measured FRET Distances with That Predicted from the Crystal Structure[e]

energy-transfer pair	measured steady-state distance (Å)	measured time-resolved discrete distance		measured time-resolved distance distribution			crystal structure $C_\alpha \rightarrow C_\alpha$ (Å)[a]	estimated dye-to-dye distances (Å)[b]
		R (Å)	χ^2	R_c (Å) [±2]	σ (Å)	χ^2		
135 ↔ 290	43	43.3	2.7	39.4	7.3	1.3	39	39
		40.3[c]	1.6	38.8[c]	6.1	1.2		
135 ↔ 412	40	40.4	2.7	39.5	3.8	1.3	40	46
412 → 135	40	39.5	2.1	38.0	3.9	1.2		
		38.7	1.4	38.1[c]	3.4	1.3		
290 ↔ 412	69	63.6	1.4	64.8	13.5	1.3	48	56
		56.6[c]	1.8	58.6[c]	13.2	1.4		
75 ↔ 290	50	51.7	4.3	46.6	13.5	1.2	40	46
202 ↔ 412	39	41.7	1.5	37.8	6.6	1.1	26	34
412 → 75	47	48.2	3.1	44.8	13.5	1.4	32	46
all[d]	–	60–70	1.1	60–80	15–30	1.1	–	–

[a] Watson et al. (1982). [b] Donor-to-acceptor distance from MD simulations based on Watson et al. (1982) crystal structure. [c] Acceptor-side FRET measurements. [d] Unfolded samples (MOPS buffer at pH 7.5 and 25 °C and 2 M GuHCl). [e] MOPS buffer at pH 7.5 and 25 °C. D ↔ A: average labeled samples (donor distributed between the two Cys sites). D → A: specific labeled samples. Unless otherwise indicated, distance determinations are from donor-side experiments. The errors on the recovered distances are dominated by "nonfitting" sources and are estimated to be ±3 Å (see the text).

The intramolecular distances for the six energy transfer pairs are recovered for the each intermediate formed during the GuHCL induced unfolding of PGK

The authors proposed a specific structural transition associated with the unfolding of PGK from the native state (left) to the first unfolded state (right).

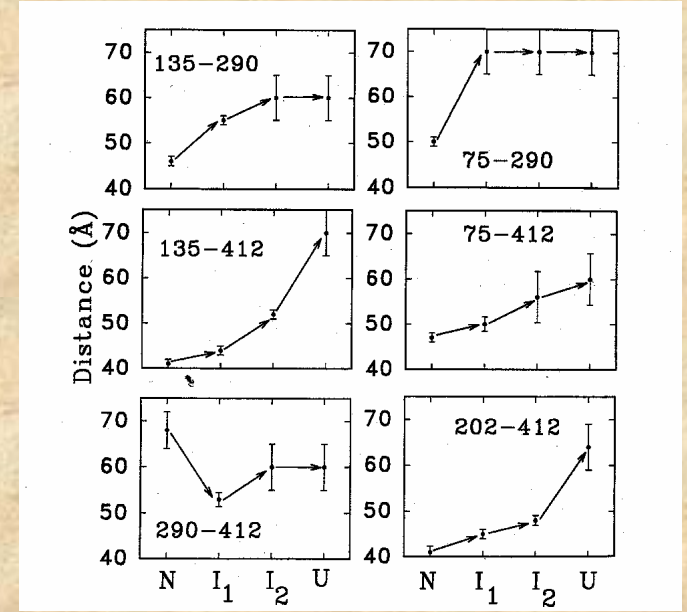

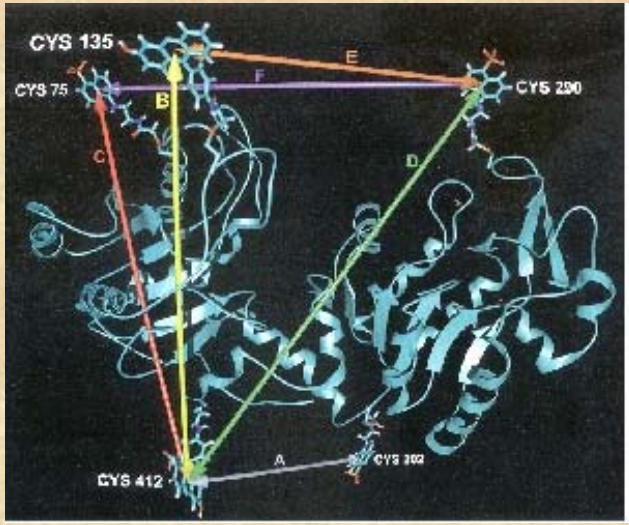

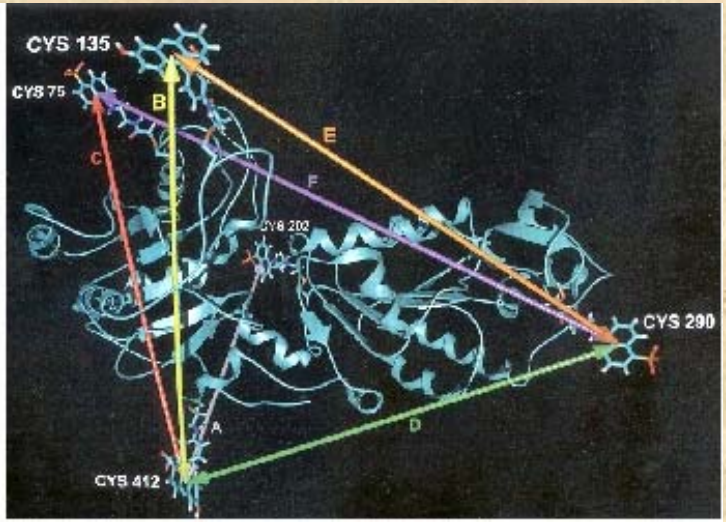

The C terminal domain (on the right of the monomer) is twisted by approximately 90º relative to the N-terminal domain resulting in an increase in the distances A,E and F and a shortening of the distance D.

The orientation factor κ^2

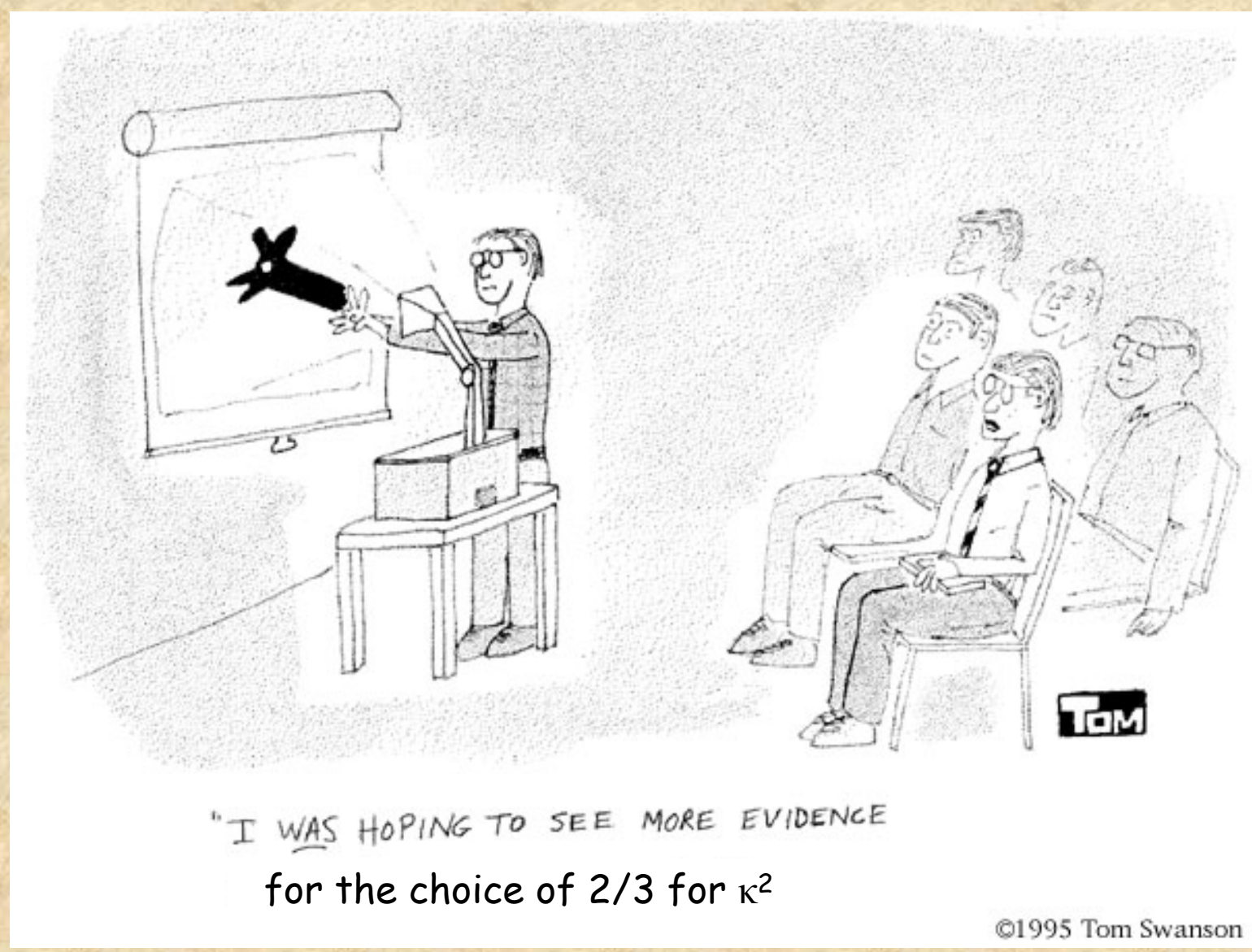

for the choice of 2/3 for κ^2

The orientation factor κ^2

$$\kappa^2 = (\cos\theta_T - 3\cos\theta_D \cos\theta_A)^2$$

Where θ_T is the angle between the D and A moments, given by

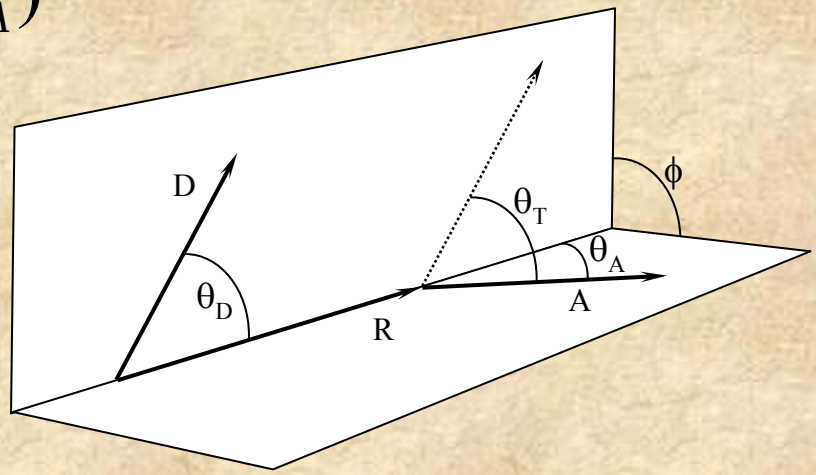

$$\cos\theta_T = \sin\theta_D \sin\theta_A \cos\phi + \cos\theta_D \cos\theta_A$$

In which θ_D, θ_A are the angles between the separation vector R, and the D and A moment, respectively, and ϕ is the azimuth between the planes (D,R) and (A,R)

The orientation factor κ^2

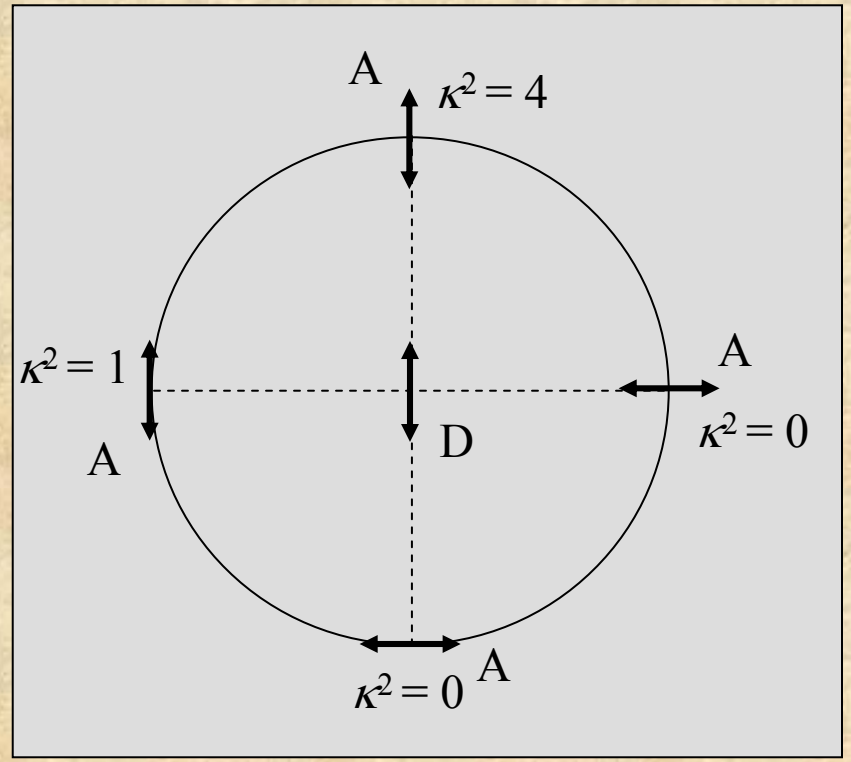

The limits for κ^2 are 0 to 4, The value of 4 is only obtained when both transitions moments are in line with the vector R. The value of 0 can be achieved in many different ways.

If the molecules undergo fast isotropic motions (dynamic averaging) then $\kappa^2 = 2/3$

From Eisinger and Dale in:"Excited States of Biological Molecules" Edited by John Birks (1976)

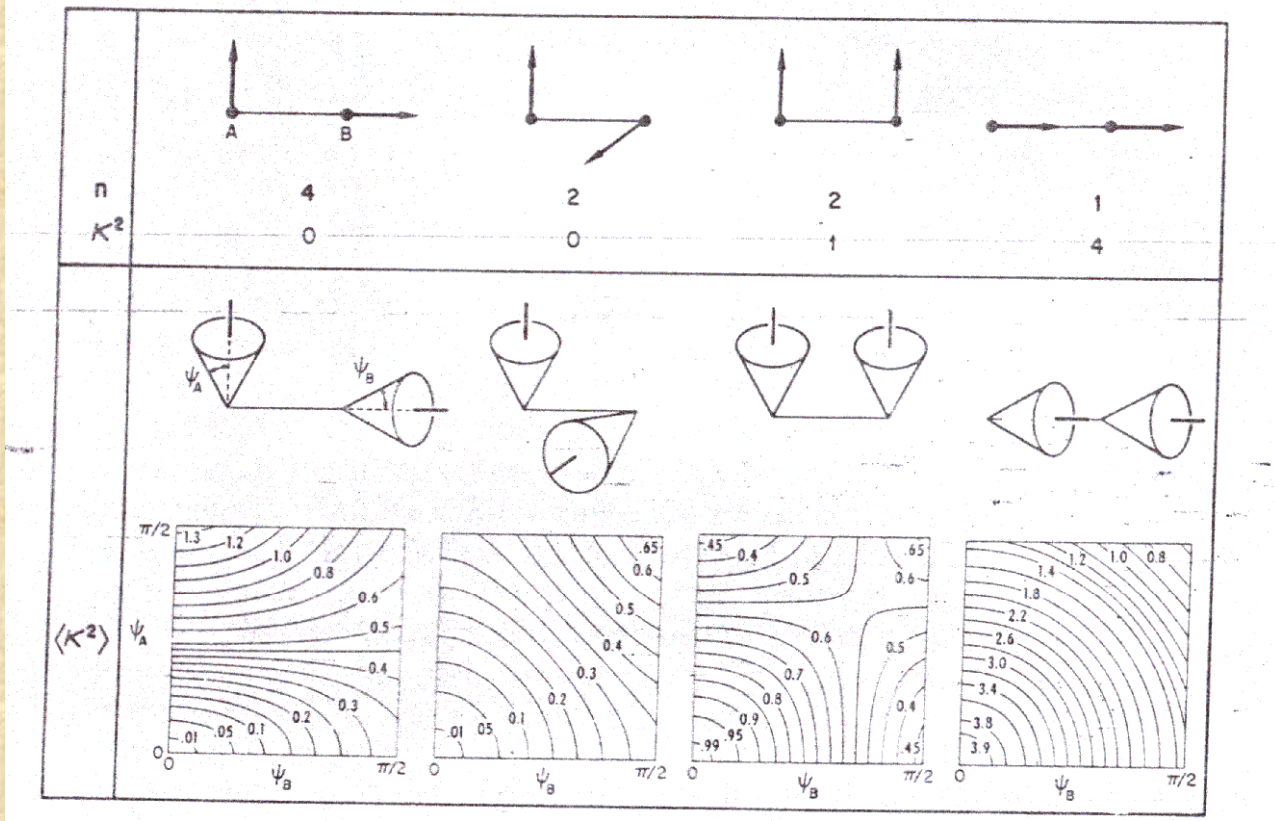

Figure 1 The upper part of the diagram illustrates the nine possible relative orientations of two transition dipoles each of which is fixed and can lie along either the x, y or z axis of a Cartesian triad. The corresponding κ^2 values are shown along with their statistical weights (n) and they are seen to lead to an average for κ^2 of 2/3, the same as for isotropically random orientations of the transition dipole moments. The lower part of the figure illustrates how these $\langle\kappa^2\rangle$ values change as the transition dipole directions are permitted orientational freedom within cones of half-angles ψ_A and ψ_B. Note that $\langle\kappa^2\rangle$ departs quite slowly from its fixed minimum and maximum values (0 and 4) as the two cones open up and that when each cone half-angle is $\pi/2$, corresponding to an isotropic distribution of the transition dipole directions, $\langle\kappa^2\rangle$ is equal to 2/3 for each of the cases considered

What if the system is static but randomly oriented?

For example for a system in a highly viscous solvent or in general if the fluorescence lifetimes are very short relative to any rotational motion.

Then $\kappa^2 = 0.476$

THE JOURNAL OF CHEMICAL PHYSICS VOLUME 48, NUMBER 6 15 MARCH 1968

Nonradiative Energy Transfer in Systems in which Rotatory Brownian Motion is Frozen

IZCHAK Z. STEINBERG

The Weizmann Institute of Science, Rehovoth, Israel

(Received 28 August 1967)

The effect of the complete restriction of rotatory Brownian motion of donor and acceptor molecules on the extent of nonradiative energy transfer in systems containing many donors and acceptors has been investigated. It is assumed that the molecules under discussion are randomly distributed and randomly oriented in space at the moment of excitation. The number of donor molecules which retain their excitation energy at time t after excitation is found to decrease exponentially with the sum of two terms: one proportional to t and the other proportional to $t^{1/2}$. This time dependence is similar in form to that found by Förster for systems in which donor and acceptor molecules undergo rapid rotatory diffusion. While the coefficient of $-t$ in the exponent is the same in both cases, the coefficient of $-t^{1/2}$ is smaller for systems in which molecular rotation is frozen than for systems in which rotatory Brownian motion is rapid.

But don't ask me to prove it!

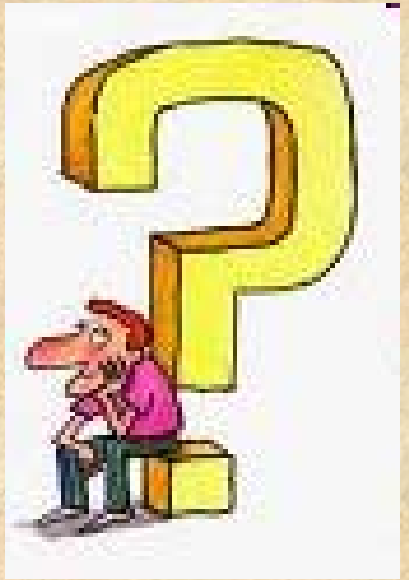

So how do we determine κ^2?

Except in very rare cases, κ^2 can not be uniquely determined in solution.

What value of κ^2 should be used ?

We can **assume** fast isotropic motions of the probes and value of $\kappa^2 = 2/3$, and verify experimentally that it is indeed the case.

We can **calculate** the lower and upper limit of κ^2 using polarization spectroscopy (Dale, Eisinger and Blumberg 1979).

Assuming $\kappa^2 = 2/3$

We can test this assumption experimentally:

***By swapping probes*:** The micro-environment of the probes will be different. Therefore, if the micro-environment affect the probes mobility and, κ^2 is not equal to 2/3, once swapped, the value of κ^2 will changed and hence the distance measured by FRET.

By using different probes: If the distance measured using different probe pairs are similar (taking into account the size of the probes) then the assumption that κ^2 is equal to 2/3 is probably valid.

Lower and upper limit of κ^2

We can **calculate** the lower and upper limit of κ^2 using polarization (Dale, Eisinger and Blumberg 1979).

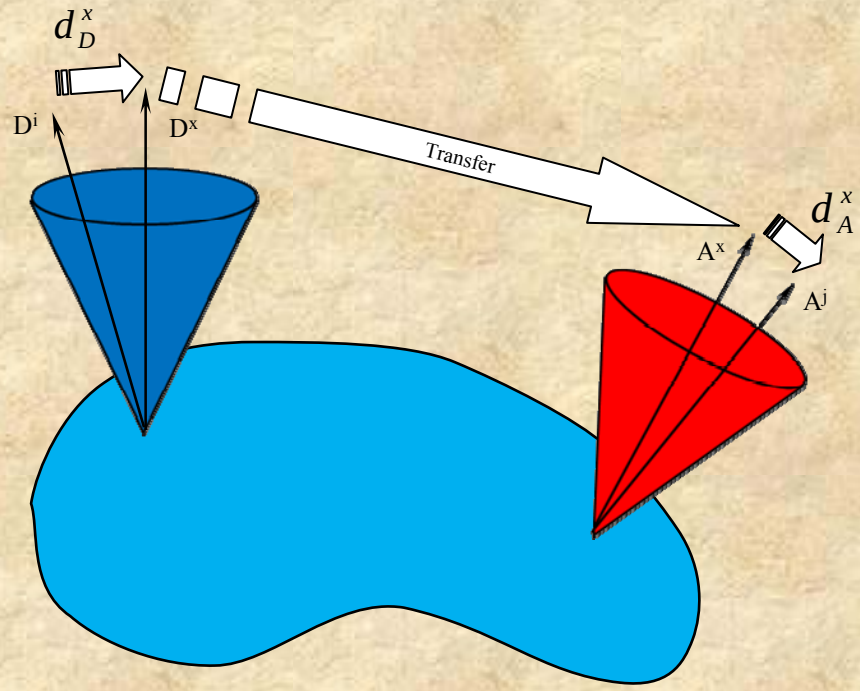

Lets consider that the each probe are rotating within a cone of axes D^x and A^x for the donor and acceptor, respectively, then 3 depolarization steps occurs after the absorption of the excitation energy by the donor: An axial depolarization of the donor, a depolarization due to transfer and an axial depolarization of the acceptor

In the Dale-Eisinger-Blumberg approach, one measures the ratio of the observed polarizations of donors and acceptors to their limiting polarizations and then uses the calculated contour plots to put limits on κ^2

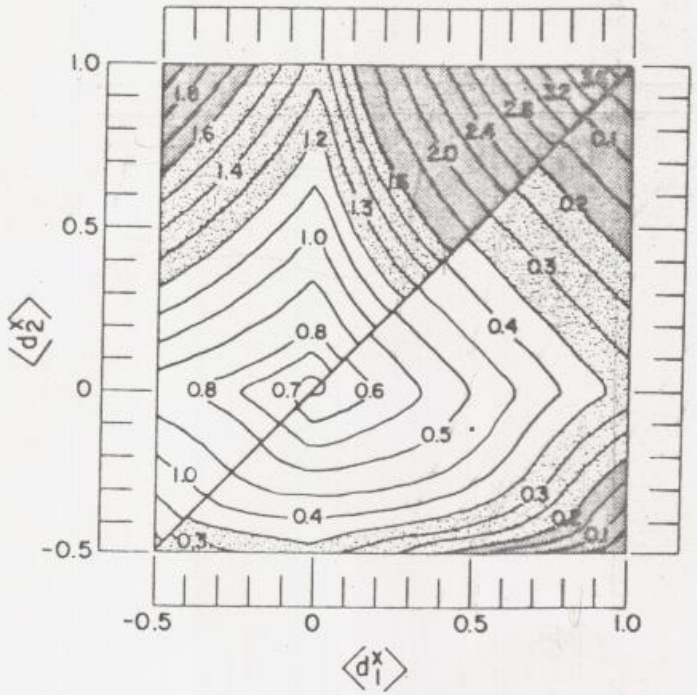

FIGURE 9 Contour plot similar to those shown in Figs. 4–8, but applicable in situations in which $\langle d_T \rangle$, and hence d_T^x, is unknown. It is obtained by maximizing and minimizing Eq. 21 and can be seen to lead to larger ranges between $\langle \kappa^2 \rangle_{min}$ and $\langle \kappa^2 \rangle_{max}$ than the plots of Figs. 4–8. In the heavily stippled regions the error in R resulting from the use of $\langle \kappa^2 \rangle = \frac{2}{3}$ instead of the indicated $\langle \kappa^2 \rangle_{min}$ and $\langle \kappa^2 \rangle_{max}$ is greater than 20%. It is between 10% and 20% in the lightly stippled regions and less than 10% in the unstippled ones.

This approach was used in:
Arbildua et al.,
Fluorescence resonance energy transfer and molecular modeling studies on 4',6-diamidino-2-phenylindole (DAPI) complexes with tubulin.
Protein Sci. (2006) 15(3):410-9.

FRET occurs between DAPI and TNP-GTP bound to tubulin – a heterodimer protein

DAPI

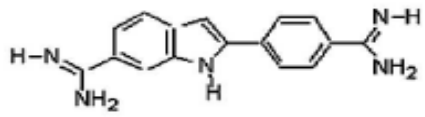

TNP-GTP

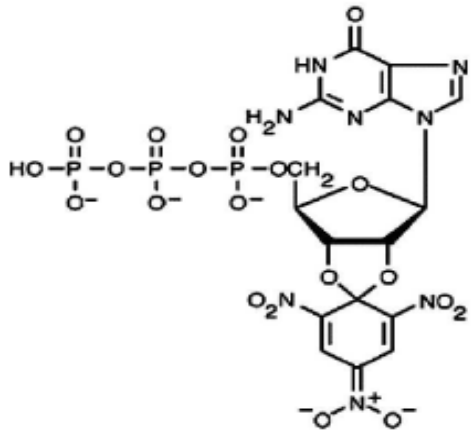

Figure 1. Structures of 4′-6-diamidino-2-phenylindole (DAPI) and 2′,3′-*O*-(2,4,6-trinitrocyclohexadienylidene)-GTP (TNP-GTP) at neutral or basic pH.

Assuming a κ^2 value of 2/3, one would calculate the DAPI-TNP-GTP distance to be ~43 Angstoms

But DAPI is bound non-covalently - hence has no local motion so its polarization is high (~0.42)

And, TNP-GTP is also non-covalently bound and has a short lifetime and hence a high polarization (~0.48)

These observed polarization values are close to the limiting polarization values for these probes: 93% and 100% respectively, for DAPI and TNP-GTP

Using the Dale-Eisenger-Blumberg plot one can then estimate that κ^2 can be anywhere between 0.02 and 3.7!

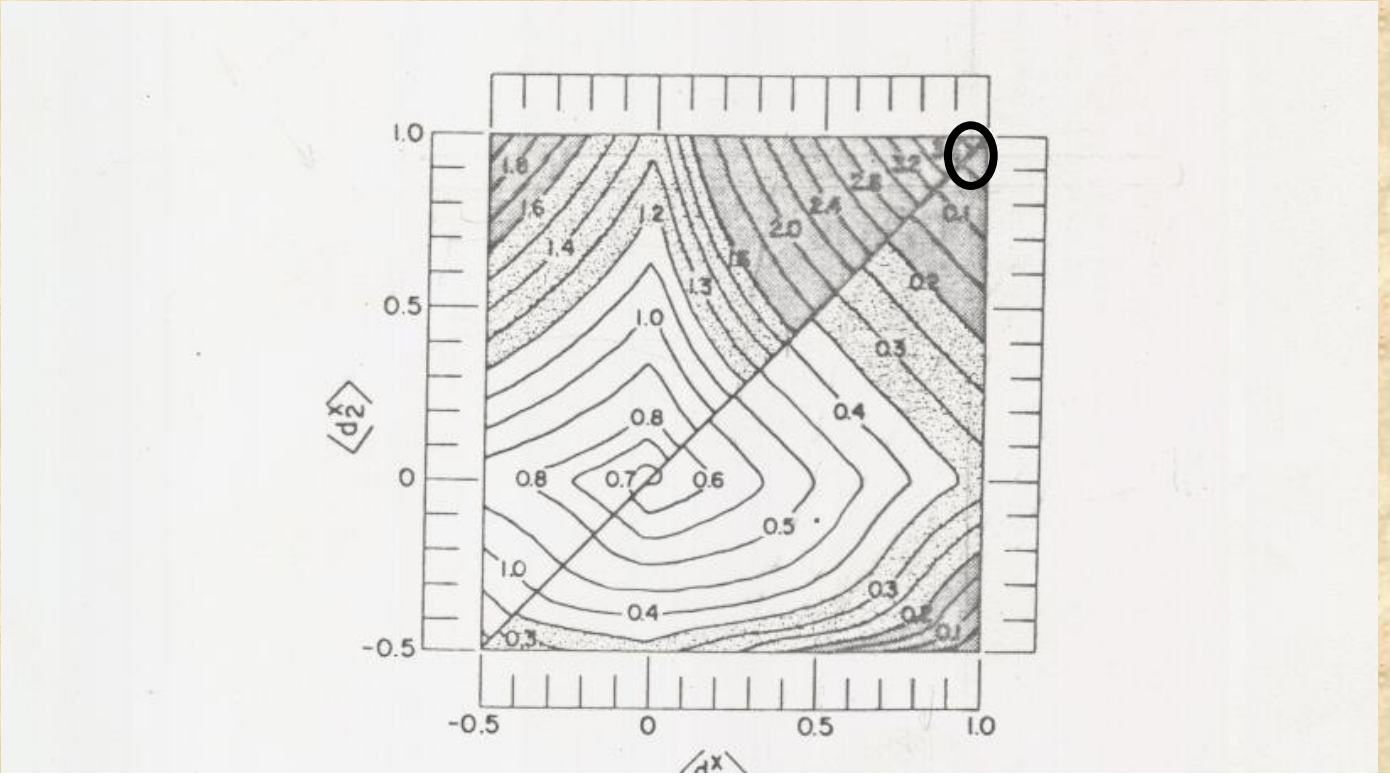

In fact the authors concluded, based on other information, that the distance between DAPI and TNP-GTP bound to tubulin was likely to ~ 30 Angstroms.

BIOPOLYMERS VOL. 13, 1607–1620 (1974)

Energy Transfer in tRNA^{Phe} (Yeast). The Solution Structure of Transfer RNA

W. E. BLUMBERG, R. E. DALE,* J. EISINGER, and
D. M. ZUCKERMAN, *Bell Laboratories, Inc.,*
Murray Hill, New Jersey 07974

TABLE II
Maximum and Minimum Values of the Orientation Factor and Ratio of Derived Separation R to that Obtained Using the Dynamic Random Average (Isotropic) Value $R_{2/3}$

Model[a]		Figure[a]	Y–A	$\langle\kappa^2\rangle$	$R/R_{2/3}$
4(1)	*cc*	10	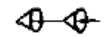	3.13 ± 0.08	1.29 ± 0.01
	cC	11	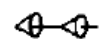	3.13 ± 0.08	1.29 ± 0.01
	Cc	11	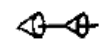	3.13 ± 0.08	1.29 ± 0.01
	CC	12	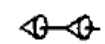	3.13 ± 0.08	1.29 ± 0.01
4(2)	*cc*	13	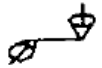	0.115 ± 0.012	0.75 ± 0.01
	cC	14	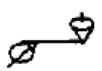	0.115 ± 0.012	0.75 ± 0.01
	Cc	14	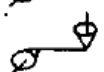	0.115 ± 0.012	0.75 ± 0.01
	CC	15	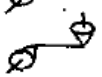	0.115 ± 0.012	0.75 ± 0.01

CCA Terminus—Anticodon Separation

Assuming an average value of 2/3 for κ^2, Beardsley and Cantor[2] estimated the separation between the *Y* base adjacent to the anticodon and acriflavine bound at the CCA terminus of $tRNA^{Phe}$ (yeast) to be about 46 Å. The analysis presented here indicates a possible range of 34–61 Å at the most.

Taking into account the uncertainty in the location of the acriflavine chromophore with respect to the CCA stem (as indicated above it may well be intercalated back into a nearby double-helical region, not necessarily in the CCA limb), the upper limit is reasonably consistent with the 77 Å separation between the extended CCA terminus and the anticodon triplet recently determined by X-ray crystallography.[2]

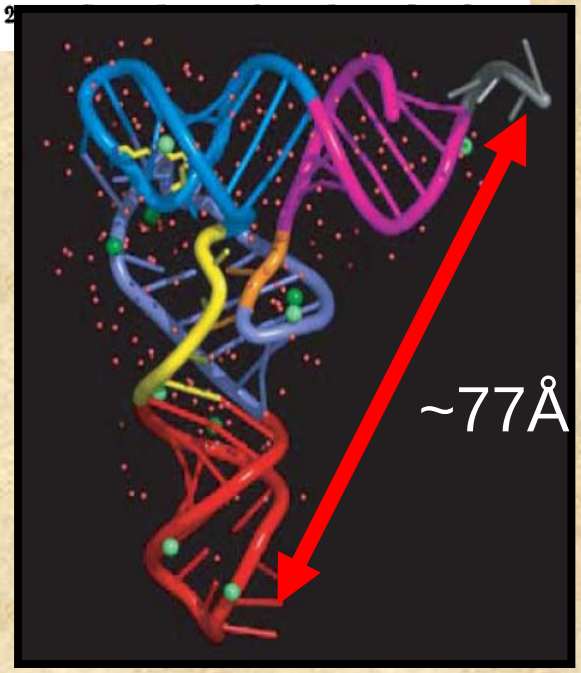

Quantitative distance determinations using FRET – i.e., as a true “spectroscopic ruler” - remain **difficult at best**

But FRET can be very powerful when used to detect changes in a system, such as alterations in distance and or orientation between donor and acceptor attached to biomolecules, i.e., due to ligand binding or protein-protein interactions

The renaissance of fluorescence resonance energy transfer

Paul R. Selvin

Recent advances in fluorescence resonance energy transfer have led to qualitative and quantitative improvements in the technique, including increased spatial resolution, distance range, and sensitivity. These advances, due largely to new fluorescent dyes, but also to new optical methods and instrumentation, have opened up new biological applications.

nature structural biology • volume 7 number 9 • september 2000

The development of Fluorescent Proteins has led to a significant increase in FRET studies

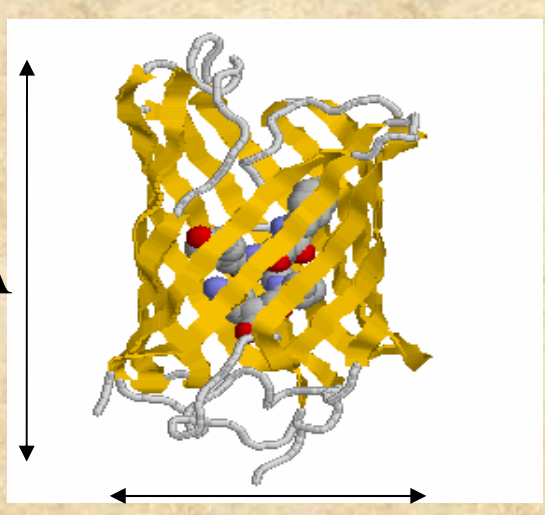

The GFP is fused to the protein of interest and expressed in the organism under study.

Fluorescent proteins with the appropriate absorption and emission properties are chosen as donors and acceptors. Such systems can be used in vitro as well as in vivo

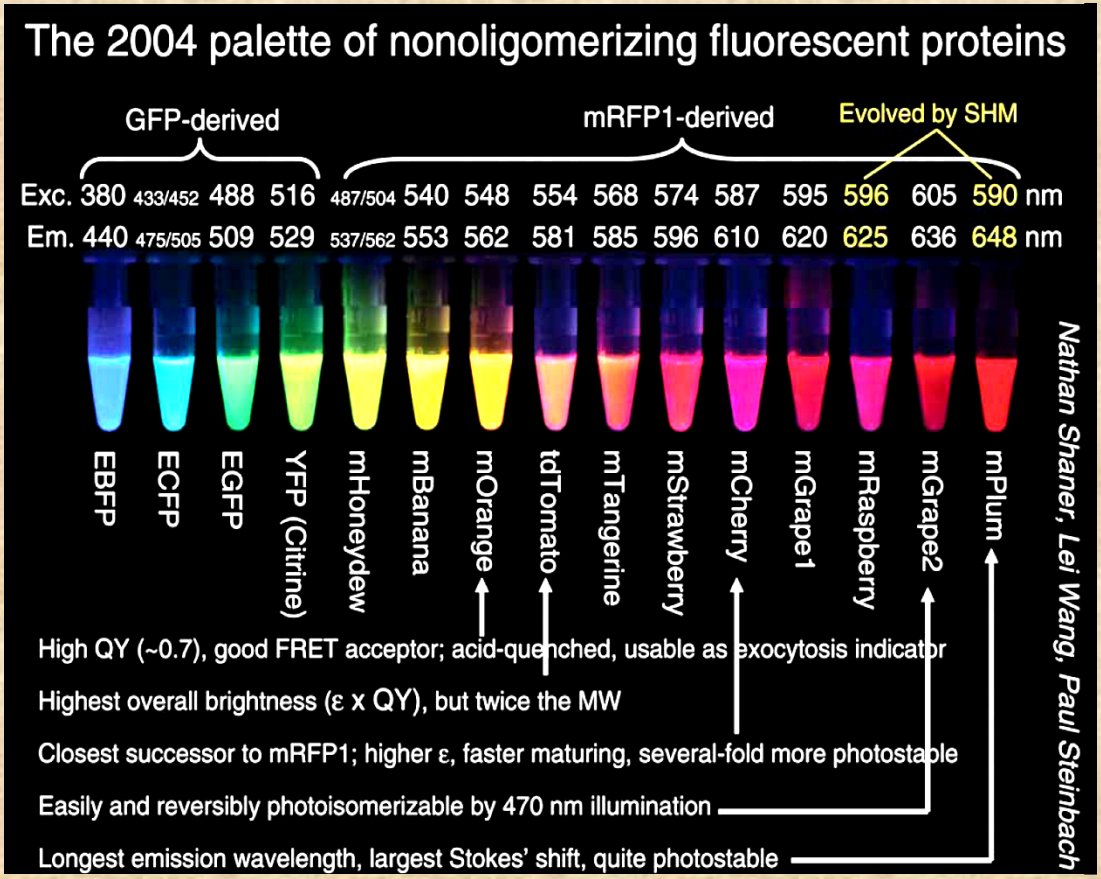

First application of FRET using of Fluorescent Proteins

Gene, 173 (1996) 13–17

GENE 09471

Fluorescence resonance energy transfer between blue-emitting and red-shifted excitation derivatives of the green fluorescent protein *

(FRET; *Aequorea victoria*; fluorescent proteins; factor X_a)

Robi D. Mitra[a], Christopher M. Silva[b] and Douglas C. Youvan[b]

We have constructed a concatemer of two GFP mutants that exhibits FRET. A blue fluorescent protein (BFP5) with an excitation band at 385 nm and an emission band at 450 nm is joined to a red-shifted GFP (RSGFP4) with an excitation band at 488 nm and an emission band at 505 nm. The two mutants are separated by a 20 amino acid flexible peptide linker that contains a Factor X_a protease site. When excited at 385 nm, two emission bands are obtained, one at 450 nm, and another at 505 nm, due to energy transfer from BFP5 to RSGFP4. Upon cleavage of the RSGFP4::BFP5 fusion with Factor X_a, the band at 505 nm disappears, and there is an increase in the fluorescence observed at 450 nm. This is the first demonstration of FRET between two GFP derivatives.

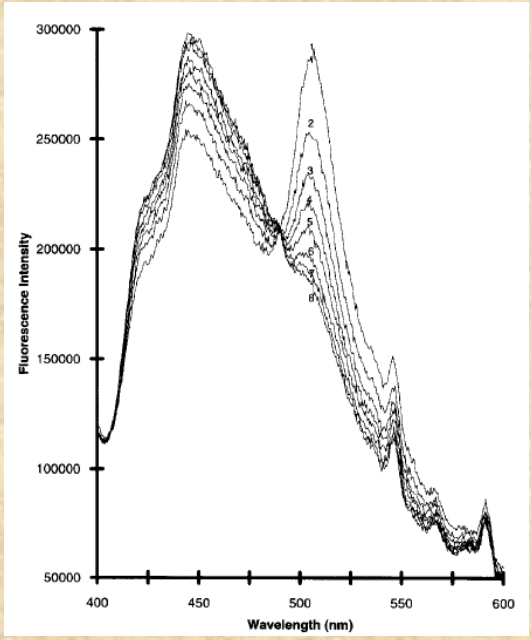

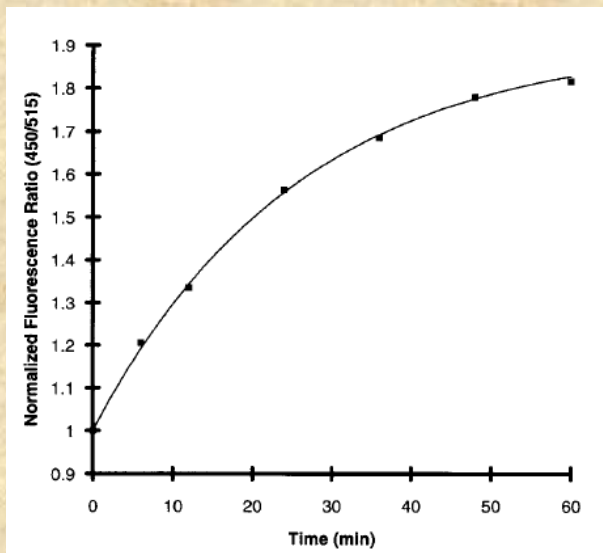

Homo-transfer of electronic excitation energy

So far, we considered the donor and acceptor molecules to be different.However, if the probe excitation spectrum overlaps its emission spectrum, FRET can occur between identical molecules.

« Il suffit qu'un transfert d'activation puisse se produire entre deux molécules voisines d'orientation différentes, c'est a dire portant des oscillateurs non parallèles, pour qu'il en résulte en moyenne une diminution de l'anisotropie de distribution des oscillateurs excites et par suite de la polarisation de la lumière émise. »

(F. Perrin *Ann de Phys.* 1929)

It suffices that a transfer of activation can occur between two neighboring molecules with different orientations, that is with non-parallel oscillators, in order to have, on average, a decrease in the anisotropy of the distribution of excited oscillators, and therefore a decrease of the polarization of the emitted light.

« …L'existence de transferts d'activation est expérimentalement prouvée pour de telles molécules par la décroissance de la polarisation de la lumière de fluorescence quand la concentration croit… »
(F. Perrin *Ann de Phys*. 1932)

…The existence of transfer of activation is proven experimentally for such molecules by the decrease in polarization of the fluorescent light when the concentration is increased…

Electronic energy transfer between identical fluorophores was originally observed by Gaviola and Pringsheim in 1924.

Über den Einfluß der Konzentration auf die Polarisation der Fluoreszenz von Farbstofflösungen.

Von **E. Gaviola** und **Peter Pringsheim** in Berlin.

Mit zwei Abbildungen. (Eingegangen am 24. März 1924.)

Tabelle 2. Uranin in ganz wasserfreiem Glycerin.

C	p	C	p	C	p	C	p
$\frac{1}{4}$	0	$\frac{1}{32}$	6,5	$\frac{1}{256}$	15	$\frac{1}{2048}$	39,2
$\frac{1}{8}$	?	$\frac{1}{64}$	8,1	$\frac{1}{512}$	19,5	$\frac{1}{4100}$	43,5
$\frac{1}{16}$	3,2	$\frac{1}{128}$	11,1	$\frac{1}{1024}$	30,7	etwa $\frac{1}{20000}$	45

(note: uranin is the sodium salt of fluorescein)

Homo-transfer of electronic excitation energy

"…Excitation transfer between alike molecules can occur in repeated steps. So the excitation may *migrate* from the absorbing molecule over a considerable number of other ones before deactivation occurs by fluorescence or other process. Though this kind of transfer cannot be recognized from fluorescence spectra, it may be observed by the decrease of fluorescence polarization…" (Förster, 1959)

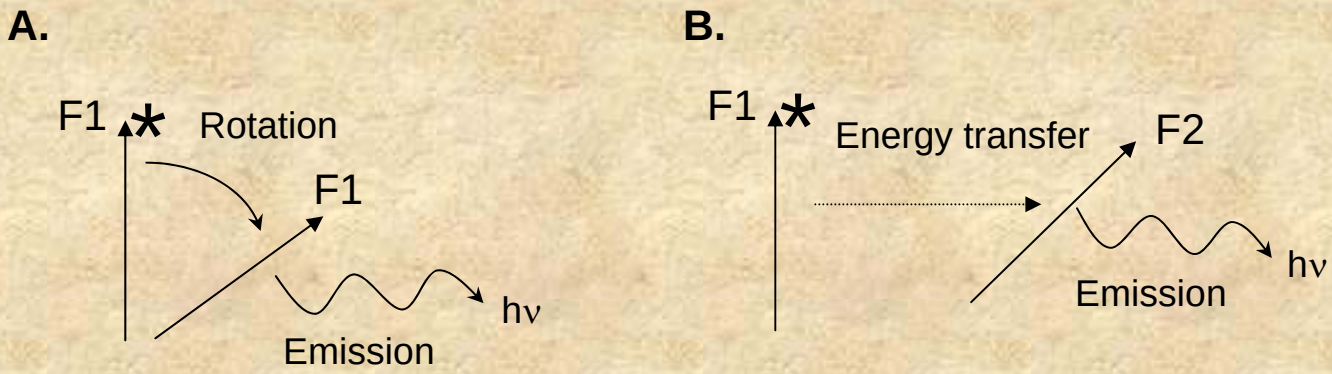

A. Depolarization resulting from rotational diffusion of the fluorophore. The excited fluorophore (F1*) rotates then emits light. **B.** The excited fluorophore (F1*) transfer energy to another fluorophore F2 which in turn emits light.

Weber's Red-Edge Effect

In 1960 Weber was the first to report that homotransfer among indole molecules disappeared upon excitation at the red-edge of the absorption band - this phenomenon is now known as the "Weber red-edge effect".

In 1970 Weber and Shinitzky published a more detailed examination of this phenomenon. They reported that in the many aromatic residues examined, transfer is much decreased or undetectable on excitation at the red edge of the absorption spectrum .

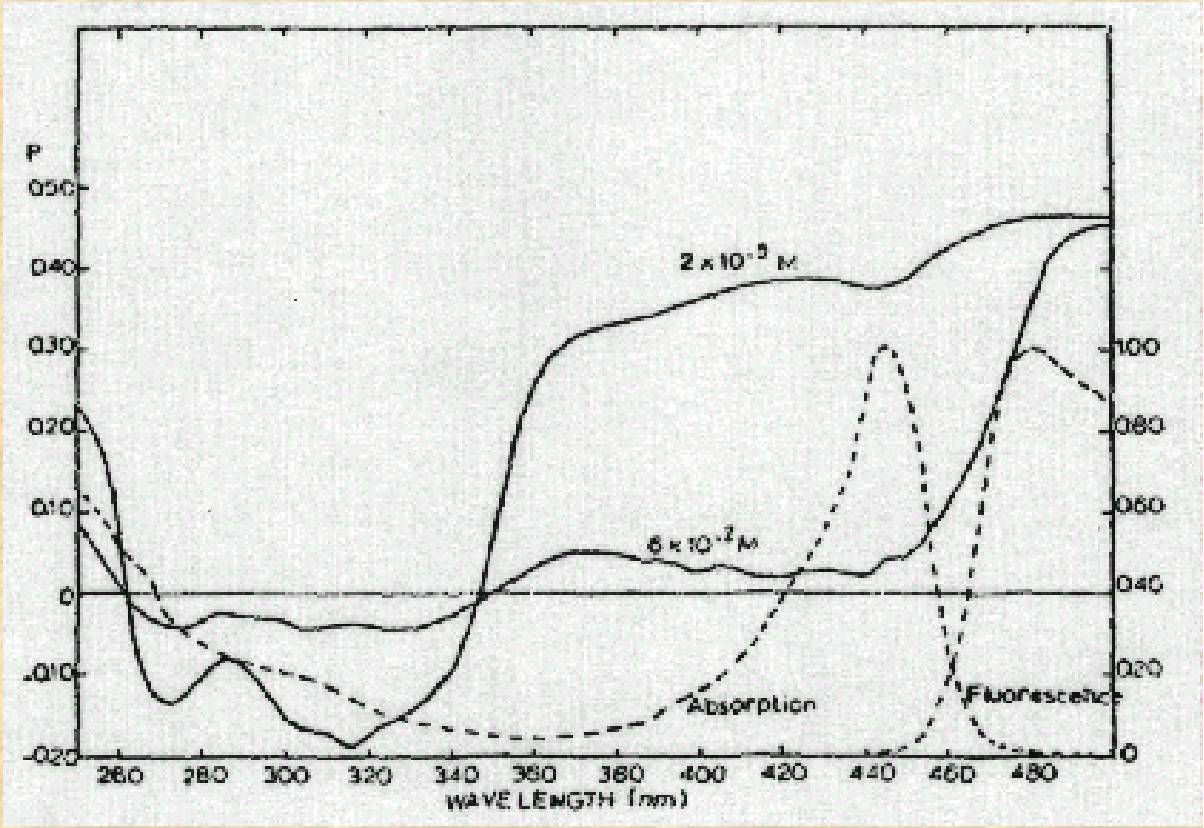

Distance determination using homotransfer

The efficiency of transfer can be calculated from a knowledge of the polarization in the absence and presence of energy transfer.

The steady state expression for the efficiency of energy transfer (*E*) as a function of the anisotropy is given by

$$E = 2(r_d - \langle r \rangle)/(r_d - r_a)$$

Where r_d and r_a are the anisotropy decay of the donor and acceptor only, respectively and $\langle r \rangle$ is the observed anisotropy in presence of both donor and acceptor. If κ^2 =2/3 then r_a = 0 and

$$E = 2(r_d - \langle r \rangle)/r_d$$

An example of homo-FRET used to study protein interactions is the work by Hamman et al (Biochemistry *35*:16680) on a prokaryotic ribosomal protein

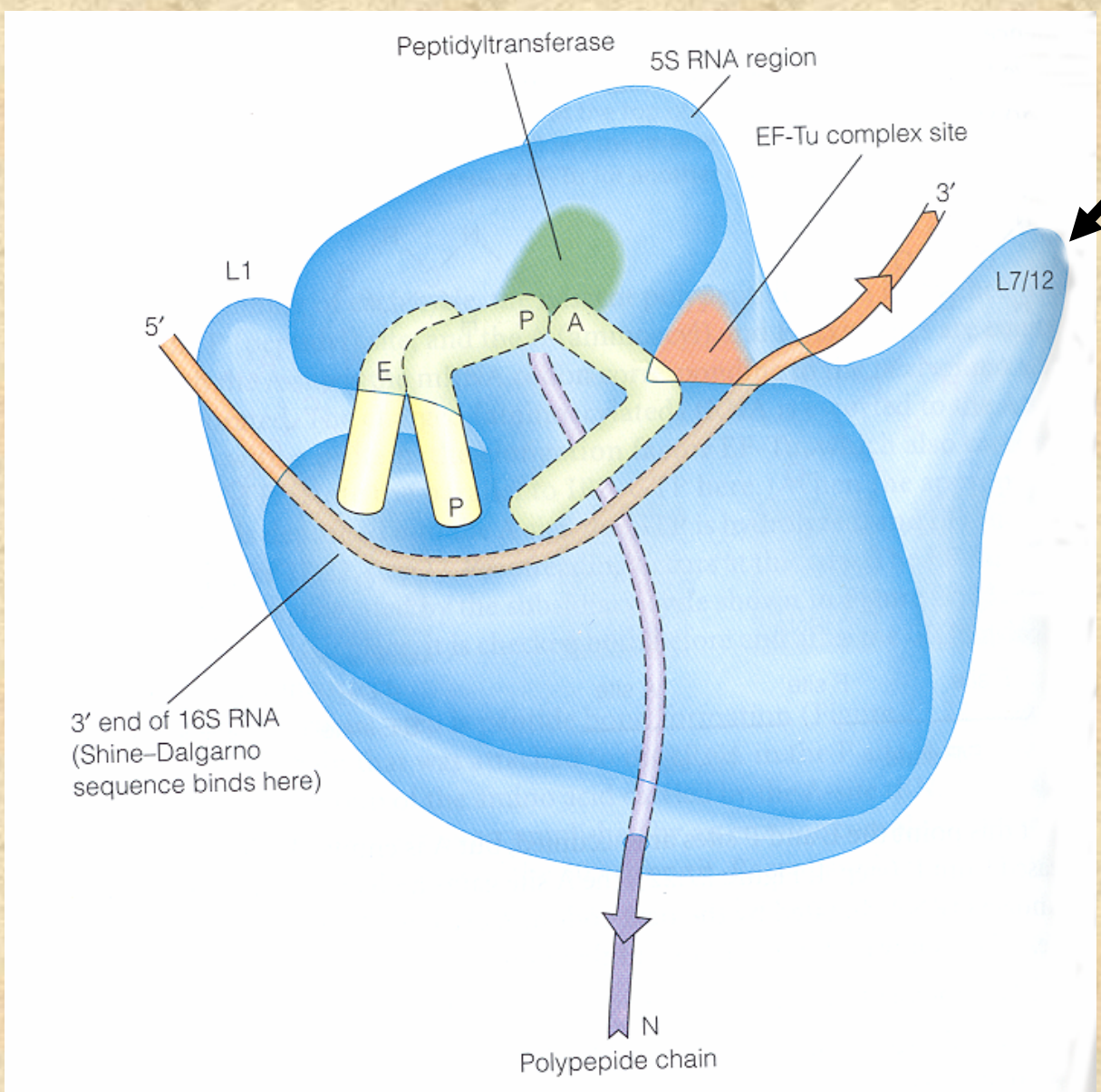

L7/L12 is present as two dimers in the ribosome. An X-ray structure of monomeric C-terminal domains led to the speculation that the C-terminal domains of L7/L12 interacted through hydrophobic surfaces as shown below

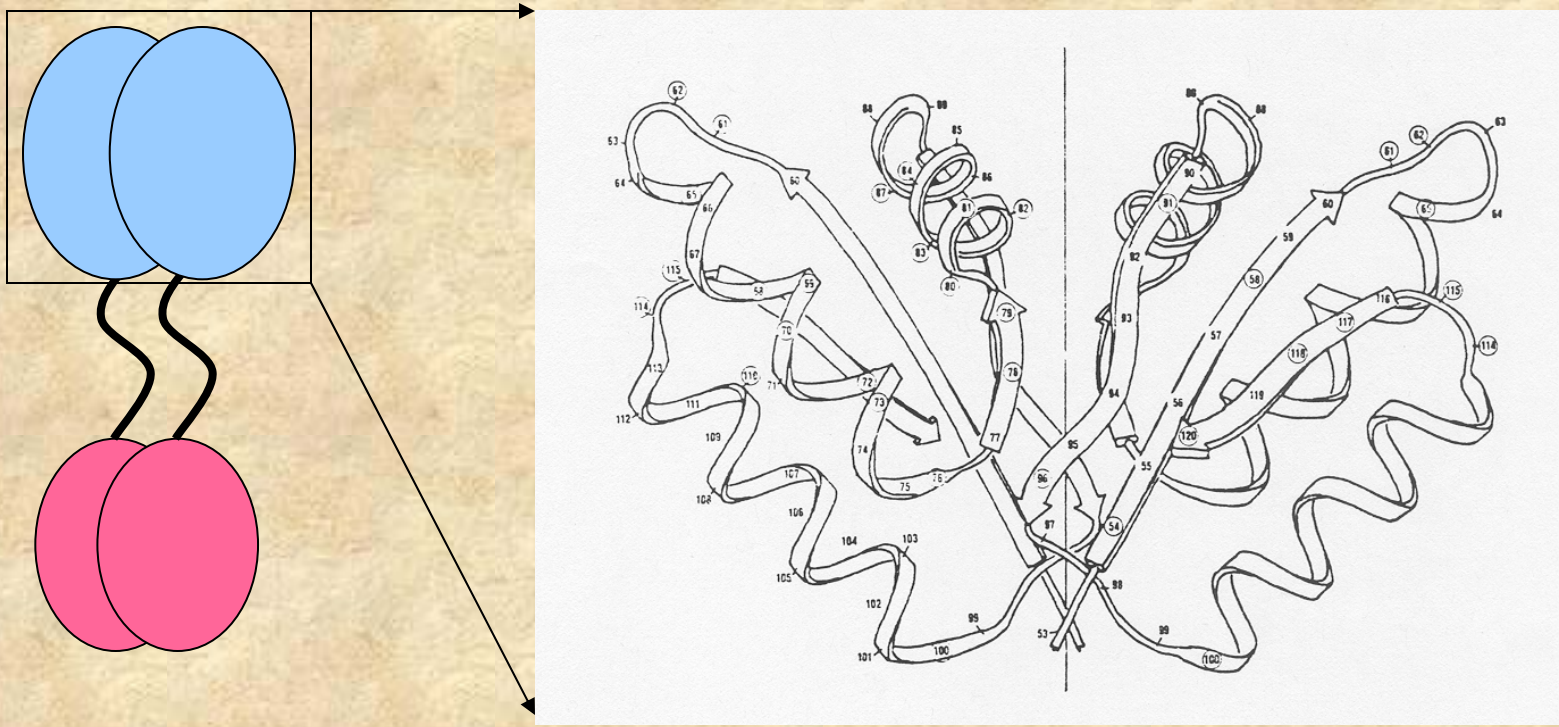

To study this protein fluorescence probes were introduced at specific locations along the L7/L12 peptide backbone.

To introduce these probes at specific locations site-directed mutagenesis was used to place cysteine residues in different locations

Sulfhydryl-reactive fluorescence probes were then covalently attached to these cysteine residues

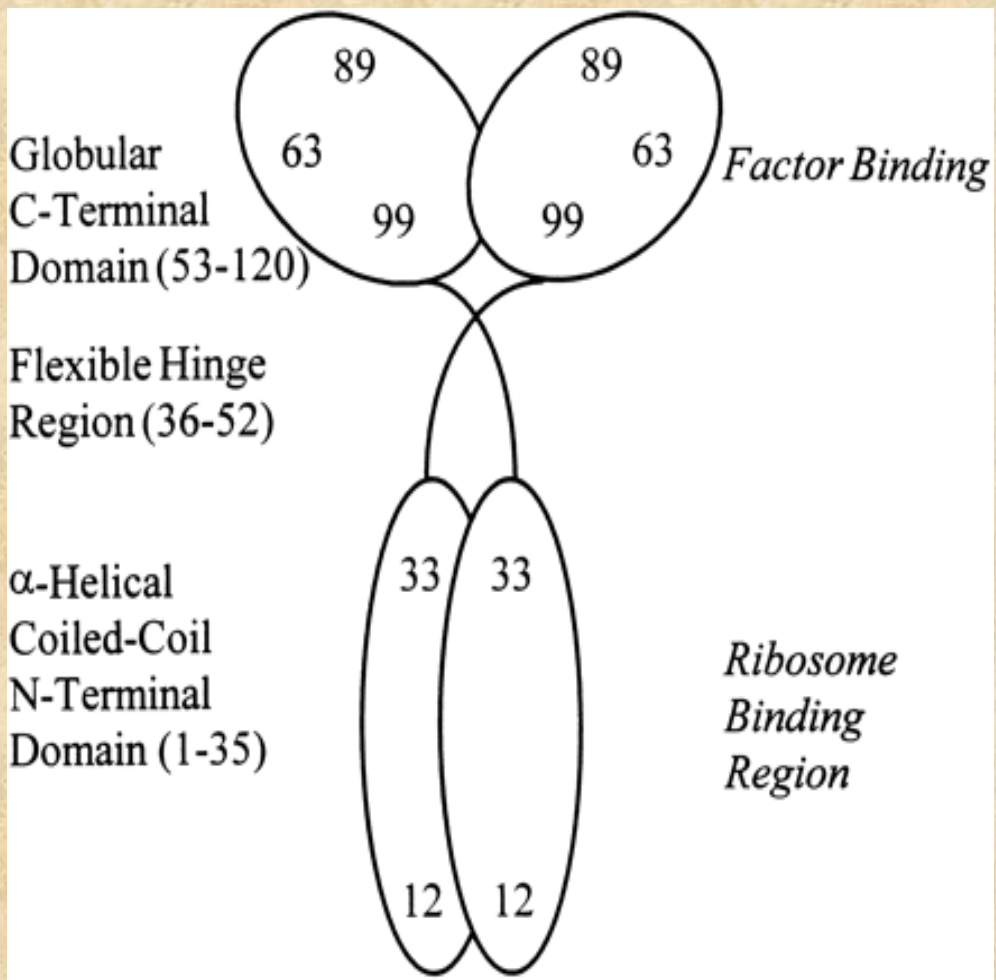

Subunit exchange experiments allowed the preparation of singly labeled dimers

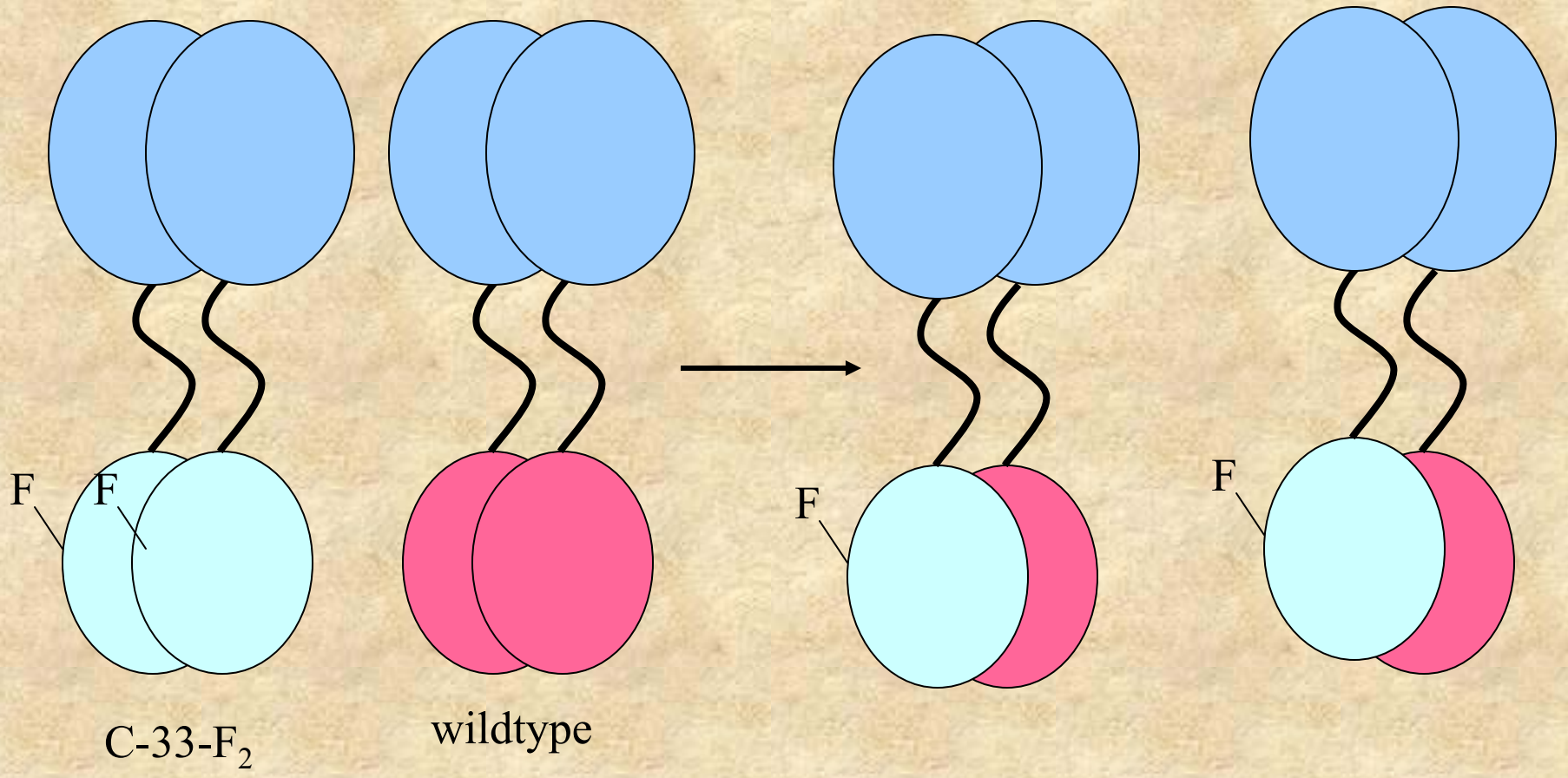

The presence of homoFRET was evident in the excitation polarization spectrum as shown by the Weber Red-Edge Effect.

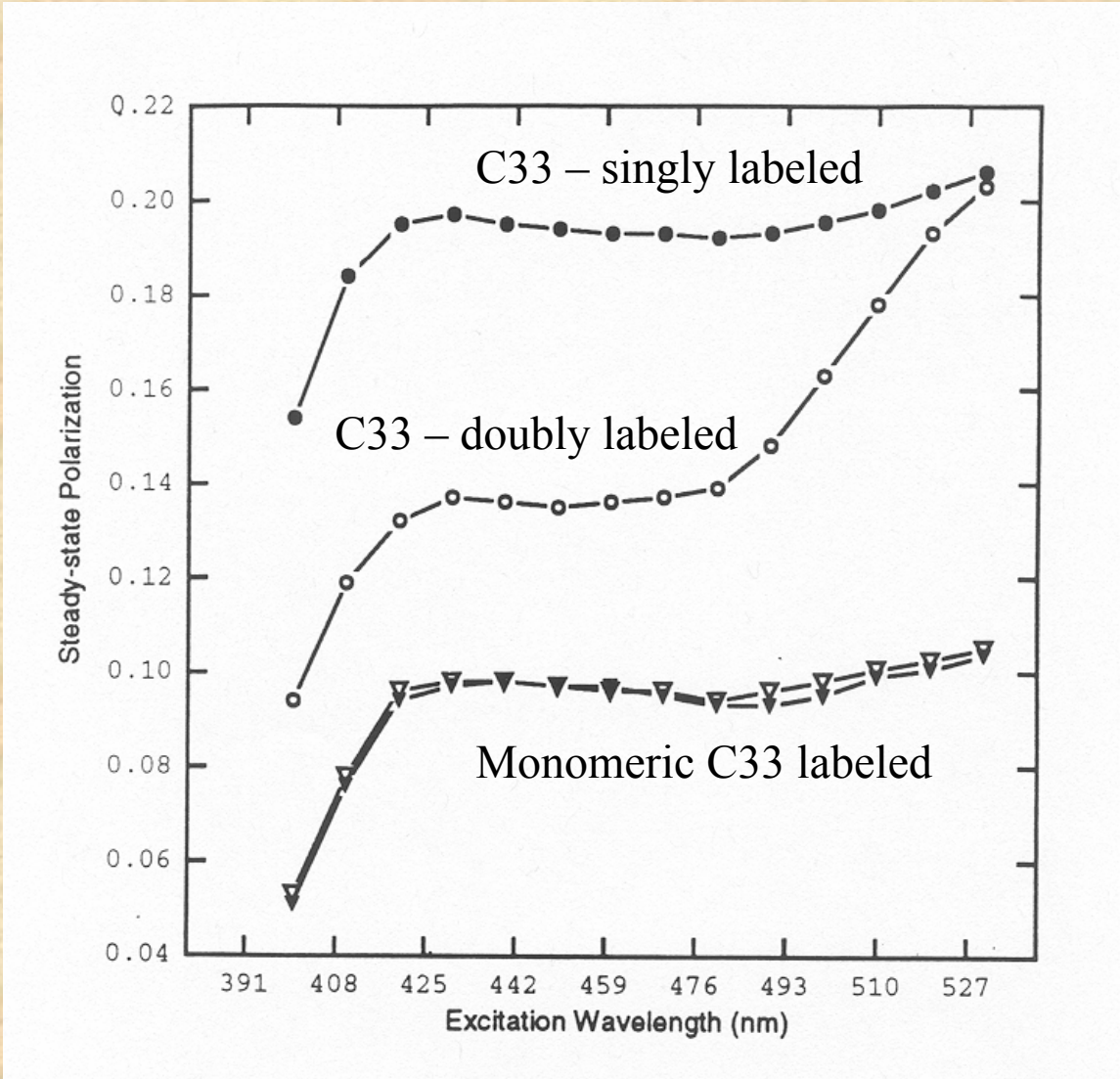

The polarization values, before and after subunit exchange, indicate which residues undergo homoFRET. The polarization data below are for fluorescein labeled constructs before (violet) and after (magenta) subunit exchange

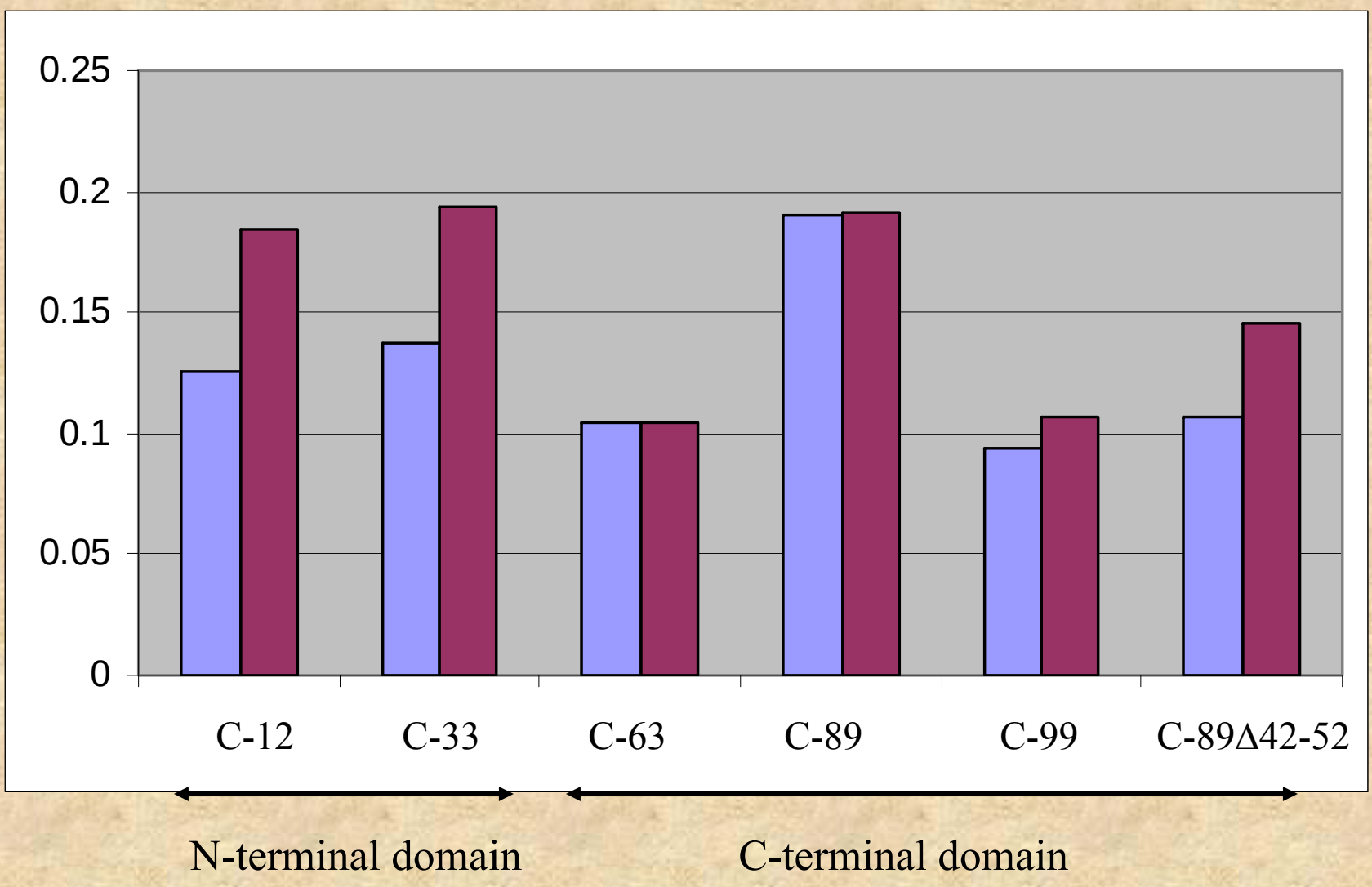

These changes in polarization due to homoFRET allow us to assign maximum proximity values for the C-terminal domains.

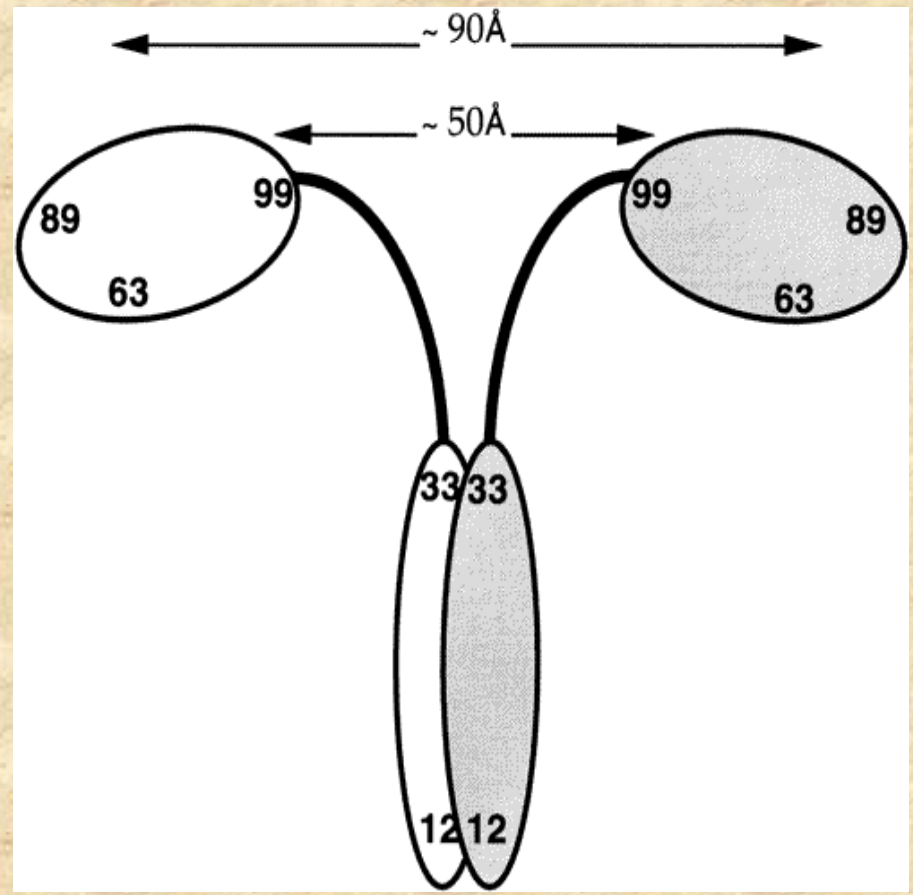

The conclusion is that the C-terminal domains are well-separated – contrary to the original model from the X-ray studies and the usual depictions in the literature

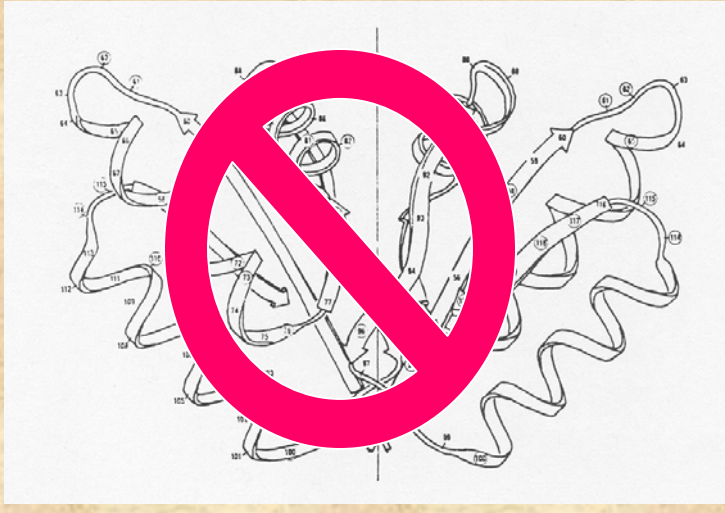

Homo-FRET Microscopy in Living Cells to Measure Monomer-Dimer Transition of GFP-Tagged Proteins

I. Gautier,* M. Tramier,* C. Durieux,* J. Coppey,* R. B. Pansu,† J-C. Nicolas,‡ K. Kemnitz,§ and M. Coppey-Moisan*

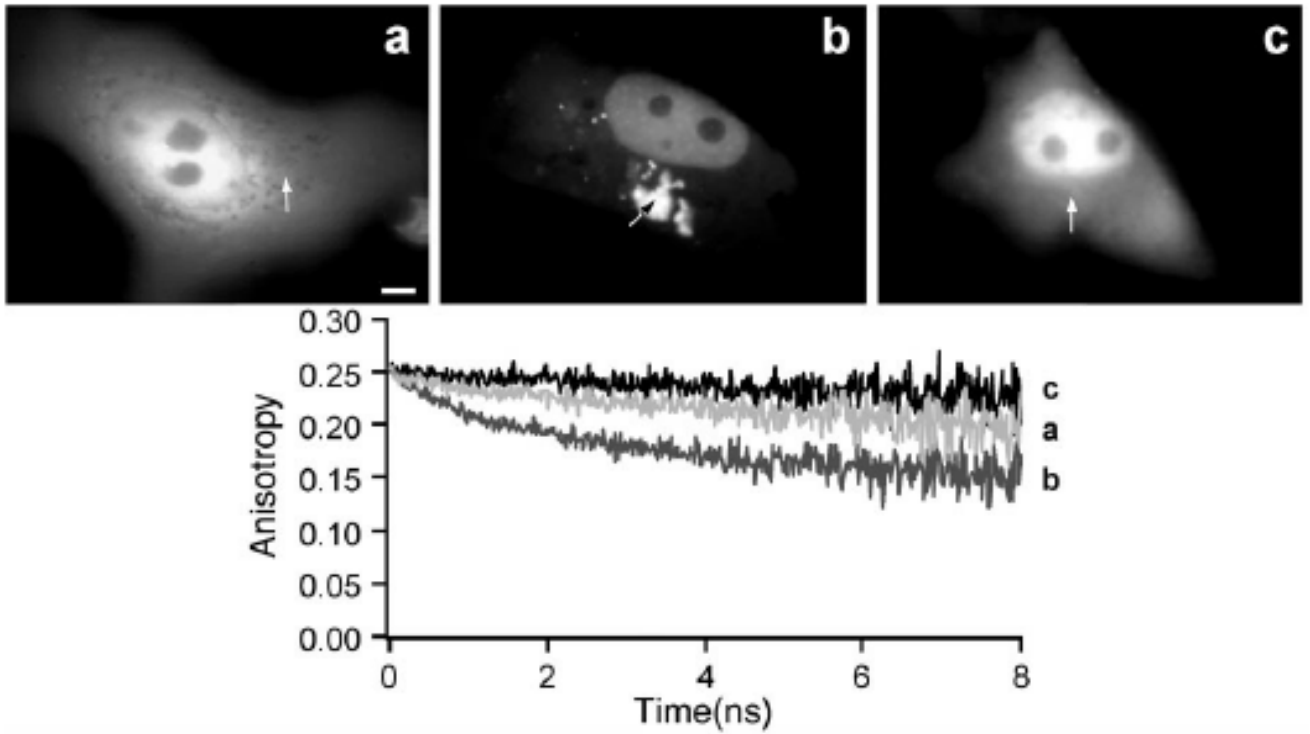

FIGURE 1 Subcellular fluorescence anisotropy decays of $TK_{27}GFP$ and $TK_{366}GFP$ proteins. (*Top*) Steady-state fluorescence images of Vero cells expressing $TK_{27}GFP$ (*a*) and $TK_{366}GFP$ (*b* and *c*). (*a* and *c*) Cells presenting only a diffuse cytoplasmic and nuclear fluorescence pattern; (*b*) Cells containing fluorescent aggregates. (*Bottom*) Time-resolved fluorescence depolarization from a cytoplasmic area of diffuse fluorescence (*a* and *c*) and from an area inside an aggregate (*b*). The subcellular location of the illuminated volume (~1 μm^3) from which the anisotropy decay was performed is indicated by an arrow. For cells containing aggregates, anisotropy decays from nuclear or cytoplasmic area of diffuse fluorescence were similar to that obtained from aggregates (*b*). Bar in *a*, 5 μm.

Biophys J, June 2001, p. 3000-3008, Vol. 80, No. 6

Other examples of homo-FRET *in vivo* can be found in: Tramier et al., 2003 "Homo-FRET versus hetero-FRET to probe homodimers in living cells" Methods Enzymol. 360:580-97.

To summarize this lecture is not intended to prepare you to start FRET measurements immediately but rather to make you aware of the salient principles and pitfalls

Several books on this topic are available as well as MANY articles in the primary literature

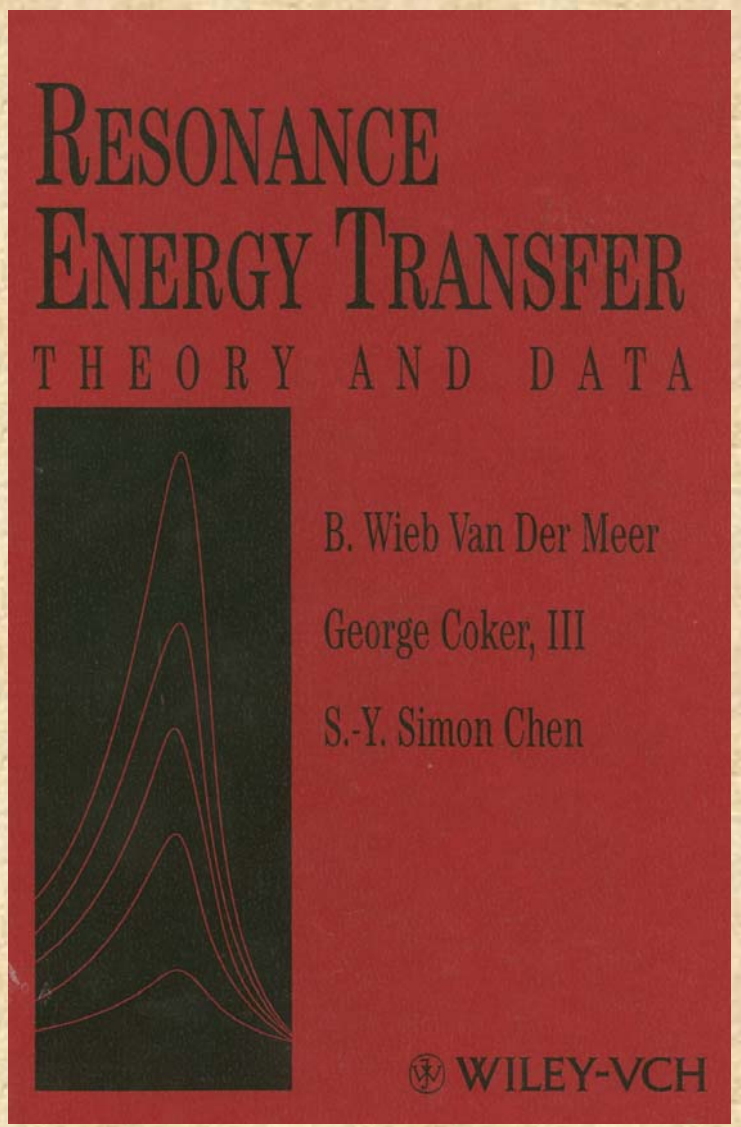

That’s all!!!